Gollner M, Oran E, Hariharan SB, Dowling J, Farahani HF, Rangwala A. 2019. Efficient remediation of oil spills over water using fire whirls. (Bureau of Safety and Environmental Enforcement Oil Spill Response Research Project # 1094).

Bureau of Safety and Environmental Enforcement (BSEE) Report: Efficient Remediation of Oil Spills over Water Using Fire Whirls

Michael Gollner, Elaine Oran, Sriram Bharath Hariharan, Joseph Dowling, Hamed Farmahini Farahani, Ali Rangwala

“Efficient Remediation of Oil Spills over Water using Fire Whirls”

Final Report

Principal Investigators:

Dr. Michael Gollner (University of Maryland)

Dr. Elaine Oran (University of Maryland)

Dr. Ali Rangwala (Worcester Polytechnic Institute)

Project Staff

Mr. Sriram Bharath Hariharan (University of Maryland)

Mr. Joseph Dowling (University of Maryland)

Dr. Hamed Farmahini Farahani (University of Maryland)

Date: 03/12/2019

This study was funded by the Bureau of Safety and Environmental Enforcement (BSEE), U.S. Department of the Interior, Washington, D.C., under Contract E17PC00016.

Acknowledgements

This study was funded by the Bureau of Safety and Environmental Enforcement (BSEE), US Department of the Interior, Washington, D.C., under Contract Number E17PC00016. The authors would like to thank Karen N. Stone (COR) and Paige Shin (CO) for support and coordination during this study. The authors are thankful to the personnel and students of the Department of Fire Protection Engineering, University of Maryland, who helped throughout this project, especially Dr. Fernando Raffan Montoya, Yu Hu, Brian Sullivan, Michael Heck and Michael Jones. The authors also thank Raymond T. Ranellone, and the personnel and students of the Fire Protection Engineering Performance Laboratory at Worcester Polytechnic Institute for their assistance with experiments within the scope of this project, especially Fredrick M. Brokaw, Chris D. Nelson and Nate Saur.

1. Executive Summary

This project is a fundamental step towards understanding the use of fire whirls to clean up marine oil spills. A series of experiments on the burning of liquid fuels on water in a traditional pool fire and a controlled fire whirl regime, from small to large scale, were designed and executed. The objectives of this project were to (1) describe and characterize the structure and behavior of fire whirls over open water; (2) understand the effects and advantages of fire whirls on in-situ burning (ISB); and to understand and quantify emissions from both traditional ISBs (pool fires) and an enhanced configuration using fire whirls at small (3) to large scales (4).

Measurements of gaseous emission (CO, CO_2, O_2) and particulate matter, the fuel burning rate, inlet velocity, temperature (gas and liquid phase), and heat flux from fires in both pool and fire whirl configurations have been conducted in small (11 cm diameter), medium (20 cm and 30 cm diameter), and large-scale (70 cm diameter) tests. Experiments with both heptane and Alaska North Slope (ANS) crude oil at various scales have shown an increased burning efficiency of fire whirls, i.e. a higher burning or heat-release rate and therefore decreased burning time for fire whirls, typically on the order of double the rate or half the time compared to traditional pool fire configurations. Emissions similarly were reduced in a fire whirl configuration, especially as scales increased. Depending on the fuel type and scale, total particulate matter production was reduced as much as 4 times for fire whirls compared to pool fires, with almost all medium and large-scale configurations exhibiting at least a 2 times reduction in total particulate matter. While heptane tests had almost all fuel removed, some less volatile components of ANS crude remained during tests, though this amount increased with increasing scales, on the order of 80%+ removal at large-scale, consistent with previous measurements on pool fires.

Finally, temperature, velocity, and heat flux data help to describe some of the processes controlling the burning process. Fundamentally, improvement in burning efficiency is caused due to an increase in heat transfer to the fuel surface, which was corroborated with experimental measurements. The phenomenon of boilover complicated the experimental process and suggestions in this area are made for future work. Ultimately, new data provided in this report have helped to improve our fundamental understanding of fire whirls and helps pave the way toward developing significantly faster, cleaner and more efficient ISB techniques.

Contents

2. Summary of Work

Experimental investigations of laboratory scale fires on the order of $10^1 - 10^2$ kW were performed at the University of Maryland (UMD). Additional experiments for fires on the order of 10^3 kW were performed at Worcester Polytechnic Institute (WPI). Fixed-frame enclosures were constructed at each scale to support formation of fire whirls under natural entrainment. The enclosures were formed using a four-wall structure, with four gaps for tangential entrainment of the air into the enclosure. This configuration sustained well-controlled fire whirls that could be studied safely and in a repeatable manner. For experiments at all scales, the ratio of gap width to enclosure length was kept constant. Parameters such as fuel type and fuel slick thickness were not varied with scale.

In all experiments, a water sublayer was used below the fuel layer to simulate ISB conditions. For experiments with ANS at the small and medium scales, the water sublayer was either mixed well such that boilover did not occur at the fuel-water interface. Boilover was not eliminated in experiments at the large scale, for both pool fires and fire whirls, in spite of using a recirculation mechanism. Experiments were conducted in three phases to study the difference in emissions behavior of fire whirls and pool fires at these scales. First, small scale experiments were conducted with detailed experiments in Phase I to understand the fundamentals of fire whirls' structure and behavior. In the small scale, the ambient circulation of the fire whirl apparatus enclosure were adjusted by varying gap size. This was used to determine an optimum condition for studying fire whirls, based on consistency of fire whirl formation under natural entrainment. Burning efficiency (fraction of initial fuel quantity consumed by fire whirl) was quantified for ANS fuel. Emissions for pool fires and fire whirls formed using heptane and ANS were measured and quantified. In Phase II of the project, the variation in the mentioned parameters was studied at the medium scale, with two fuel pool sizes. Phases I and II were conducted at UMD. Finally in Phase III, a large-scale experimental campaign was performed at WPI, characterizing the behavior of fire whirls at a scale relevant to ISB situations. The findings from this phase served as a proof-of-concept fire whirls show potential to be further studied and developed such that they may be employed and integrated with traditional ISB techniques to reduce the airborne emissions, and improve the efficiency of oil spill remediation. A summary of the three executed phases are provided below.

2.1. Summary of Phase I

This phase included bench-top experiments of burning liquid fuels over water in an 11 cm fuel pool to understand the fundamentals of fire whirl formation and behavior over water. Fire whirls were formed in a fixed-frame, four-wall fire whirl setup with natural entrainment, and the emissions, effectiveness, and other relevant parameters were compared with corresponding pool fires.

Task 1 of Phase 1 of the proposed work, "Fire whirl structure and fundamental behavior", lasted between months 1 and 9, and involved studies of fire whirl behavior at the small scale. The experiments initially were performed to configure and optimize a basic fire whirl setup in terms of the gap width to fire whirl enclosure size and also obtain preliminary information on mass loss, and residue measurement from ANS crude oil experiments.

Task 2 of Phase 1 of the proposed work, "Effectiveness, combustion efficiency, and emissions" lasted between months 3 and 12. These experiments utilized various sensors to measure particulate matter (PM) emissions, gaseous emissions (CO, CO_2), O_2 consumption, mass loss rate, inlet velocity, temperature (gas and liquid phase), and heat flux feedback. The experiments were also conducted for the pool fire regime, such that a basis for comparison could be established. The fuels used in the experiments were heptane and ANS crude oil. Results from small-scale experiments will be presented in June 2019 at the 42nd Arctic and Marin Oilspill Program (AMOP), to be held in Halifax, Canada.

2.2. Summary of Phase II

Phase II included medium-scale laboratory experiments of liquid fuels burning over a water layer, in 20 and 30 cm fuel pools, to study the change in fire whirl characteristics at the medium scale. Emissions, effectiveness, and combustion efficiency were also characterized at this scale, and the results for fire whirls and pool fires were compared. Phase II included demonstration of fire whirl formation with heptane and ANS crude oil similar to Phase I, after which measurements related to emissions and other combustion parameters were conducted.

Task 1 consisted of construction of a new fire whirl enclosure with the appropriate dimensions, similar to that of the small-scale configuration. After achieving consistent fire whirl formation at this scale, comparisons of burning rate and combustion efficiency between fire whirl and pool fire regimes were performed. Results were also compared with results from Phase I.

Task 2 included the emissions measurements of fire whirls and comparisons to pool fires, as well as identifying any changes in trends from the small-scale results. Experiments utilized various sensors to measure gaseous emission (such as CO, CO_2, O_2) and particulate matter, mass loss rate, inlet velocity, temperature (both in the gas and liquid phase), and heat flux. Findings from the medium-scale experiments will be presented at the 11th U.S. National Combustion Meeting, to be held in Pasadena, CA, March 2019. A manuscript incorporating these results, was submitted to this meeting as an extended abstract, was submitted and accepted by the CO, Karen Stone.

2.3. Summary of Phase III

Phase III of the project pertains to large scale experiments, with a fuel pool diameter of 70 cm. At this scale, the burning rate and heat transfer mechanisms of liquid-fuel fires are closer to realistic scenarios. Large-scale experiments were performed at WPI in the UL Fire Protection Engineering Performance Laboratory under a calorimeter, which is rated up to 6 MW ($\sim 10^3$kW). Similar to Phases I and II, initial efforts were devoted to construction of the fire whirl enclosure at the large scale and performing preliminary experiments to ensure consistent fire whirl formation. Dimensions of the larger fire whirl enclosure were designed based on knowledge of fire whirl formation at the smaller scales, and the ratio of gap-size to enclosure length were kept constant.

The Large Oxygen Depletion System (LODS) at WPI provided gas species measurement similar to the smaller scales. Gaseous emission (such as CO, CO_2, O_2) and PM were obtained from the exhaust duct of the system. In addition, the inlet velocity at different heights in the gaps, temperature (gas and liquid phase), and heat flux (to fuel surface, and to surrounding environment) were captured. Heptane and ANS crude oil were used in both pool fire and fire whirl regimes, and the fuel slick thickness was kept the same as experiments at the smaller scales. For experiments

with ANS, post-extinction residue was collected using absorbing pads, and overall mass loss was calculated to determine combustion efficacies.

Data from fires ranging from 0.2 m in height to those over 5 m have been obtained and analyzed. Scale modeling has focused on emissions factors, which quantifies the mass of effluent divided by the mass of fuel consumed, providing a quantitative means to assess the improvement offered fire whirls over pool fires. The parameters characterizing the fire whirls formed in this study, namely the circulation (defined based on inlet velocity and enclosure side length) and heat-release rate (HRR) is also presented. Additionally, the large-scale experiments serve as justification for attempting design of future ISB technology to generate controlled fire whirls in the open water. Major findings from this work at a wide range of length scales will be summarized in a ground-breaking paper and be submitted to a high-impact journal in the near future. Further analysis of large-scale experiments, to be presented as a proof-of-concept, will also be submitted for publication by Summer, 2019, and there are plans to submit it for presentation at the International Oil Spill Conference (IOSC) 2020.

3. Background

Oil spills are disastrous in nature and pose a serious threat to surrounding populations [1,2], response workers [3], and ecosystems [4–6]. In addition to the above, the effects of oil spills include disruption to local oil exploration infrastructure, marine transportation, and potentially widespread economic impacts [7]. Rapidly advancing oil recovery technology as well as increased interests in local production continues to increase the probability of oil spills' occurrence [8]. An efficient, effective, and robust treatment technique is crucial to mitigate their impact. In this regard, in situ burning (ISB) is one of the most reliable and effective oil spill treatment techniques [9–11], particularly in conditions where remoteness, harshness of the climate, and scale of the incident make it impossible for mechanical recovery or dispersant techniques to be deployed and utilized immediately after the spill. Decades of laboratory and mesoscale testing of in situ combustion of oil have shown that the composition and concentration of emitted emissions from ISB is an acceptable tradeoff in relation to inshore and offshore contamination and its environmental consequences and cleanup costs [9,12]. In fact, an efficient ISB has been shown to effectively eliminate at least 90% of the released liquid oil in some cases [13–15]. ISB remains a relatively fast and portable method of treating oil spills, which is especially important as 70% of the untreated oil spills may emulsify during the first 24 hours [11,16]. Despite their importance and effective use, ISB techniques are still challenged by the airborne emissions they release (especially near shore), oil slick thickness, the degree of weathering and emulsification, and the intensity of ambient wind and waves. In general, burns over water are oxygen-starved [7,17,18]; hence, ample black soot can be seen in almost any ISB, such as that shown in *Figure 3.1*. In fact, one of the major operational limits of current ISB practices is the after-burn emission concentrations, particularly at the downwind distance of the burn close to the populated areas. For instance, the maximum 1-hour averaged concentration of Particulate Matter of ten micrometers or less (PM_{10}) must not exceed 150 $\mu g/m^3$, according to ISB guidance from the U.S. National Response Team, Science and Technology Committee [17]. Reduction of PM production requires high efficiency at the time of burning, including reaching ample oxygen concentrations, high temperatures over the fuel surface, and completeness of combustion [9]. The premise of the current study is that fire whirls may be able to achieve lower emissions and faster burning rate than conventional ISB.

Figure 3.1: Shown is a controlled in-situ burn of oil spill after the 2010 Deepwater Horizon/BP spill in the Gulf of Mexico (USCG). The dark cloud indicates highly inefficient combustion and high levels of soot and other pollutants released into the atmosphere.

The fire whirl is one of the most dramatic structures which arises at the intersection of combustion and fluid dynamics, forming when the right conditions of wind and fire interact [19]. The resulting intensification of combustion imposes higher heat feedback to the fuel surface, increasing the rate of burning. The unique vortex structure also increases the amount of oxygen available to the fire and, alongside higher temperatures within the fire, can reduce the production of PM within the plume.

There is enough evidence that fire whirls generate higher burning rates in comparison to corresponding pool fires. Several studies of emissions from traditional ISB point to high emission of soot during ISBs. For instance, the Newfoundland Offshore Burn Experiment (NOBE) [9] was conducted using crude oil contained with a U-shaped fire-proof boom, where the rate of emissions

was compared with typical rates of emissions from slash burns of agricultural debris and other emission sources such as power plants and woodstoves [7,9]. Results from the experiments, presented as emissions factors (g effluent per kg fuel burned) and emissions rates (kg total emissions per hour) are compared with other known sources in *Table 3.1*, assuming a burning rate of 200 barrels per hour during the NOBE experiment [9].

Table 3.1: Collected emission data from the NOBE experiment compared with other sources [7,9]. Source: *http://response.restoration.noaa.gov/oil-and-chemical-spills/oil-spills/resources/in-situ-burn-emissions-comparisons.html*

Substance	Average Emission Factor for NOBE (g/kg-fuel-burned)	Emission rate (kg/hr)	Comparable Emission from Known Sources
CO_2	2,800	75,600	approx. 2 acres slash burn
CO	17.5	470	approx. 0.1 acres slash burn or ~1,400 wood stoves
SO_2	~15	405	7,400 (kg/hr) (avg. coal-fired power plant)
Total smoke Particle	150	4,050	approx. 9 acres slash burn or ~58,400 wood stoves
<3.5 micrometer smoke particle	113	3,050	approx. 9 acres slash burn
<3.5 micrometer soot	55	1,480	approx. 38 acres slash burn
PAHs	0.04	0.1	approx. 9 acres slash burn or ~1800 wood stoves

One of the most regulated and potentially dangerous products of combustion during an ISB is the production of Particulate Matter (PM). These fine particles, classified in groups less than 10 or 2.5 micrometers (PM_{10} & $PM_{2.5}$) in diameter, pose the greatest health hazards as they can be transported into lungs and, sometimes, even bloodstreams. *Figure 3.2* illustrates a schematic comparison between the size of these particles, fine beach sand, and a human hair.

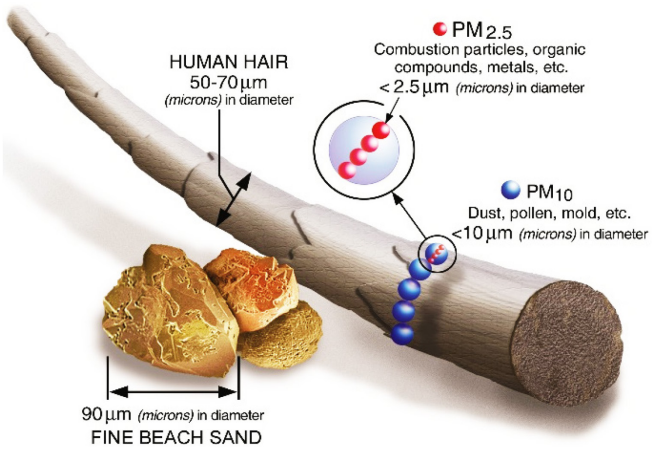

Figure 3.2: Schematic comparison between the size of particulate matter PM10 and PM2.5 with human hair; Source: https://www.epa.gov/pm-pollution/particulate-matter-pm-basics#PM

Very fine particles ($PM_{2.5}$) also create haze in the atmosphere, which is a primary cause of reduced visibility, in particular at downwind distance of large fires such as ISBs [20]. The Environmental Protection Agency (EPA) established a National Ambient Air Quality Standard for PM_{10} of 150 $\mu g/m^3$ averaged over 24 hours. This limit was later adopted by the National Response Team (NRT), Science & Technology Committee, averaging production over 1 hour. Thus, the efficiency, effectiveness, safety and completeness of the combustion of fire whirls will be, also, characterized by measuring $PM_{2.5}$ and PM_{10} in this study. Additional gases such as CO, and CO_2, while not as closely regulated, have an impact on climate and human health, and will also be measured when available to further understand both emission factors and the cause of soot formation in fire whirls.

4. Experimental Approach

The methodology of the project at the different scales is explained in this section. This includes a generic explanation of the experimental approach (fire whirl generation mechanism) and the different measurement techniques and sensors used at different scales. The details related to the measurements at each scale and the specific setups are presented in the relevant sections. Experiments of Phase I and Phase II were conducted at UMD, and those of Phase III were performed in the Performance Fire Laboratory at WPI.

Fixed-frame four-wall configurations were used to generate fire whirls in this project at all scales. This fire whirl mechanism generation creates an on-source quasi-steady fire whirl [19]. This is the most stable form of fire whirls, providing a good comparison with regular burning of liquid fuels, i.e. pool fires. Four-walled setups are also simple to construct and potentially adaptable for later use in applications. For all experiments, a circular pan was used to hold the water sub-layer and the fuel slick. Pans of different depths for experiments at the various scales. Fuel slick thickness over the water sublayer was nominally about 5 mm, and some experiments with 7 mm were performed at the large scale. *Figure 4.1* shows the schematics of the fixed-frame configuration that was used in this project from the top and side view along with important parameters labeled. At different scales of the project, the below configuration was increased proportional to the fire size (heat-release rate).

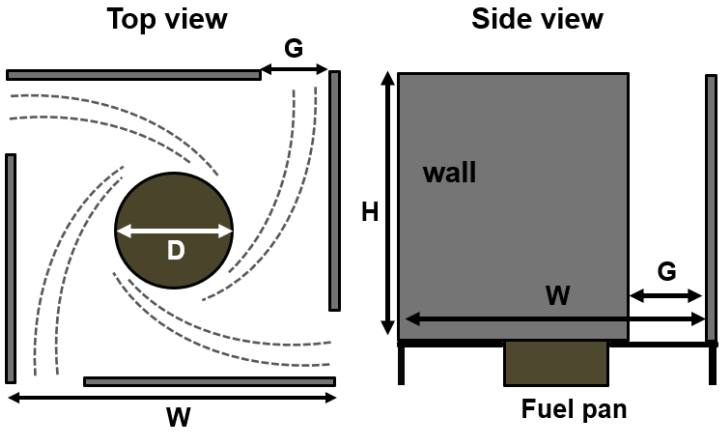

Figure 4.1: Generic experimental setup used at different scales. The ratio of the gap width to enclosure length ($G/W = 1/4$) was maintained constant for experiments at all scales.

Different pan diameters were used in the different scales of this project. The dimensions of the fire whirl enclosure were also increased along with the increase in the fuel pan diameter from small to large scale tests. *Table* 4.*1* summarizes the enclosure dimensions at different scales tested in this project. Liquid fuels in the fuel pans (burning rig) were burned with and without these walls to have two different flame regimes, a fire whirl and pool fire, respectively. Except for the fire whirl apparatus dimensions, the test condition and other parameters (such as fuel type and fuel layer thickness) were kept similar for the pool fire and fire whirl tests.

Table 4.1: Dimensional details of the experimental configurations. Refer *Figure 4.1* for nomenclature.

	Pool diameter ***(D, cm)***	**Gap width** ***(G, cm)***	**Enclosure length** ***(W, cm)***	**Enclosure height** ***(H, cm)***
Small-scale	11	15	61	61
Medium-scale	20, 30	25	100	100
Large-scale	70	45	175	240

Two liquid fuels, n-heptane and ANS crude oil, were used for experiments. Experiments were performed at each scale with both fuels, such that results could be compared across scales. Heptane (C_7H_{16}) is a pure liquid hydrocarbon with a relatively low flash point (−4.0°C) and was chosen to isolate the effect of fuel composition and provide a steady burning rate. This helped to subsequently stabilize the fire whirl and its burning rates. Particularly at small-scales, it is important to eliminate the need to account for potential changes in flash point as well as to reduce uncertainties involved in vapor pressure-temperature relationships. On the other hand, ANS crude oil was used to mimic a realistic spill. Multi-component fuels such as ANS, with their constituent species having a wide range of flash points, provide a chance to study the influence of a fire whirl on complex fuels and their residue after extinction of the fire. *Table 4.2* shows important characteristics of the fuels that were used in the experiments. Some preliminary exploratory

experiments were also conducted on West Texas intermediate crude oil and Diesel, used in specific scales.

Table 4.2: Physical properties of the fuels used in this study.

Fuel	Density (kg/m^3)	Flash point (^{o}C)	Boiling point (^{o}C)
Heptane	684	– 4	98
ANS Crude oil*	866	25–35	> 38
West Texas intermediate	867	32	> 35
Diesel	830	50	120–350

*Crude oil properties are a strong function of their evaporation level and %weight, thus great variation exist in their reported properties.

For experiments at the different scales, a systematic approach was taken towards instrumentation. The exhaust ducts of the suction hoods were connected to IR gas sensors to measure the CO and CO_2 concentrations. Initially, a SERVOMEX Siemens ULTRAMAT 23 infrared was used to measure analyze CO and CO_2, and a Rosemount Analytical instrument with a paramagnetic O_2 sensor was used for measuring O_2 consumption. However, a newer device from Cal Instruments (ZPA ND-IR with O_2 Analyzer) was used to perform final measurements of CO, CO_2, and O_2 concentrations in the exhaust duct. The sensitivity of the sensors that were used in the project were in the ppm range. Nitrogen was used as zero reference for CO, CO_2, and O_2. The gas sensors were all calibrated with their respective calibration gases on each day that experiments were performed. The span gas for the IR sensor contained 8% CO_2 (80,000 ppm) and 0.8 % CO (8,000 ppm), with N_2 making up the remainder. The newly purchased Cal Instruments gas analyzer is shown in *Figure 4.2*. Experiments at the large scale conducted at WPI used similar sensors to measure effluent concentrations.

In order to measure other effluents, such as NO_x, SO_x, and unburned hydrocarbons (C_xH_y) an E-instruments E-8500 multi-gas analyzer was used on selected tests. However, even when the

instrument was used to probe directly in the flame, the concentration of these species in the effluent was lower than the sensitivity of the instrument, and it was thus difficult to distinguish between actual signals and electronic noise from the sensors. Thus, emission factors for these species are not quantified here. It is suggested that in future work, discussed in *Section 10*, that sensors with higher sensitivity to low concentrations of these species be used to obtain reliable measurements. Regardless, their presence in the exhaust duct does not affect measurements of CO, CO_2 and PM, which were reliably detected and measured.

A DustTrak DRX was used to measure the concentration of particulate matter in the exhaust duct. The exhaust was sampled from the duct at a rate of 3 L/min using the internal pump in the instrument. In order to use the device on particulate matter (PM) from crude oil and heptane, a photometric calibration of the DustTrak was performed. *Figure 4.2* shows the gas analyzer and the DustTrak DRX instrument used in this project. The details of the sampling systems and the sensors are given in the respective sections of this report.

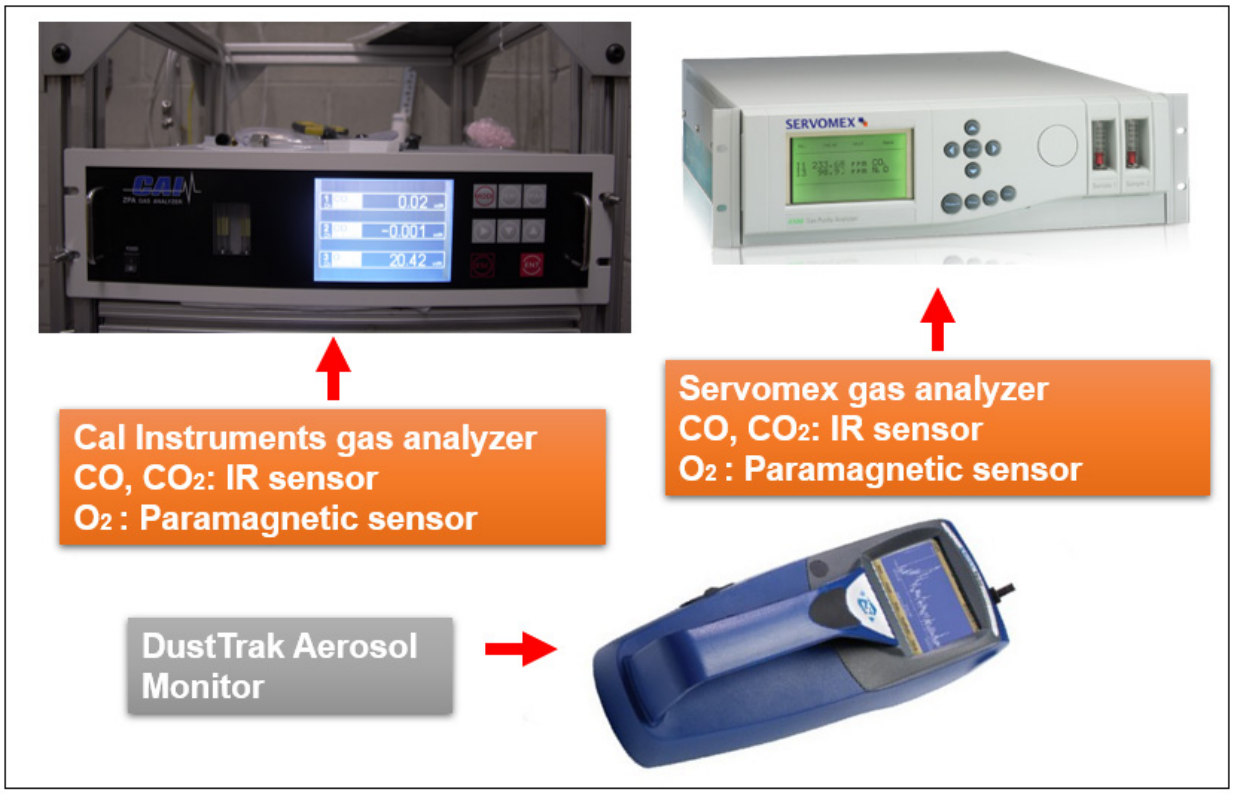

Figure 4.2: System for gas and particle measurements used in the project except for a similar gas analyzer used at WPI for large-scale experiments.

For all the experiments of the fire whirl, a combination of hot-wire anemometers and vane anemometers were positioned at the inlet gaps, at different heights above the bottom surface. The velocity of air flow into the enclosure was measured to calculate a circulation representative of the fire whirl formed. More details on the quantity and positioning of the flow meters at different scales are presented in their respective sections.

For experiments at all scales, the water sublayer was mixed/stirred continuously to prevent (or delay) boilover. In small and medium scale experiments stirring was performed with a magnetic stirrer. In the large-scale experiments a pump was used to directly circulate the water. Details are provided in their respective sections. In the small and medium scales, a load cell was placed under the fuel pan to measure the mass loss rate of liquid fuel. The mass loss rate of the fuel has direct correlation with the heat-release rate (HRR) and is an important parameter in studies related to fire science. Because of the excessive weight of the fuel/water container at the large-scale, the use of a load cell was not possible, and thus mass loss rate was not measured directly. However, oxygen consumption calorimetry was used to calculate the corresponding heat-release rate for large-scale tests.

A heat flux gauge was installed during some experiments at the center of the pool to measure heat feedback from the flame to the fuel. The component of heat feedback from the flame to the fuel surface is a critical parameter influencing the energy balance of the fuel layer. It is dependent on flame dynamics and geometry, and also influences these characteristics. A tree of K-type thermocouples were placed in the centerline of the pool to measure the change in temperature of the liquid fuel and also the water sublayer. Temperature measurements help in understanding the evolution of the water and fuel temperatures that may lead to boilover. The use of the heat flux gauge and thermocouples helped in understanding the flame feedback and the effect of the liquid-phase on burning rate in the different flaming regimes, i.e. fire whirl and pool fire. An alternative method to calculate heat flux feedback using and energy balance in the water sublayer was also used to estimate heat fluxes, presented in respective sections.

5. Small-Scale Experiments (Phase I)

Experiments at the small-scale, in Phase I, were conducted at the University of Maryland, lasting between months 3 and 12. A fixed-frame four-wall configurations was used to generate fire whirls. Experiments were conducted using ANS crude oil and heptane in both pool fire and fire whirl regimes. Results of experiments at the small-scale are reported in this section.

5.1. Small-Scale Apparatus

The experimental configuration for small-scale experiments is shown in *Figure 5.1*. The apparatus was placed under a large fume hood. Fiberglass curtains were draped around the hood, such that they were lower than the base of the experimental platform, to ensure all effluents were collected. For the small-scale apparatus, polycarbonate panels (61 cm × 61 cm) were used for the four walls of the setup and were positioned in a way that allowed for the gap size to be adjusted as required. The bottom surface of the enclosure consisted of a flat piece of ceramic fiber-board insulation, with a recess in the center to position the fuel dish. Experiments with gap sizes between 5 and 25 cm were performed to observe fire whirl formation upon ignition. A gap size of 15 cm was found to consistently form fire whirls quickly, and also remain as fire whirls for the entirety of the burning duration. The wall panels were removed for pool fire experiments.

A cylindrical dish, made of quartz (11 cm diameter, 6 cm deep) was positioned within the recess in the insulation, with the enclosure floor surface flush, such that no lips were formed within the enclosure. The pan was placed over a load cell, which was used to measure the mass loss during the experiment. First, water was filled in the container to the required level, and then the fuel layer was added over the water for each experiment before ignition.

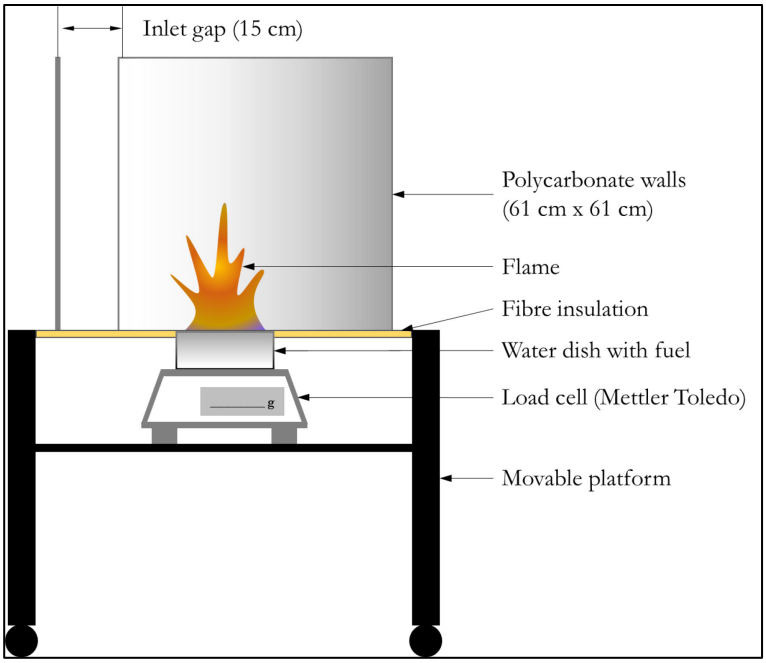

Figure 5.1: Experimental configuration for small-scale experiments.

Combustion products (effluents) were collected through a suction duct (28 cm in diameter), which was connected to a long channeling duct where effluents were mixed. The duct was instrumented with thermocouples, and effluents were sampled by instruments through tubes after being well mixed. An image of the cross-section of the exhaust duct is shown in *Figure 5.2*. The volumetric flow rate through the duct was estimated to be 0.1143 m^3/s, based on a 0.5 V operating voltage in the differential pressure sensor, with a maximum flow rate of 0.8 m^3/s at ~3.5 V. The thermocouples were positioned 5 cm, 10 cm and 14 cm from the wall of the duct. During operation, the maximum spread of temperature was less than 2 K between the thermocouples, which justified a constant temperature and well-mixed assumption across the duct. Two sampling tubes were used in the suction duct, each with 17 holes, 2 mm in diameter, along the length of the tube. This ensured sufficient sampling from across the flow channel. Combustion products encountered the differential flow meter, the particulates sampling tube, and the gas sampling tube, in that order. The holes in the sampling tubes faced downstream of the ambient duct flow. The two sampling tubes were offset by 45 ° (around the duct axial axis), to prevent interference as they were close to each other. A picture from inside the duct showing the above arrangement is shown in *Figure 5.2*.

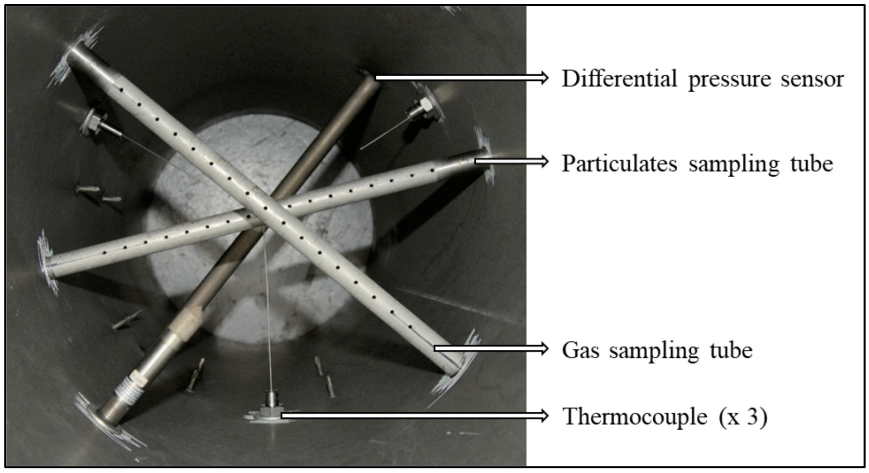

Figure 5.2: Sampling tubes and the pressure and temperature sensors in the exhaust duct.

Concentrations of effluent gases, in particular O_2, CO and CO_2 were determined from measurements made with the Cal Instruments gas analyzer, for which sampling was enabled by a two-head pump to provide the required flow rate. Particulate emissions from the fire were measured by a DustTrak DRX, and sampling was performed by the internal pump of the instrument. A photometric calibration of the DustTrak was performed by capturing data on the DustTrak simultaneously with a separate filter and pump setup to gravimetrically measure the soot generated. The measured soot mass and that measured by the DustTrak was compared to determine the appropriate settings for future experiments. The instrument was factory calibrated using Arizona Test Dust [21], and the baseline mass concentrations calculated by the instrument were based on this density. To adjust for the density variation between the test dust and the soot in our experiments, a gravimetric calibration was performed. In parallel to the DustTrak, a separate pump sampling system was operated at the same flow rate, and the exhaust gases were channeled through a fine particulate filter, which collects all the PM. The filter elements were weighed on a high-precision mass balance before the experiment, and the DustTrak and parallel pump system operated for the same amount of time. Post experiment, the filter element was again weighed to determine the amount of soot deposited in the test duration. A density adjustment was made according to the expression below [22]. Once this correction factor is determined, the values were either programmed into the instrument directly, or applied during data processing.

$$Concentration, \frac{mg}{m^3} = \frac{\left\{\begin{matrix} Filter\ Post\ Weight\ (mg) - \\ Filter\ Pre\ Weight\ (mg) \end{matrix}\right\}}{\frac{2}{3} \times \frac{\left\{\begin{matrix} DustTrak™\ Monitor \\ Flow\ Rate\ (L/min) \end{matrix}\right\}}{1000}} \times Total\ Sample\ Time\ (min)$$

In some experiments, boilover was observed at the fuel-water interface. To prevent these boilover events a magnetic stirrer was positioned under the fuel pan for all the experiments. This additional mixing prevented boilover since the mixing caused the entire water bulk to raise in temperature, preventing a stratified water sublayer, and eliminating boilover. This is described in detail later in the temperature section. An array of thermocouples were placed in the centerline of the liquid fuels to capture the liquid-phase temperature during the experiment. This was used to monitor the water temperature and anticipate boil over and control the level of stirring required.

The experimental apparatus and a fire whirl formed by burning of heptane in the apparatus is shown in *Figure 5.3*. *Figure 5.4* shows visual comparison of ANS crude oil burning in the pool fire and fire whirl regimes, both formed in the small-scale configuration.

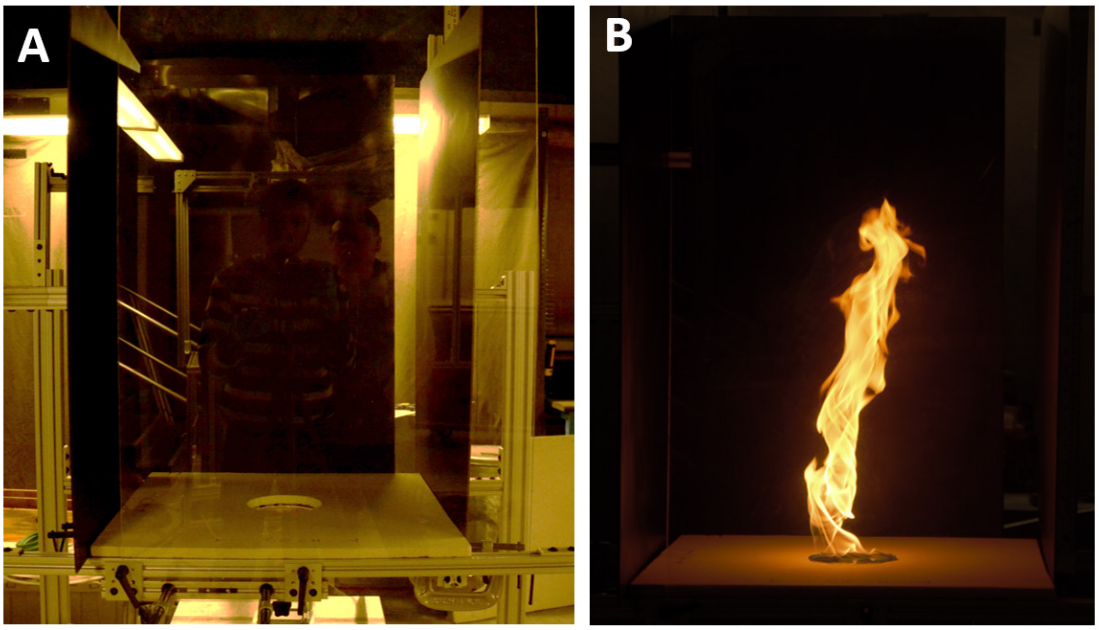

Figure 5.3: (A) Small-scale fire whirl apparatus. (B) A fire whirl formed using heptane in the small-scale apparatus.

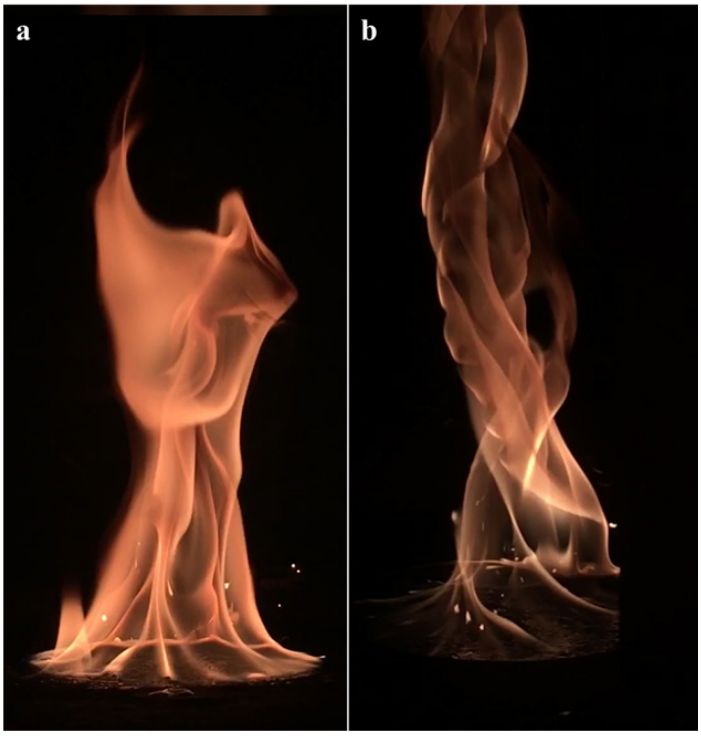

Figure 5.4: ANS crude oil burning in a (a) pool fire, and (b) fire whirl, both formed in the small-scale apparatus.

5.2. Small-Scale Results

5.2.1. Mass Loss Analysis

As part of Task 2, quantification of burning rates of liquid fuels was a parameter of interest to aid in understanding the differences between pool fires and fire whirls. Heptane and ANS crude oil were used to perform experiments on mass loss. A fuel quantity of 40 ml was used for each test. This quantity ensured sufficient time in the fire whirl regime, since a delay of about 30 s was observed between ignition and stable fire whirl formation. 40 ml of fuel was used for both fuels and flame regimes to maintain consistency.

The gap sizes were maintained constant at 15 cm for fire whirl experiments. This gap width was set based on preliminary experiments and found to reliably generate a fire whirl for both fuels used in these experiments. Absolute mass readings were logged from the Mettler Toledo load cell

to a computer using BalanceLink software. Experiments were repeated a minimum of three times for each case.

The results of these experiments are shown in the following figures. *Figure 5.5* shows the mass loss with time for heptane pool fires and fire whirls. For a fuel quantity of 40 ml, pool fires consume the fuel in around 3 minutes, while the fire whirls burn the same quantity of heptane in about half the time. The total mass loss for both regimes is around 25 g. Markers of different colors represent data from individual experiments, and the minimal spread for each case show good repeatability.

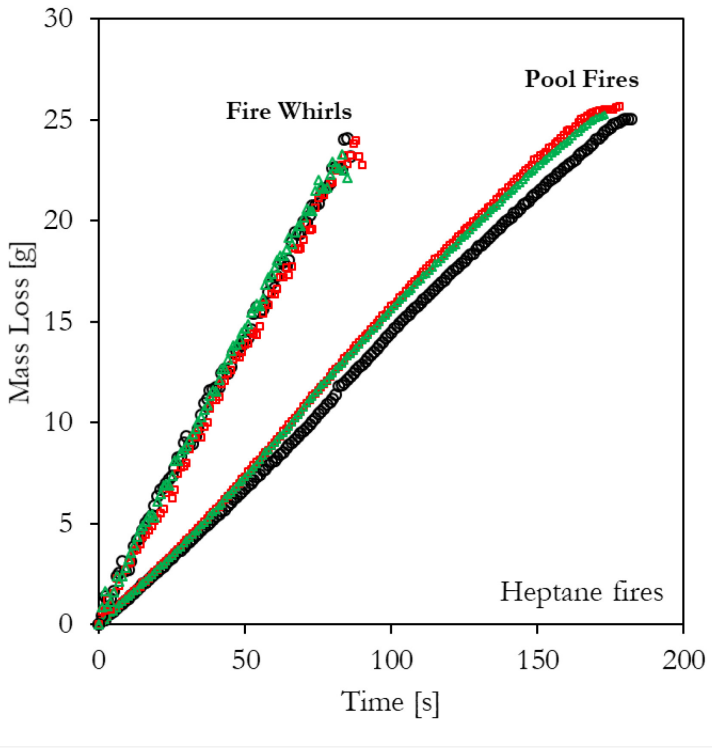

Figure 5.5: Fuel mass loss with time, for heptane pool fires and fire whirls, at the small scale.

Given the minimal spread of data for each case, and average mass loss rate can be determined by using a linear fit to the data. The slope of the linear fit gives the mass loss rate and is shown in *Figure 5.6.* The average mass loss rate for heptane pool fires was about 0.14 g/s, and that of fire whirls is 0.26 g/s. A higher mass loss rate for fire whirls as compared to pool fires is expected since the burn time (from *Figure 5.5)* for fire whirls is lower for the same initial mass of fuel. For

heptane, variation in the fuel thickness with time (as the fuel was consumed by the fire) does not seem to affect the mass loss rate. This may be attributed to heat feedback to the fuel layer, which is more than sufficient, and roughly constant throughout the burn time, leading to steady evaporation of the fuel, which is a single component hydrocarbon.

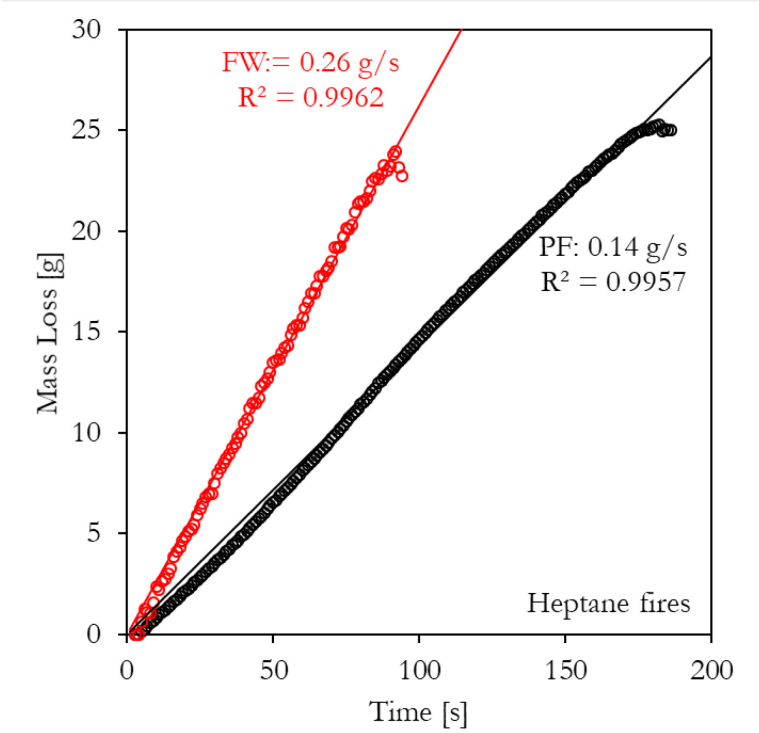

Figure 5.6: Average mass loss rate estimations of heptane using linear fits to the average mass loss data from *Figure 5.5*.

The mass loss results for ANS crude oil are shown in *Figure 5.7*. For all mass loss experiments involving crude oil, a stirrer was used at the base of the water/fuel dish, in the water sublayer, to prevent boilover at the interface of the water and crude oil. The total mass loss for fire whirls was around 18 g, and that of pool fires was around 15 g. These values are smaller than those seen in *Figure 5.5*, due to the low volatility of heavy hydrocarbons that are present in crude oil, and do not burn entirely. Thus, after each burn, some residue remained on the water surface that was

collected with oil absorbing pads. The total burn time for 40 ml of ANS was about 200 s for fire whirls, and about 300 s for pool fires.

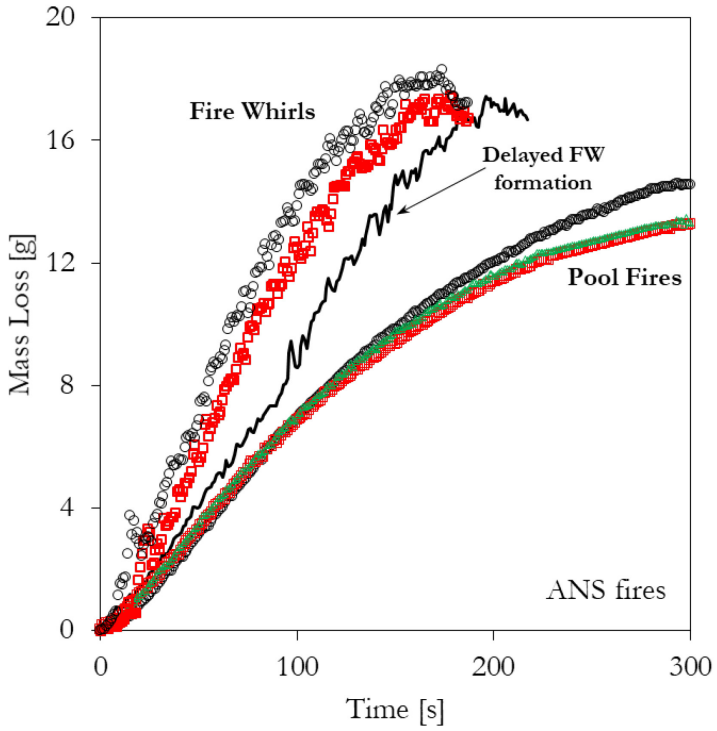

Figure 5.7: Fuel mass loss with time, for ANS pool fires and fire whirls, at the small scale.

In one experiment, fire whirl formation was delayed more than usual, and the initial pool fire burned with a rate similar to that of the pool fire experiments (see *Figure 5.7)* Once a transition to the fire whirl occurred (around 80 s after ignition), the slope of the mass loss curve changed quickly, and followed a trend similar to that of the other fire whirl experiments that did not show delayed fire whirl formation. In the delayed case, the total fuel consumed was also slightly lower than the other fire whirl experiments, owing to the initial pool fire burning prior to transition. The peak mass loss rate in this case was not as high as the other fire whirls because the initial pool fire had reduced the fuel thickness to a level where the higher burning rates were not possible. The effect of this was also seen in the total burn time, which was slightly longer than the other fire whirls.

Although the mass loss curves for ANS burning are not straight lines as in the case of heptane fires, a linear fit of the data can provide a basis for comparing the different fires. The linear fit for ANS pool fires and fire whirls are presented *Figure 5.8*. As in the case of heptane fires, fire whirls generally have a higher burning rate. The linear fit does not capture the complex nature of burning in multi-component fuels. In contrast to the relatively constant mass loss rate for Heptane, the curves for ANS showed a significant drop in burning rate over time. In the case of pool fires, the average mass loss rate is 0.056 g/s, but roughly 50 s after ignition, it peaks around 0.08 g/s, and then steadily declines until extinction. For fire whirls, the mass loss rate peaked at around 0.15 g/s, roughly twice that of the ANS pool fire, and the average rate is 0.11 g/s. The peak occurred between 30 – 50 s after ignition, and then declines until extinction. The continuous drop in mass loss rate may be attributed to the continuously diminishing fuel depth, which is known to affect burning rate, as well as the fact that with time, the fraction of heavier hydrocarbon molecules that require progressively more heat flux feedback for evaporation increases. This behavior is different from heptane, which is a single component fuel.

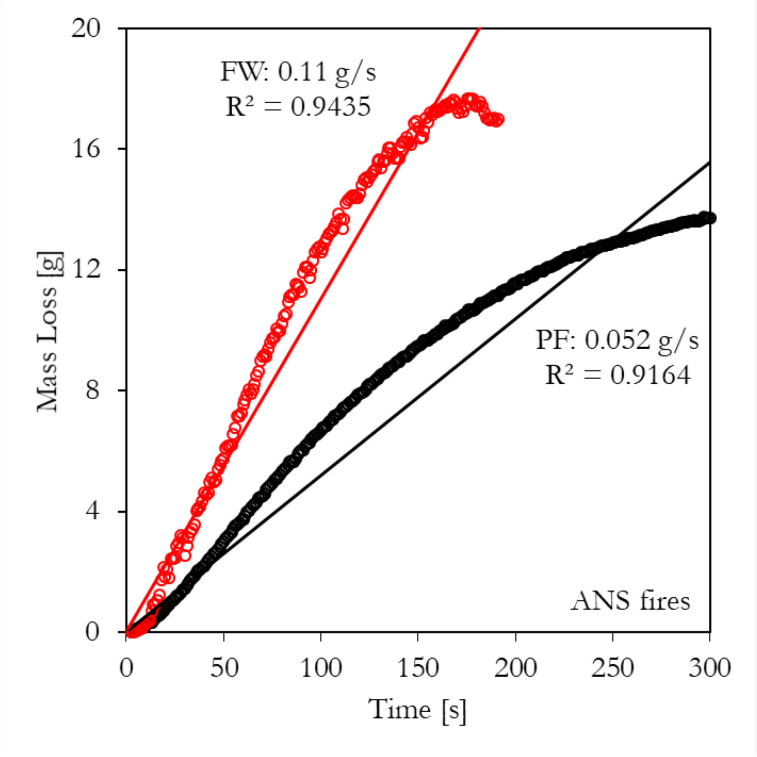

Figure 5.8: Average mass loss rate estimations of ANS using linear fits to the mass loss data from *Figure 5.7*.

Experiments at the small-scale burned about 50% of the initial mass of ANS crude oil. However, fire whirls burned slightly more crude oil, most likely due to increased heat fluxes to the fuel surface, which enable the evaporation of hydrocarbons with higher molecular weight. The fire whirl consumption efficacy was about 53%, while the pool fire burned just over 40% of the initial oil mass. *Figure 5.9* shows the comparison of the oil consumed by the fire, for the fire whirl and pool fire regimes at the small-scale. This is expected to increase at larger scales, as heat fluxes to the fuel surface increase.

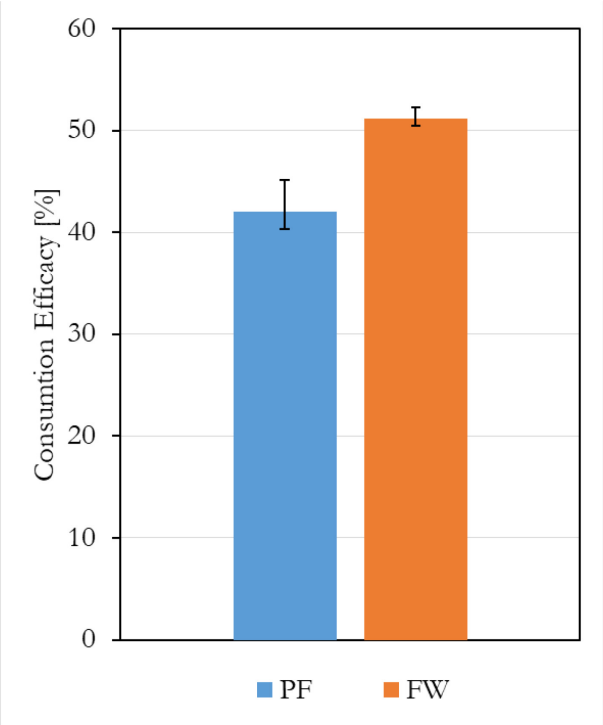

Figure 5.9: Comparison of consumption efficacy for ANS pool fires and fire whirls, calculated from mass-loss data.

5.2.2. Particulate Emissions

Particulate emission measurements were obtained using a TSI DustTrak DRX. Experiments were performed using heptane and crude oil, and for both flame regimes. The particulates sampling

tube was connected to the inlet of the DustTrak, which was operated at an internal sampling flow-rate of 3 L/min (5×10^{-5} m^3/s). Data reported here includes the total particulate matter concentration (TPM in mg/m^3) as a function of time. These values have been corrected for particle density based on a gravimetric calibration. Based on this data and the flow rate of exhaust, an approximation of the PM emitted per unit mass of fuel (in g-of-PM per kg-of-fuel) is reported later. The results of these are shown in *Figure 5.10*. The figure depicts averaged values of particulate emissions obtained from a minimum of three experiments for each case. As expected, the concentration of particulate emissions of crude oil was higher than that of heptane for both flame types.

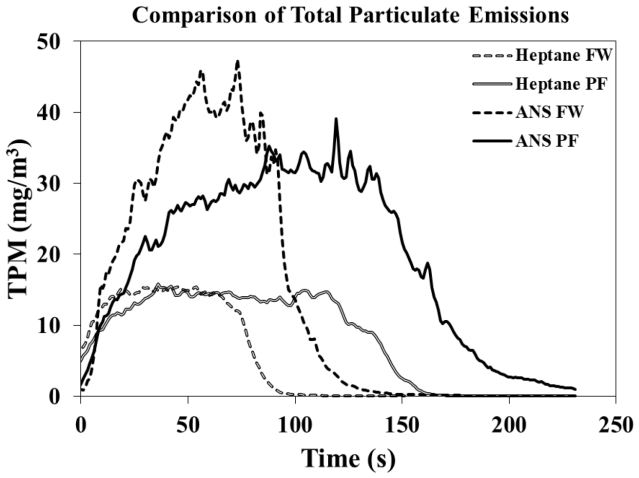

Figure 5.10: Comparison of Total Particulate Matter (TPM) emissions from pool fire and fire whirl regimes, for both heptane and ANS fires.

For heptane, upon ignition, the concentration of particulates emitted was quite similar for both the fire whirl and the pool fire, however, the total quantity of particulates emitted was higher in the case of the pool fire owing to the longer burning period. Similarly, for crude oil, the initial concentration of particulates was higher from the fire whirl, but the total quantity of particulates was higher for the pool fire case.

The total time period of emissions for ANS crude was observed to be slightly longer than the burning period determined from the mass loss rate experiments. At the end of the burning period,

a significant amount of visible smoke was observed to continue to emanate from the residual fuel. These were sometimes accompanied by small flames on the insulation surface, which had small drops of fuel deposited as a result of the splashing from boilover which occurred towards the end of some experiments. The particulate emission period was nearly the same for heptane.

Similar to the mass loss rate, particulate concentrations reached a near steady-state for heptane, but not for ANS crude. This may be attributed to the vaporization order of the various components of crude oil [23], as well as the decreasing fuel thickness over the course of the experiment as the fuel was continuously consumed by the fire.

The total quantity of particulate emissions is calculated as,

$$TPM\ (mg) = \dot{V}\left(\frac{m^3}{s}\right)\int_0^{t_b} TPM\ \left(\frac{mg}{m^3}\right)\ dt\ (s)\ , \qquad Eq.\ 1$$

where TPM *(mg)* is total, or cumulative particulate emission, $\dot{V}$ is the volumetric flow rate through the sampling duct, a constant, TPM *(mg/m³)* is particulate concentration measured in the duct, which is a function of time (*Figure 5.10*), and t_b is the particulate emission period. The resulting TPM (g) normalized by the mass of fuel consumed from mass loss measurements, which for each case is shown in *Table 5.2*. This quantity is referred to as an Emission Factor (EF) and represents the relative amount of pollutant released per unit mass of fuel consumed. As expected, EFs of TPM were higher for crude oil than heptane, and higher for pool fires than fire whirls. Here, TPM refers to a sum of PM_1, $PM_{2.5}$, PM_4 and PM_{10} concentrations, of which $PM_{2.5}$ is directly measured using an IR photometric sensor in the DustTrak. The relative concentrations of the remaining fractions are calculated based on a factory calibration. More details on this are available in [21].

Table 5.2: Average TPM (g) EF (TPM (g) / kg of fuel consumed).

$EF_{TPM} = \frac{\textbf{TPM (g)}}{\textbf{Mass of fuel (kg)}}$	**ANS Crude**	**Heptane**
Pool Fire	52.3	26.8
Fire Whirl	37.9	16.4

Since the instrument makes a direct measurement of only one size fraction of particulate matter ($PM_{2.5}$) it is worthwhile to compare the fuels and flame regimes on the basis of this parameter as well. The variation of $PM_{2.5}$ emissions with time for all the conditions are shown in *Figure 5.11*. The instrument's direct measurement of $PM_{2.5}$ is observed to follow the same trends as the total concentration and shows that most of the particulates emitted are at or below the $PM_{2.5}$ size range. The values shown here adjust for the difference in density of soot relative to the in-factory calibration aerosol, with a gravimetric calibration factor of (1/1.34).

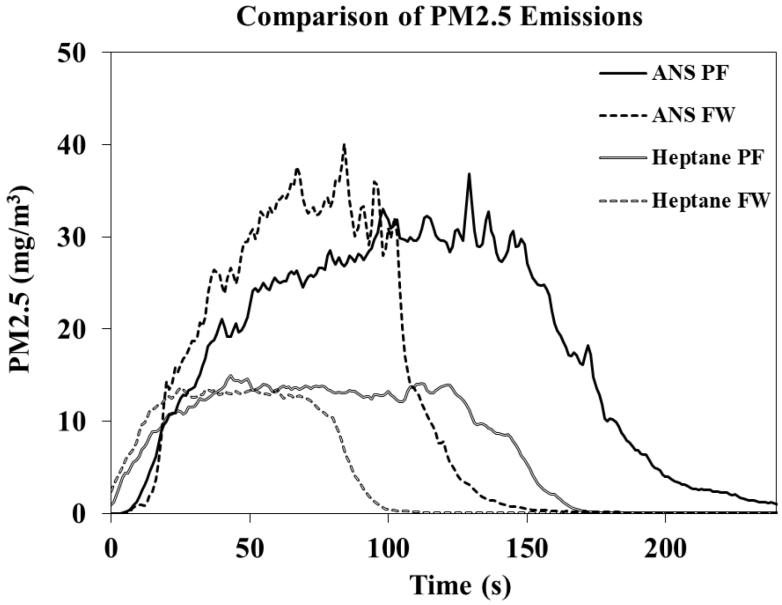

Figure 5.11: Comparison of PM 2.5 emissions from pool fires and fire whirls for two fuels, heptane and ANS crude. Results are averages of at least three experiments for each case.

5.2.1. Gas Emissions

The exhaust duct was instrumented with a sampling tube to analyze the effluent gas composition. The primary gases of interest are CO and CO_2. CO_2 provides an overall measure of the combustion process (the production of CO_2 is related to the chemical heat-release rate) and CO. The ratio of CO to CO_2 production provides a measure of the completeness of combustion resulting from locally ventilated or under ventilated conditions during burning. For the small-scale pool fire (11 cm diameter), the suction through the exhaust duct caused dilution of combustion

products. The concentrations of these species for the different cases are presented in *Figure 5.12* and *Figure 5.13*. The analyzer was calibrated using pure Nitrogen as zero gas and a gas mixture containing 0.8% CO and 8% CO_2 as the span gas, although measurements at this scale are much smaller than this range. CO_2 concentrations of heptane and ANS for the different flame regimes are shown below. For both fuels, the peak CO_2 concentration for fire whirls were higher than that of pool fires. In addition, the burning duration for fire whirl is shorter, and consistent with mass loss experiments. CO_2 concentrations therefore represented the burning rates and closely follow what was captured in the mass loss measurements.

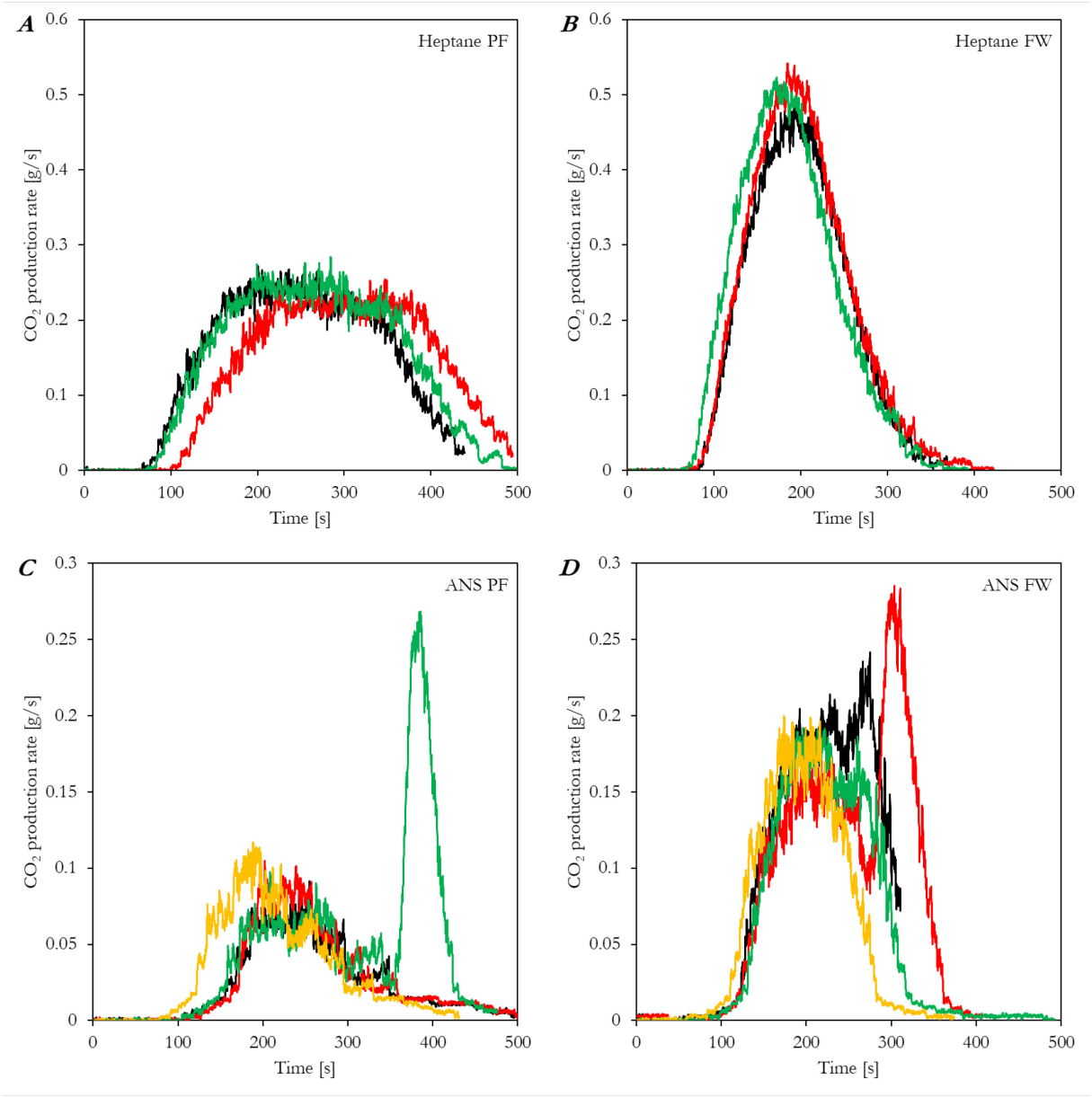

Figure 5.12: Comparison of CO_2 production rates for both pool fires and fire whirls, formed using both heptane and ANS crude oil.

The CO concentrations observed at this scale were very small, on the order of the error from the instrument. This indicates that combustion is relatively complete with good mixing, as would be expected at this scale. At larger scales the center of the diffusion flame will have less access to external oxidizer and may start to be significantly less efficient, something that the fire whirl may help improve. Experiments at larger scales will start to demonstrate the true level of this effect.

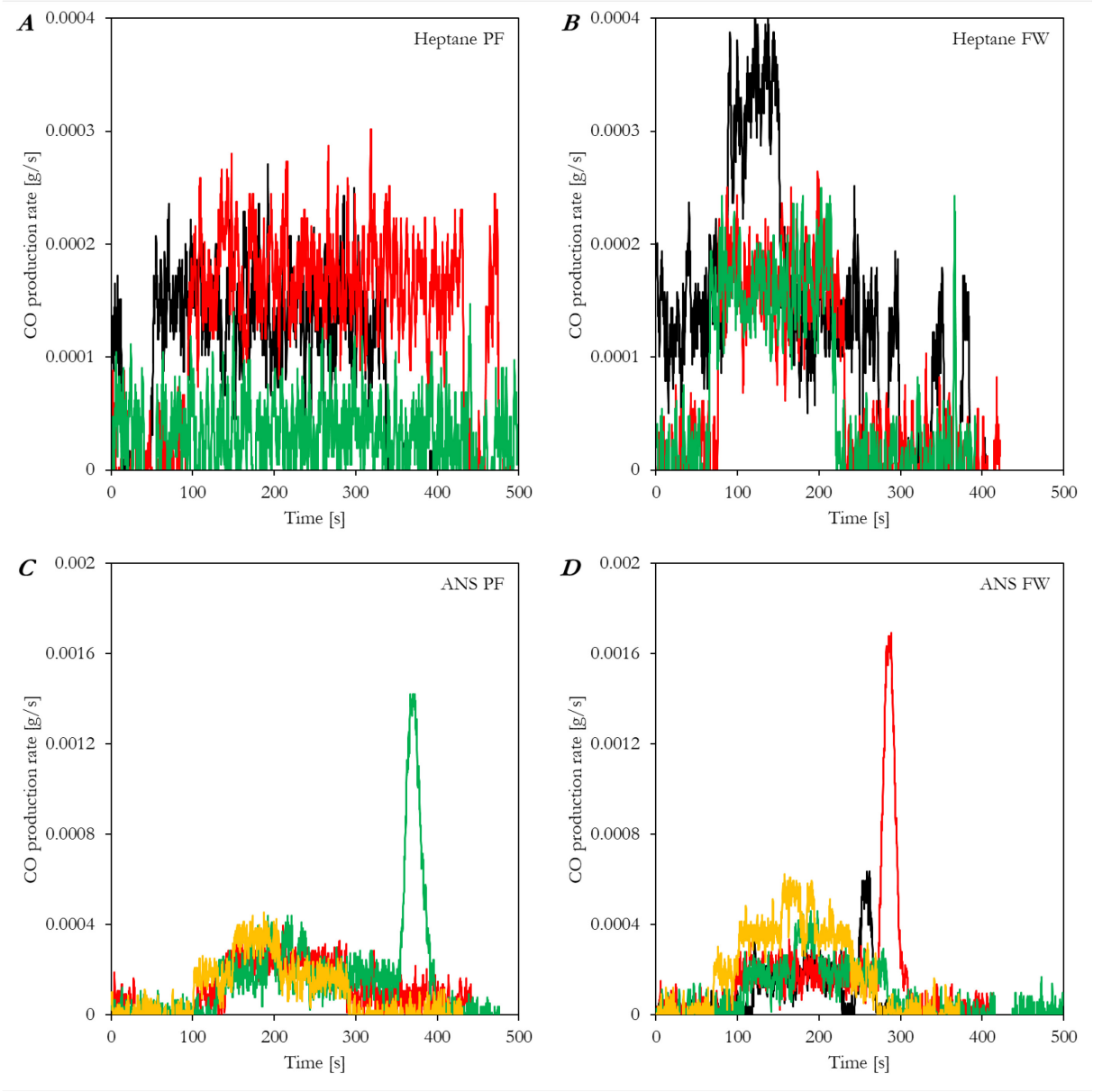

Figure 5.13. Comparison of CO production rates for both pool fires and fire whirls, formed using both heptane and ANS crude oil.

Based on these experiments, CO_2 emission factors for each fuel and burning configuration were calculated and are shown in *Figure 5.14*. The CO_2 emission factor is slightly higher for heptane fire whirl as compared to the heptane pool fire. However, the CO_2 emission factor is reduced for the ANS fire whirl compared to the pool fire case. However, the CO_2 emission factor of ANS fire

whirls is significantly higher than that of ANS pool fires. These results suggest that a larger fraction of the carbon in each of these fuels is converted into CO_2. This also explains, in part, why the particulate emissions were lower from the fire whirl cases: since more of the carbon from the fuel was bring converted to CO_2, a lower amount was left behind to form soot. In comparison the emissions factors from wildland fires are typically 1500 g of CO_2/kg-of-fuel [24]. This value is given to provide context and is not intended to be used as a direct comparison.

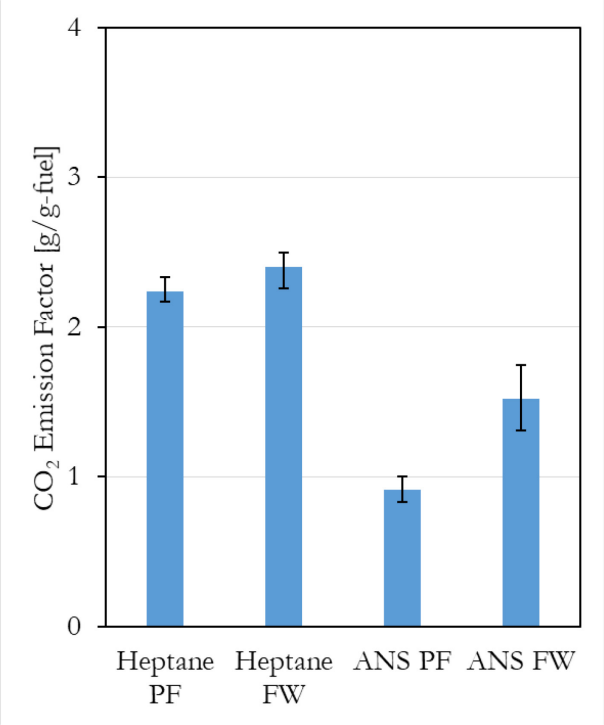

Figure 5.14. Comparison of CO_2 emission factors for both flame regimes and fuels.

Similarly, CO emission factors for each fuel and burning configuration were calculated and are shown in *Figure 5.15*. The CO emission factor of an ANS fire whirl is significantly reduced compared to the pool fire case. Reduction of CO along with PM emissions in fire whirl configurations indicates improved access to oxygen and cleaner combustion. The CO emission factor for heptane tests also show a decline in CO from the fire whirl regime when compared to the pool fire regime. Given the small size of fire and availability of oxygen in the small-scale experiments, it is expected that larger fires, with higher turbulence, will show more convincing trends of the CO emission factor.

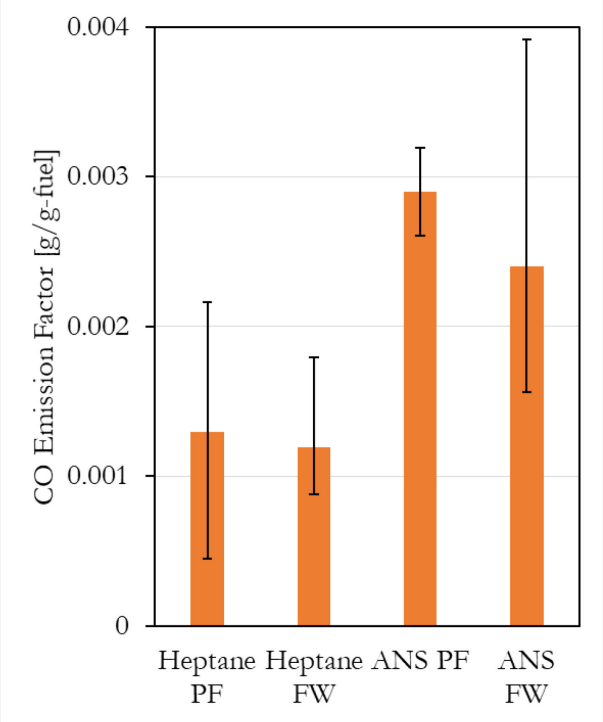

Figure 5.15. Comparison of CO emission factors for both flame regimes and fuels.

Similar to CO_2 and CO, O_2 concentration measured in the duct for each flame regime and fuel type is shown in *Figure 5.16*. The trends are similar to those seen with CO_2 and represent the instantaneous heat-release rate of the fire. For the ANS fires, one instance of boilover in each case, pool fire and fire whirl, is visible as a sharp spike in the O_2 consumption data. Similar to an emission factor for CO_2 and CO, a consumption factor is defined for O_2, and the consolidated results are presented in *Figure 5.17*. In calculating the consumption factor, data from experiments that showed boilover were ignored since they do not represent stable burning conditions.

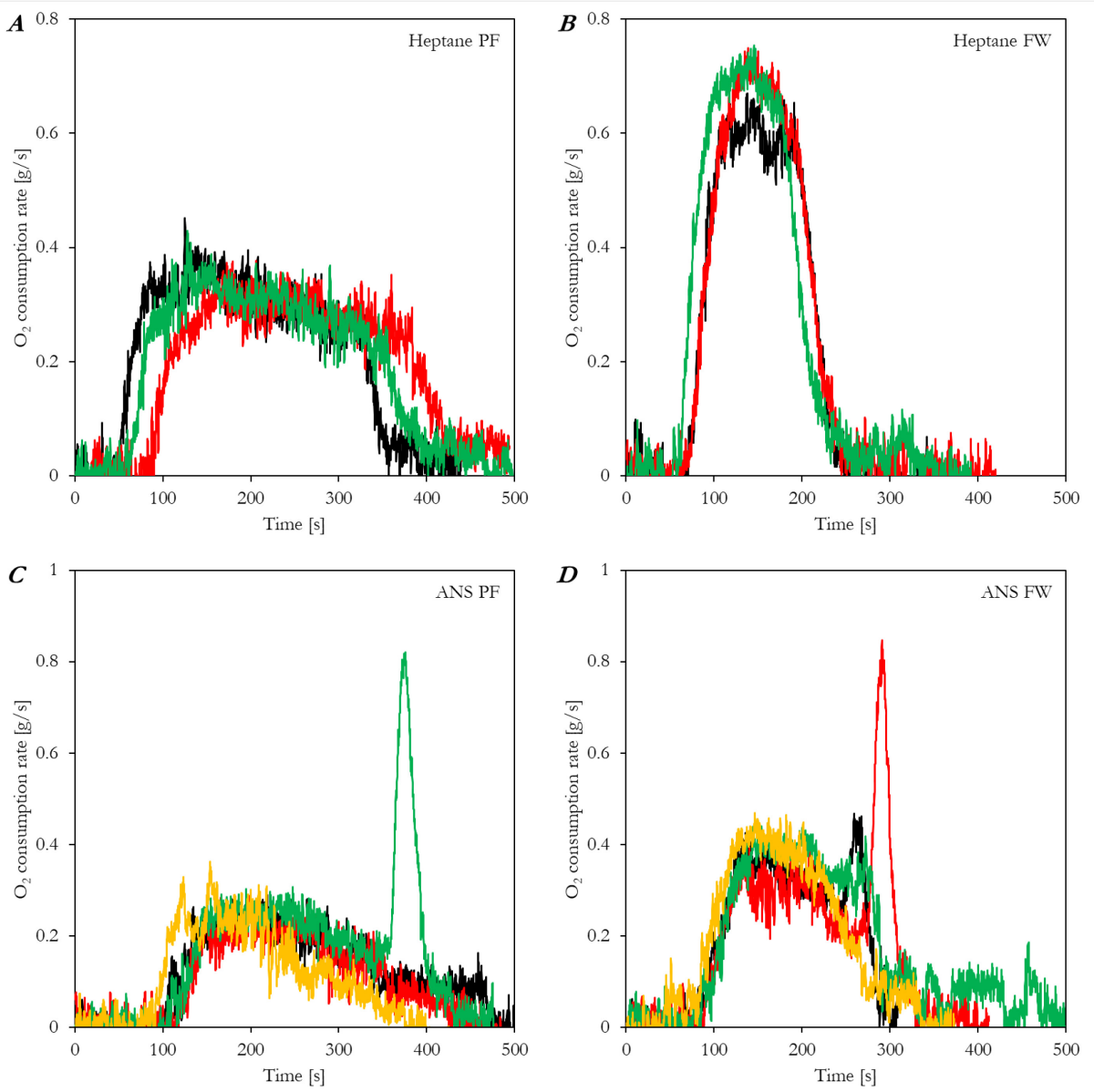

Figure 5.16. Comparison of O2 consumption rates for both flame regimes and fuels.

In *Figure 5.17*, similar to the emission factors of CO_2, the difference between heptane pool fires and fire whirls is not significant. However, a slightly higher consumption of O_2 is observed in the case of ANS fire whirls as compared to ANS pool fires.

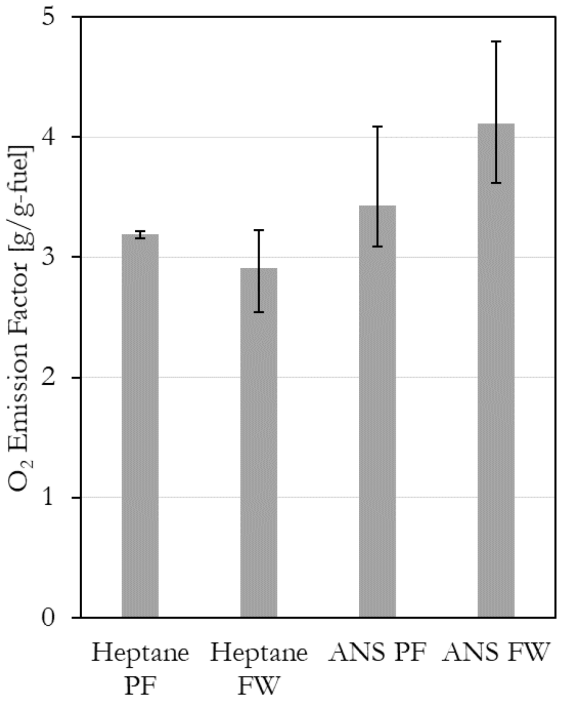

Figure 5.17. Comparison of O_2 consumption factors for both flame regimes and fuels.

5.2.2. Fuel Consumption Efficacy

For experiments with ANS crude, the residue on the water surface after extinction was collected using 3M adsorbent pads (3M™ Petroleum Sorbent Static Resistant Pad HP-556). Pads from every experiment were dried in an oven at 70 °C for 24 hours to remove any water content in the pads both prior to testing and after collection of the residual fuel. Because most volatiles were expected to burn off during the combustion process before drying, there should be little components of the crude oil other than water lost during the drying process. The pads were then weighed on a precision load cell to determine the residual weight. These measurements were performed for both pool fires and fire whirls. The results are shown in *Figure 5.18*.

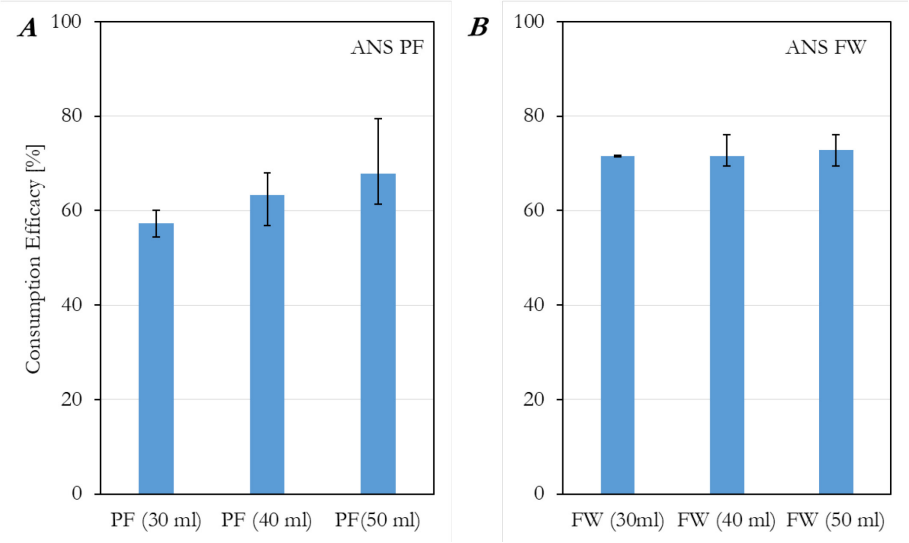

Figure 5.18. Comparison of consumption efficacies ANS pool fires and fire whirls, formed using different initial fuel slick thicknesses. With increasing initial slick thickness, overall fuel consumption is enhanced slightly for the pool fire regime at this scale. Significant variation was not found with the fire whirl regime at this scale.

For residual weight loss experiments, three different fuel quantities were tested in the same size (11 cm diameter) dish to determine the effect of the fuel slick thickness on this quantity. 30, 40 and 50 ml of ANS crude were used in these experiments, with the lower bound set by the limiting condition required for sustained combustion at this scale. The residual weight increased for all cases with increasing fuel quantity. As expected, the residual weight was higher for pool fires for all initial fuel quantities, resulting in lower consumption efficacies. However, the difference between the residual weight for pool fires and fire whirls seemed to converge with increasing fuel quantity. This corresponds directly with initial fuel depth, which was 3.2, 4.3 and 5.4 mm for the 30, 40 and 50 ml of initial fuel deposited, respectively. In medium-scale tests with larger fuel quantities, residual weight is measured using mass-loss data rather than physical measurements using adsorbent pads as the sensitivity of measurements is higher when boil over is avoided. This method is simpler and potentially more accurate, but it had to be verified at this scale first.

5.2.3. Liquid-Phase Temperature and Boilover

In previous experiments with ANS crude, boilover was observed towards the end of the burn and resulted in skewed mass loss results as some fuel spilled onto the test apparatus. This effect was compounded if fresh (thus, cold) water was not used for each test. To avoid this, a magnetic stirrer was introduced to the bottom of the fuel dish to mix the bottom water layer during the experiment and prevent boiling at the interface of the water and crude oil. Fresh water was also used for every experiment to ensure similar initial conditions (i.e. water sublayer temperature) every time. Experiments were run with the stirrer at different speeds, with the lowest speed that prevented the oil from boiling over being used for all experiments. This minimized vibrations on load cell data that could be introduced from the stirrer when run at higher rotation speeds.

To measure the temperature variation over time ***without the stirrer***, an array of 4 thermocouples were positioned as shown in *Figure 5.19*. One thermocouple was placed immediately above the fuel layer in the flame, one was positioned right at the water-crude oil interface, and two were more positioned below in the water. The results of the temperature measurement are shown in *Figure 5.20*. The flame temperature is consistently beyond 750 K. Data from thermocouples in the liquid phase (without TC 1) is shown on the right-hand side of *Figure 5.20*. A clear increase in temperature of around 70 K, to the boiling temperature of water, can be seen at the interface. This indicates that the very top layer of water increases to a boiling temperature while the water in the lower layers in the dish remains close to the initial temperature condition. A strong temperature fluctuation is also seen at the interface towards the end of the experiment, which is when boilover occurred. Towards the end of the experiment, a temperature gradient in the water layer is observable with an increasing TC 3 temperature, which is 1 cm below the water-crude oil interface. This was an indication of effective mixing within the water layer, which delayed boilover.

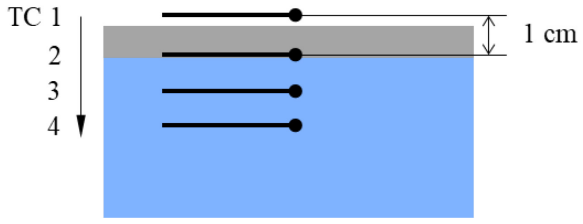

Figure 5.19. Thermocouple positioning for experiments without the stirrer.

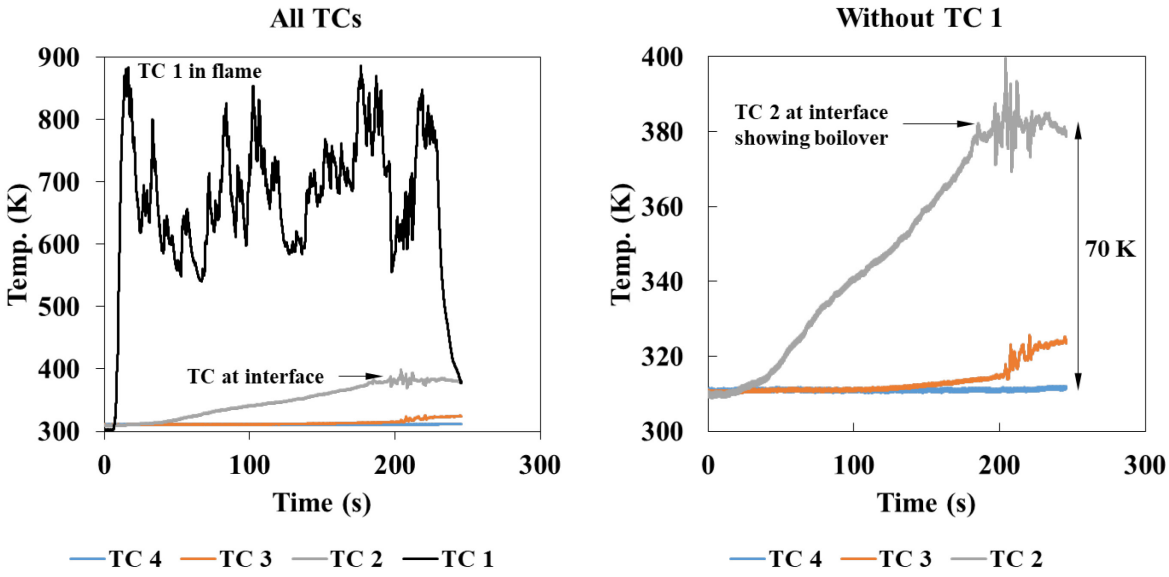

Figure 5.20. Variation of temperature at water-crude oil interface and bulk water for experiments without the stirrer. Results from one experiment are shown here, and results from similar experiments showed little variation.

To understand the effectiveness of the stirrer in preventing boilover, a similar array of thermocouples was used ***with the stirrer*** operating during the experiment. For experiments with the stirrer, 4 thermocouples – 3 within the water and 1 in the fuel layer were positioned as shown in *Figure 5.21*, and the temperature variation with time is shown in *Figure 5.22*.

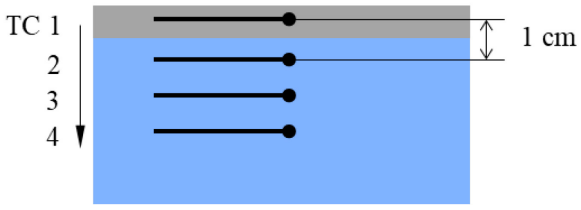

Figure 5.21: Thermocouple positioning for experiments with the stirrer.

Upon ignition, the temperature of the fuel layer rose beyond 340 K due to the evaporating fuel. In the figure on the right, TC1 is not shown for better clarity of the water temperature. The water temperature, essentially a bulk temperature introduced because of the stirrer, increased to a maximum of 315 K, which is a rise of about 15 K. This temperature was therefore too low for boilover and showed that the stirrer was effective in ensuring a low temperature at the water-crude oil interface. The small increase in temperature introduced by the mixing (15 K) is unlikely to affect the burning rate or other results. This stirrer technique is much simpler than the use of a recirculating bath and is also effective at the medium scale.

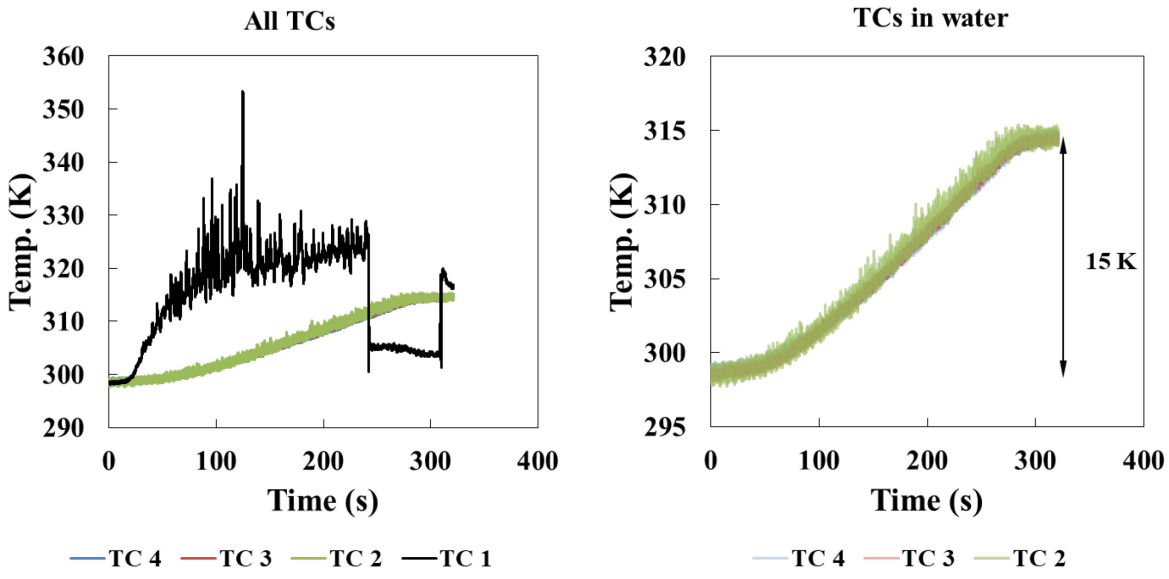

Figure 5.22. Variation of fuel layer (TC1) temperature and bulk water temperature with stirrer.

Using the rise in water bulk temperature over the course of the experiment involving each flame regime and fuel type, and the mass of water used in each experiment, an average heat flux feedback was calculated. The total heat transfer was measured as $Q = mC_{p,water}\Delta T$, where m is the mass of water in the dish, $C_{p,water}$ is the heat capacity of water, and ΔT is the rise in temperature of the water sublayer. This was then divided by the burn time and fuel pool area to determine an average heat flux feedback in both time and area of the fuel pool for each case. The results are shown in *Figure 5.23*.

The heat flux feedback from heptane fires are lower than ANS in both pool fire and fire whirl regimes. This could potentially be attributed to the higher concentration of soot formed in ANS fires, which contribute to higher incandescence and higher radiative feedback to the fuel pool. Flame geometry considerations, arising from different boiling points for these fuels, may also need to be accounted for when attempting to explain this difference. Nevertheless, the average heat feedback of fire whirls are generally higher than the pool fire scenario for both fuels, which indicates the higher burning rate of fire whirls. Heat feedback from heptane in pool fire configuration was 9 kW/m^2 while heptane fire whirl averaged around 11 kW/m^2. Similarly for ANS crude oil, average pool fire heat feedback is about 12 kW/m^2, which increases to 13 kW/m^2 for the fire whirl regime. This value is, of course, spatially averaged and may be greater at the center of the pool or during peak burning rates, which is not captured in this time and space average.

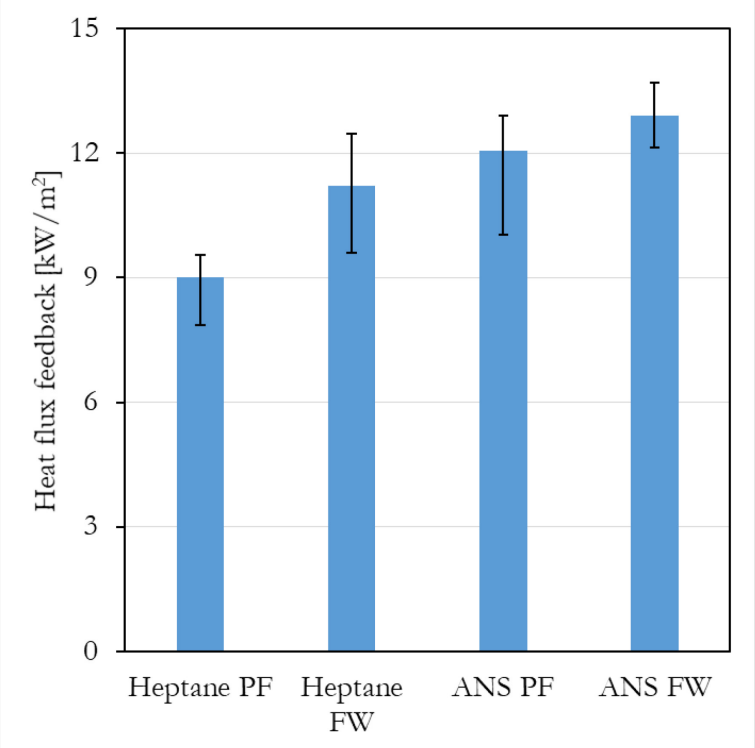

Figure 5.23: Average heat feedback from the flames to the fuel layer, shown for both pool fire and fire whirl regimes formed using heptane and ANS crude oil.

Another consideration in explaining the higher heat feedback in case of fire whirls is the flame temperature. In *Figure 5.24*, measurements of flame temperature at different heights (*H*) above the

fuel layer. In general, it can be seen that for the pool fire cases, the highest temperatures are seen closest to the fuel layer, and the temperature reduces continuously with height. In contrast, the high temperature region in fire whirls is longer, caused by the elongated shape of the fire whirl. The temperature distribution in the vertical direction is more stratified in the case of the pool fire, and the generally higher temperatures can contribute to a higher radiative heat feedback to the fuel layer in the case of the fire whirl regime.

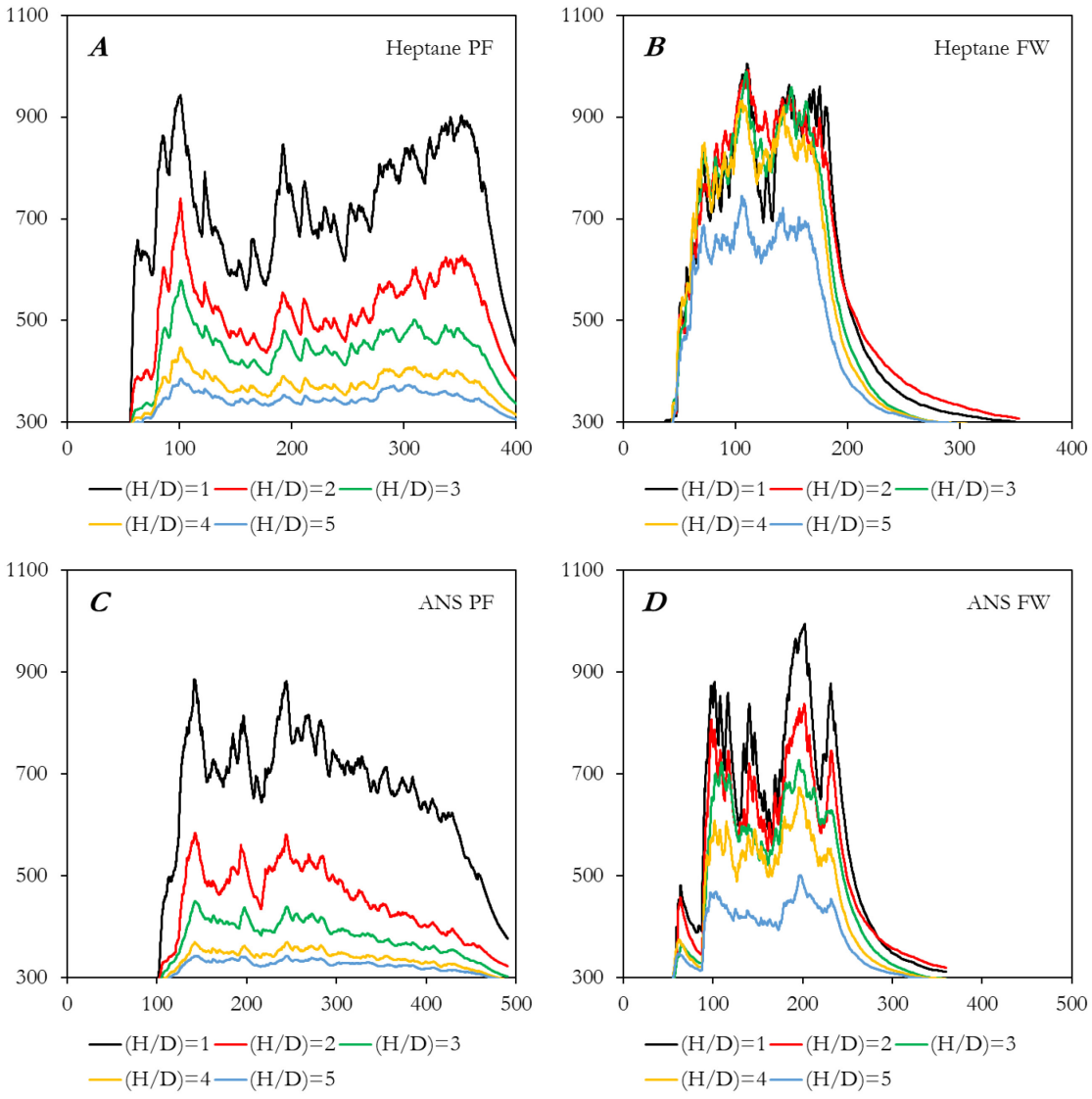

Figure 5.24: Flame temperatures at different heights (H) above the fuel layer, obtained for pool fires and fire whirls formed using heptane and ANS crude oil at the small scale (D = 11 cm). Here, data from a single experiment is shown so that the data is not smeared by averaging. However, trends were very similar in other repetitions of the experiment.

5.2.4. Inlet Velocity

In literature, the configuration used here for forming fire whirls is termed as a fixed-frame, self-entraining fire whirl apparatus. In this configuration, entrainment into the enclosure is controlled by the buoyancy generated within the enclosure and the gap size at the inlets to the enclosure. The velocity of this air entrainment is useful to help characterize the conditions under which fire whirls will form and can be related to formation under a variety of different configurations and conditions. More details may be found in [19].

For the fire whirls in this study, a constant gap size of 15 cm was used, and the inlet velocity variation with height is shown in *Figure 5.25*. These values are averaged over time and between several repetitions, with the standard deviation between measurements shown as error bars in the figure. The inlet velocity for heptane fire whirls were higher than those of ANS crude and may be attributed to the higher mass loss rate (and consequently higher HRR) and higher buoyancy within the enclosure during the heptane tests. The inlet velocity decreased slightly with height but was expected to be relatively constant beyond a height of 10 cm, based on previous work on fire whirls [25]. This data is used to estimate the circulation entering the enclosure in *Figure 5.25–B*. This will be compared with the results from other scales later.

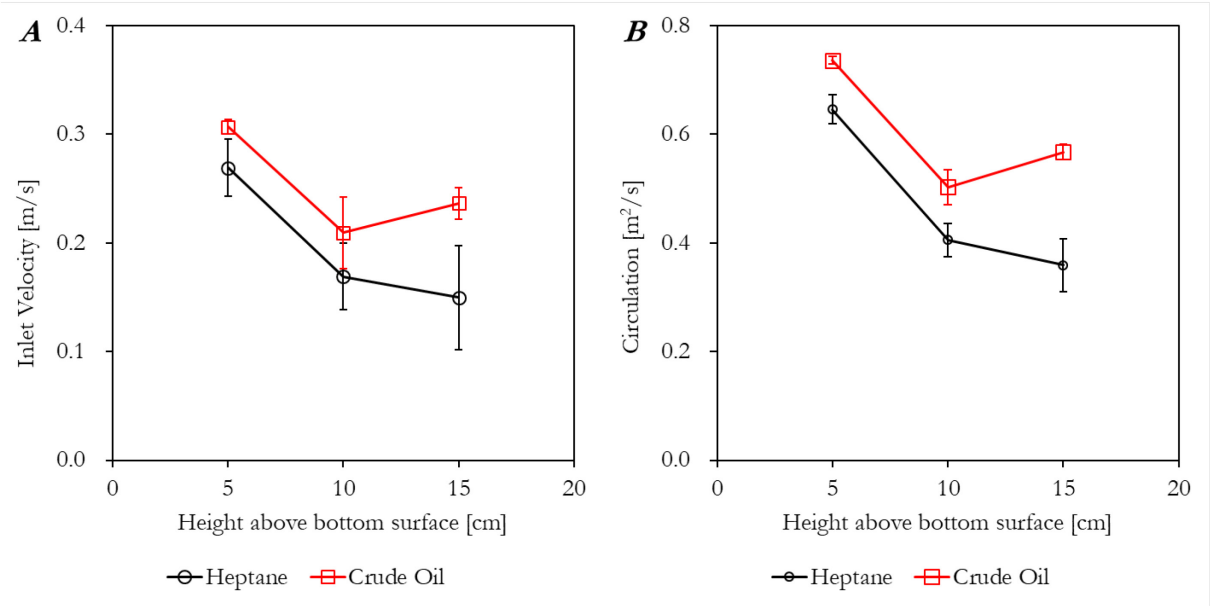

Figure 5.25: (A) Variation of inlet velocity with height for fire whirls formed using heptane and ANS crude. (B) Corresponding values of circulation calculated using the enclosure side as the length scale.

5.3. Discussion of Small-Scale Results

The small-scale experiments were conducted in an 11 cm diameter fuel pan, burning heptane and ANS crude oil, with two flame configurations (pool fire and fire whirl). Measurements of mass loss, PM and gas emission (CO and CO_2), liquid-phase temperature, and inlet air velocity through the gaps were recorded for the analysis. The results of the experiments at this scale indicate the potential for fire whirls to reduce the hazardous emission by fires.

Mass-loss analysis showed the heptane burning rate was higher than ANS crude oil, which is due to the higher volatility of heptane. In addition, both fuels showed improvement in burning rate when the fire whirl configuration was used. In the small-scale tests conducted, the ANS crude oil did not burn more that 42% of its initial volume, owing to its heavier hydrocarbon components; however, when fire whirl configuration was used, it burned about 51% of the initial fuel mass. Comparing PM emission factors, it can be seen that PM measurements also showed improvement in the fire whirl burning configuration. Due to the small size of the fire at this scale the fires were relatively well mixed and burning clean as the CO production rates were very small. Higher heat fluxes and flame temperatures help to explain the increase in burning rate achieved with fire whirls.

6. Medium-Scale Experiments (Phase II)

The medium-scale experiments were conducted at the University of Maryland and lasted between months 9 and 18. The fire whirl apparatus used for the medium-scale tests used a fixed-frame four-wall configuration. Experiments were conducted by burning ANS crude oil and heptane in both pool fire and fire whirl regimes. A new gas analyzer (Cal Instruments) was purchased and used in the medium-scale experiments due to breakage of the previous ULTRAMAT 23 gas analyzer used in small-scale experiments. The results of the medium-scale tests are reported in this section.

6.1. Medium-Scale Apparatus

The fire whirl apparatus used for the medium-scale tests used a similar configuration as explained in the small-scale experimental setup section. The fuel pool diameter and enclosure size were increased proportionally to account for the larger heat-release. For example, the ratio of the inlet gap width to the enclosure length was kept as ¼, similar to the small-scale experiments. For all experiments, the enclosure length was 100 cm, with a constant gap size of 25 cm. In the medium-scale setup, the walls were 120 cm by 120 cm made of an Aluminum/LDPE sandwich. One wall was made of a transparent polycarbonate sheet for capturing images and observational purposes. The enclosure floor area was 100 cm x 100 cm. Two different pan diameters (20 cm and 30 cm) were used for the medium-scale experiments. *Figure 6.1* shows the experimental setup with important dimensions labeled.

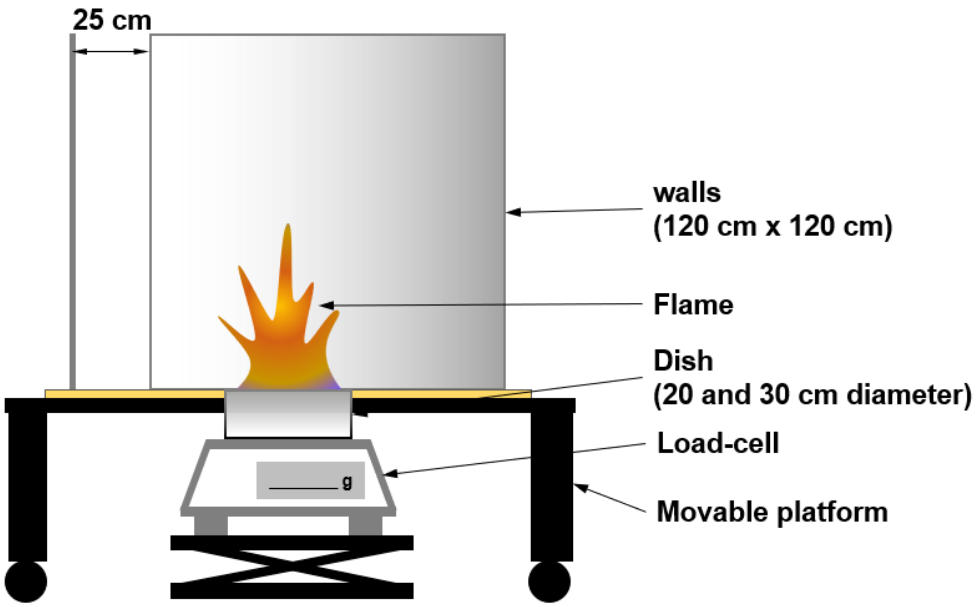

Figure 6.1: Schematic of fire whirl apparatus, used for experiments at the medium scale.

The apparatus is similar in construction to the small-scale setup, with the floor enclosure constructed out of ceramic insulation boards. Steel panels were laid on insulation board to form the top surface and ensure improved operability and ease of access. The fuel pans were held at the bottom on a platform jack, on which a load cell was positioned to obtain mass loss data. Fire whirls formed within the enclosure are shown in *Figure 6.2*.

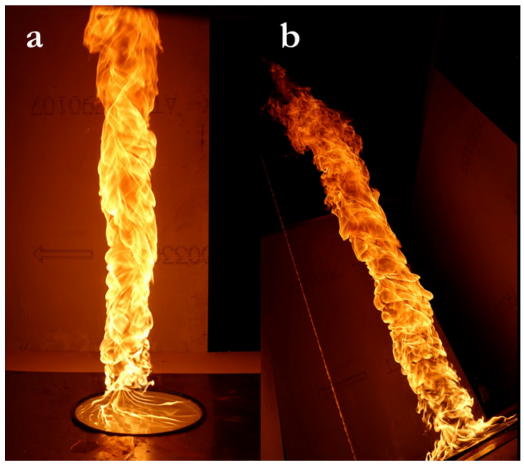

Figure 6.2: Images of fire whirls formed with the 30 cm pan, using heptane, Note the camera is tilted to depict the fire whirl shown in (b).

Both heptane and ANS crude oil (initial slick thickness of ~5 mm) were used in the experiments of both flame regimes. Temperature at the center of the pool was also measured with an array of thermocouples. Two vane anemometers (Testo 405*i*) were positioned at one inlet, with one at 25 cm above the enclosure surface, and the other 50 cm above the enclosure surface. A magnetic stirrer was placed below the fuel pan to mix the water sublayer. This was done to ensure the boilover was prevented for the duration of the experiment.

6.2. Medium-Scale Results

6.2.1. Mass Loss and Fuel Consumption

Mass loss trends of the fuels for the medium-scale experiments are reported in this section. First, the mass loss results of the heptane in fire whirl and pool fire flame regimes are reported, followed by those of ANS crude oil. Experiments for each case were repeated for a minimum of three times to ensure repeatability of the experiments. The average presented herein are derived from three repetitions for each case.

Figure 6.3 shows the individual mass loss trends for heptane burned in the 20 cm and 30 cm diameter pan, in both pool fire and fire whirl regimes. *Figure 6.3–A and B* show results for the 20 cm scale. As can be seen, the pool fire lasts for a longer duration and burns at a slower rate when compared to the fire whirl, while consuming the quantity of fuel (~110 g of heptane). The fire whirl was approximately three times faster in removing the fuel from water. *Figure 6.3–C and D* show results for the 30 cm scale. Again, the fire whirl burns at a higher rate, consuming about ~240 g of fuel in about 150 s.

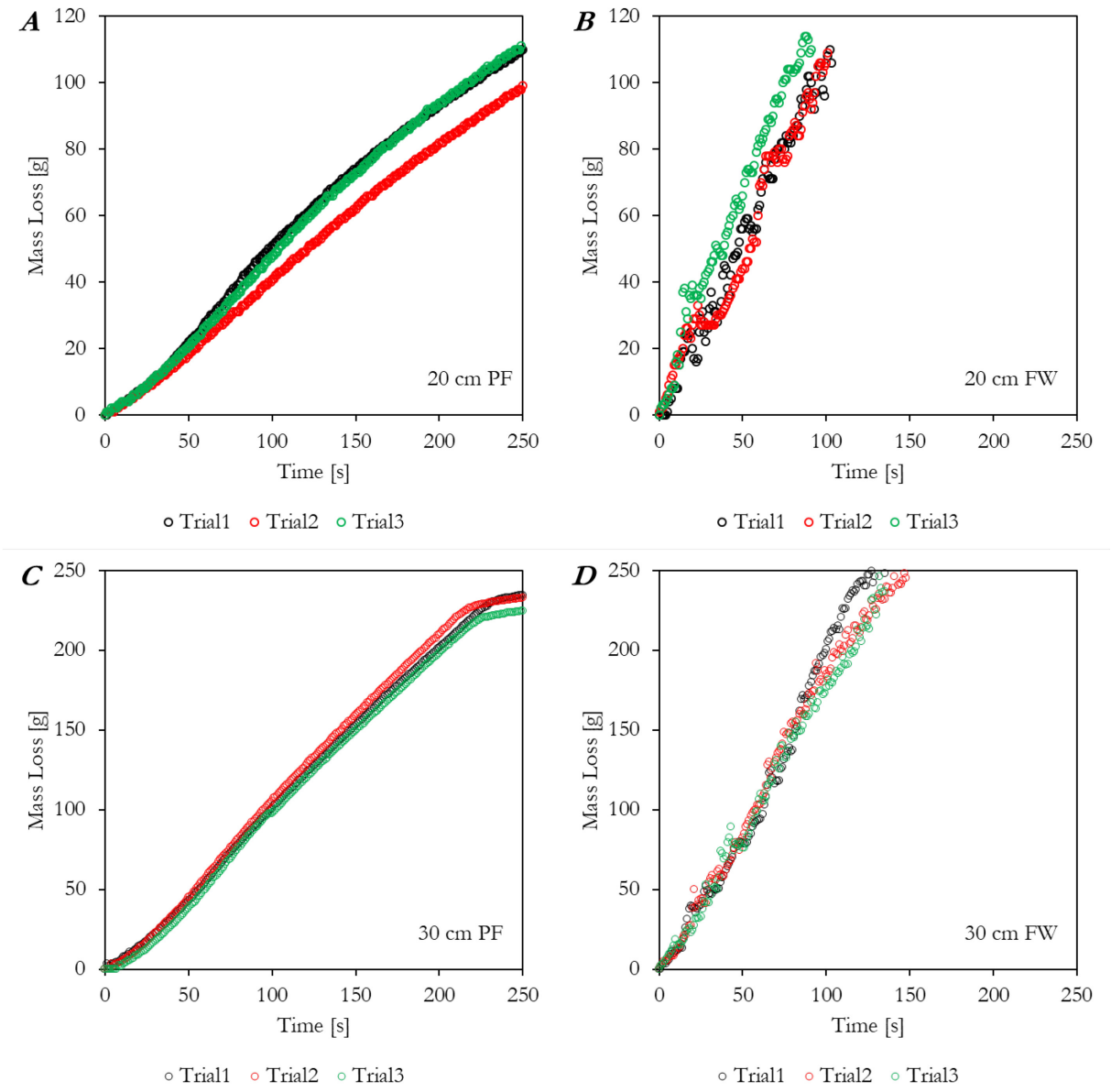

Figure 6.3: Mass loss behavior of heptane fires for both 20 and 30 cm scales. (A) 20 cm PF, (B) 20 cm FW, (C) 30 cm PF, and (D) 30 cm FW.

The mass loss of the Heptane tests were averaged, and a linear fit for each case to obtain an average burning rate the slope of the fitted lines. A comparison of all heptane fires is shown in *Figure 6.4*. As expected, the 30 cm fire whirl case had the highest average mass loss rate equal to 1.8 g/s, while the 20 cm pool fire was the slowest, at about 0.45 g/s.

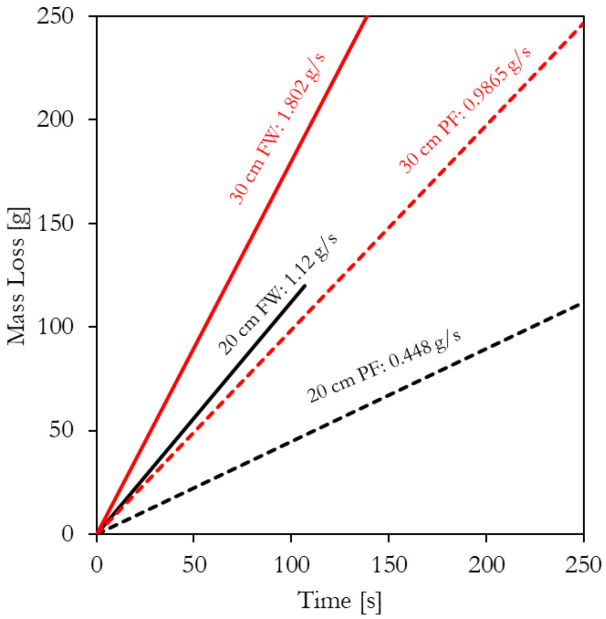

Figure 6.4: Comparison of average mass loss rates for heptane fires (20 and 30 cm).

Figure 6.5 shows the individual mass loss trends and their averages for ANS crude oil fire whirl and pool fire tests in 20 cm and 30 cm fuel pools. Crude oil, with an initial thickness of 5 mm was burned over water with some leftover remaining as residue. The burning behavior shows a similar trend to heptane tests, with roughly linear mass loss behavior. Mass-loss rates are higher in the fire whirl regime for both scales, and consequently the duration of burning is shorter. The steep jump in the mass-loss rate observed in the 30 cm pan is due to boilover towards the very end of the experiment. As evident, boilover can be influential in increasing the overall burning rate as flame volume is increased when fuel droplets are ejected into the flame. This also causes an abrupt extinction of the fire when a large amount of oil is ejected out of the fuel pool. Boilover behavior is complex and deserves further study on its effectiveness in improving the burning rate, implications on emissions, and a sometimes-observed behavior where boilover causes an abrupt extinction.

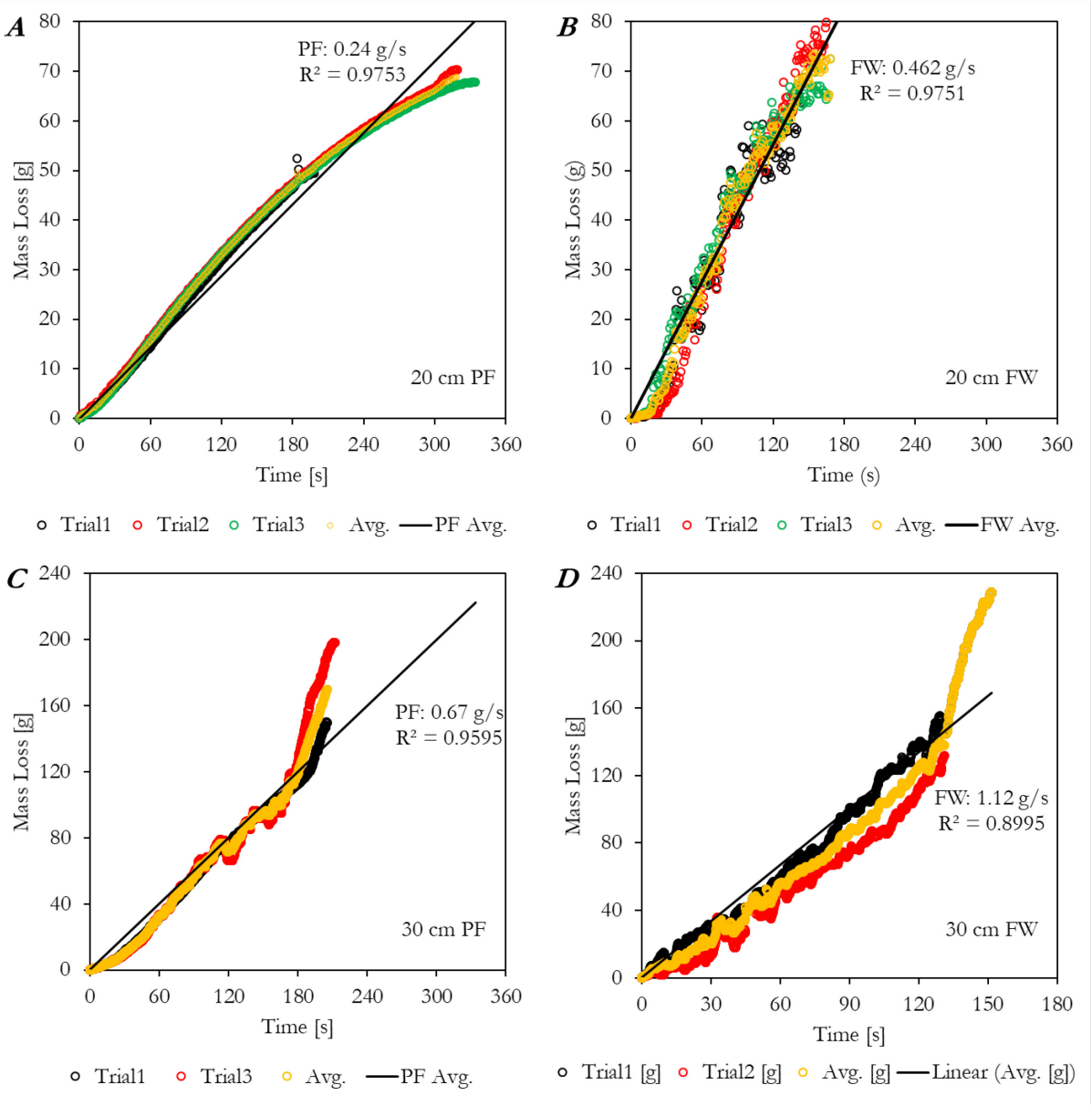

Figure 6.5: Mass loss behavior of ANS fires for both 20 and 30 cm scales. (A) 20 cm PF, (B) 20 cm FW, (C) 30 cm PF, and (D) 30 cm FW.

A linear trend is fitted to each data set to obtain the average mass loss rate using the slope of the line. Average mass loss rates of ANS fires are shown in *Figure 6.6*. The average mass loss rate of pool fires increased from 0.45 g/s in the 20 cm pan to 0.67 g/s in the 30 cm pan. No significant difference between 20 and 30 cm scales is observed in terms of the mass loss rate.

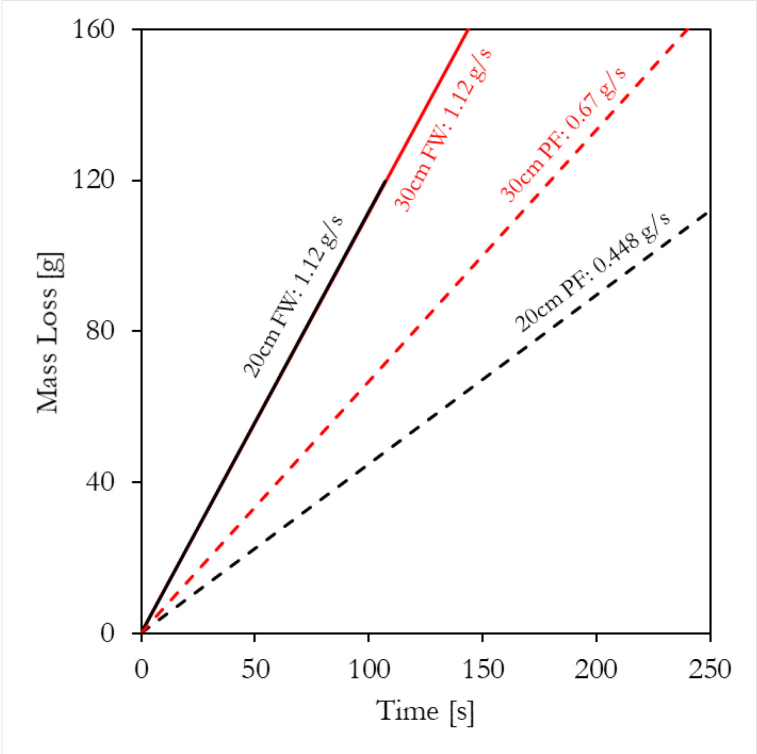

Figure 6.6: Comparison of average mass loss rates for ANS fires (20 and 30 cm).

The pool fire and fire whirl consumed different amount of ANS crude oil in both diameter pans. *Figure 6.7* shows the removal percentage in terms of the total initial crude oil mass for the two flame regimes. In general, the consumption efficacy of the fire whirls was higher, meaning a lower residual mass was left after flame extinction. The fire whirl in the 30 cm pool removed the most oil, amounting to about 70%, while the corresponding pool fire removed less than 60%. The 20 cm pool fire removed about 50% of the oil, and the corresponding fire whirl removed about 55% of the oil.

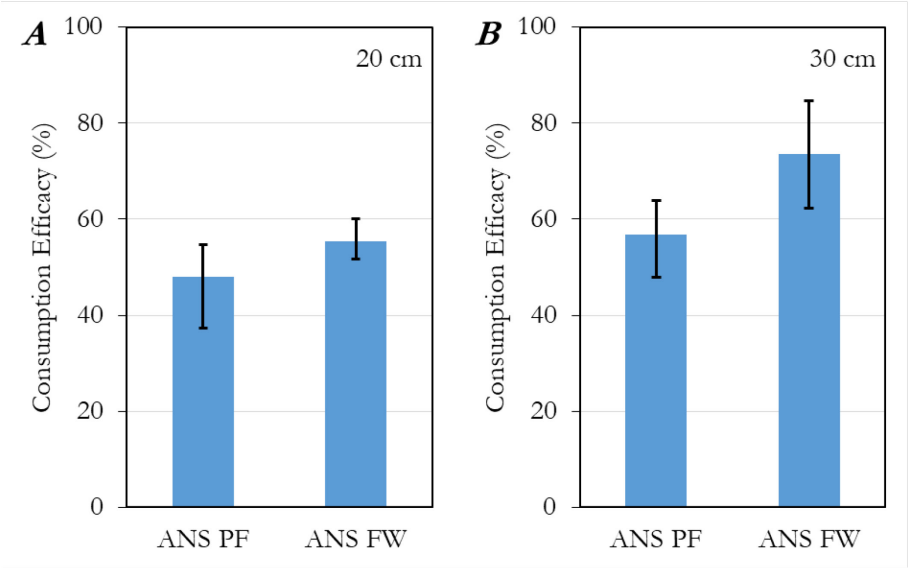

Figure 6.7: Comparison of fire whirl and pool fire consumption efficacies for ANS crude oil at the 20 cm and 30 cm scales.

6.2.2. Particulate Emissions

Particulate matter emissions over time were captured for medium-scale fire whirls and pool fires using both Heptane and ANS crude oil. The results of PM emission for the tests conducted in the 20 cm pan for both heptane and ANS crude oil are presented in *Figure 6.8*. The colored curves each represent different repetitions of each case, and the emission rate of Total PM is presented in units of mg/s. For both fuels, the fire whirl emits lower PM amounts, and does so in a shorter period of time, which ultimately results in smaller accumulative TPM emission as the area under the curve is smaller. In case of the heptane fires, changing the regime from a pool fire to fire whirl reduces emissions significantly as the peak TPM emission rate is reduced from around 15 mg/s in the pool fire case to about 8 mg/s for a fire whirl. The ANS peak TPM emission rate did not vary with a change in the flame regime to a fire whirl, although the duration was much shorter and thereby the total TPM emission factor was ultimately much lower, as shown later in this section (*Figure 6.10*).

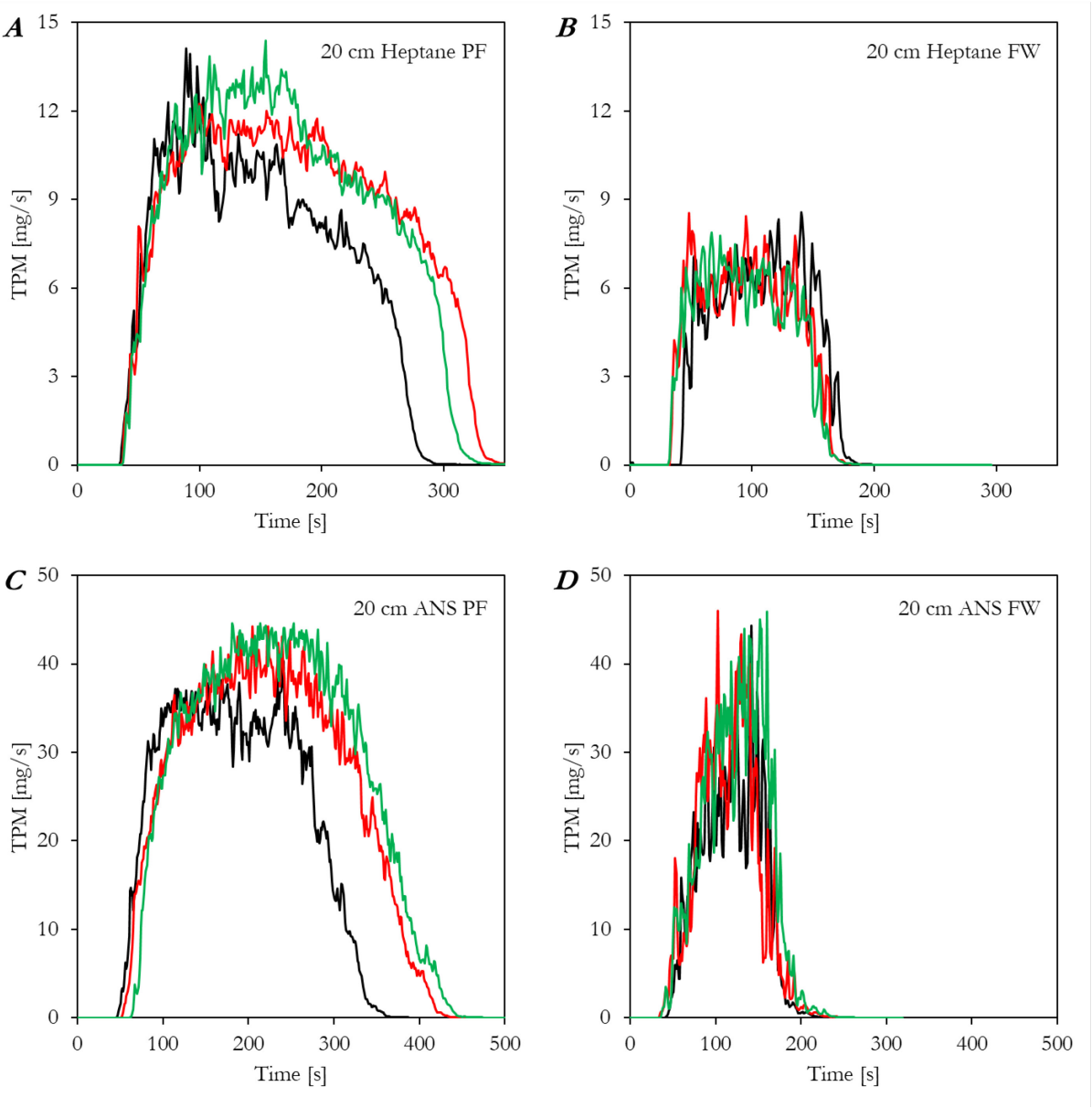

Figure 6.8: Comparison of TPM emission rate from 20 cm pool fires and fire whirls, for both Heptane (A and B) and ANS crude oil (C and D). Note the three lines represent three repetitions for each case.

The results of PM emissions measurements for the tests conducted in the 30 cm pan are presented in *Figure 6.9*. As can be seen, for both fuels the fire whirl produced lower PM emissions with a shorter burning duration, which ultimately results in smaller cumulative TPM emission as the area under the curve is smaller. In particular, the ANS fire whirl burned with significantly

lower PM emissions compared to the pool fire. In the case of ANS fires at 30 cm, using a fire whirl configuration instead of a pool fire significantly reduces the peak TPM emission rate from around 100 mg/s to about 50 mg/s. The peak TPM emission rate did not vary much between the heptane fires, though the emission duration was much lower in case of the fire. Thus, the total TPM emission factor is ultimately much lower for the fire whirl, shown in *Figure 6.11*.

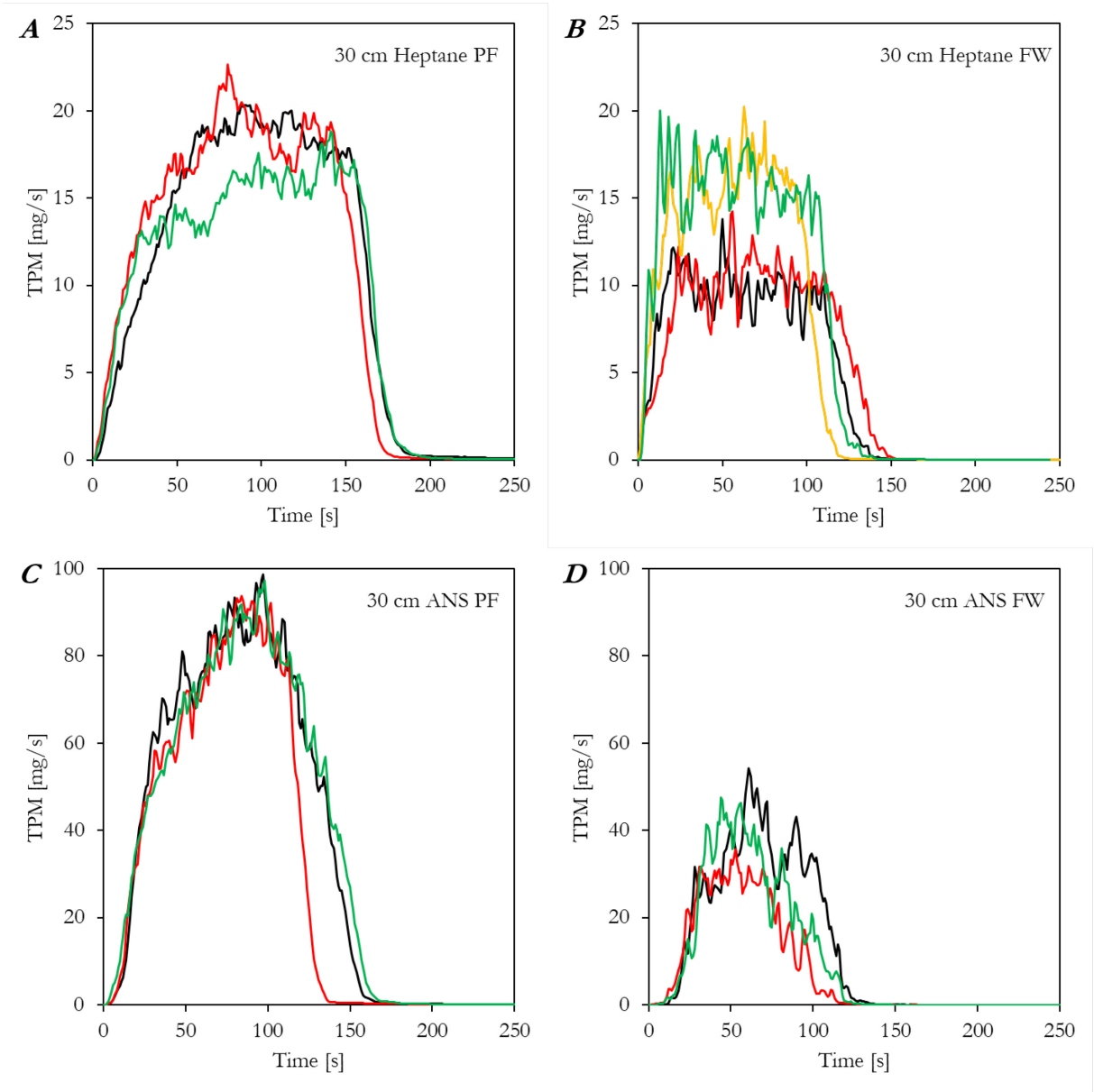

Figure 6.9: Comparison of TPM emission rates of 30 cm pools fires and fire whirls, for both heptane (A and B) and ANS crude oil (C and D).

Emission factors of PM represent the total PM emission normalized based on the consumed amount of oil (g-PM per kg-fuel-consumed). *Figure 6.10* compares the emission factors obtained from experiments with the 20 cm fuel pool. For heptane, the EF dropped from 23 g/kg for the pool fire to about 8 g/kg for the fire whirl. The EF for ANS tests in the 20 cm pan also showed the same trend, decreasing from about 140 g/kg for the pool fire to around 40 g/kg for the fire whirl. This reduction is significant and could potentially decline further with scale.

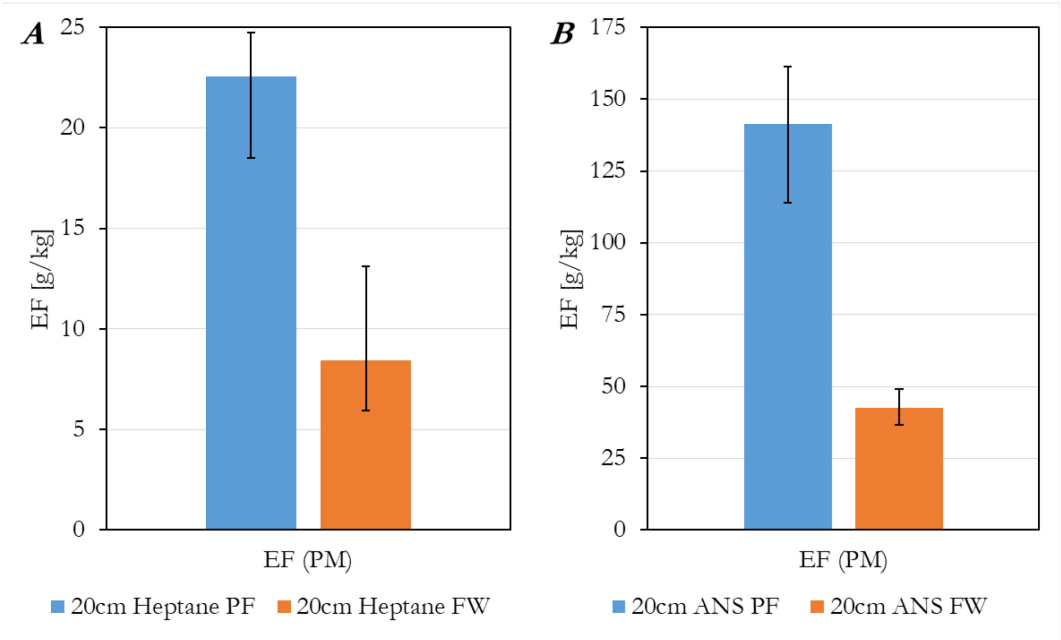

Figure 6.10: Comparison of particulate matter EF for 20 cm heptane and ANS fires.

Figure 6.11 compares the emission factors obtained from experiments with the 30 cm fuel pool. The heptane pool fire at 30 cm is slightly cleaner compared to the 20 cm in terms of soot production. Nevertheless, the fire whirl's EF at a 30 cm pan size declined from 9 g/kg to about 3 g/kg. The EF for ANS tests in the 30 cm pan also showed the same behavior decreasing from 38 g/kg to around 14 g/kg.

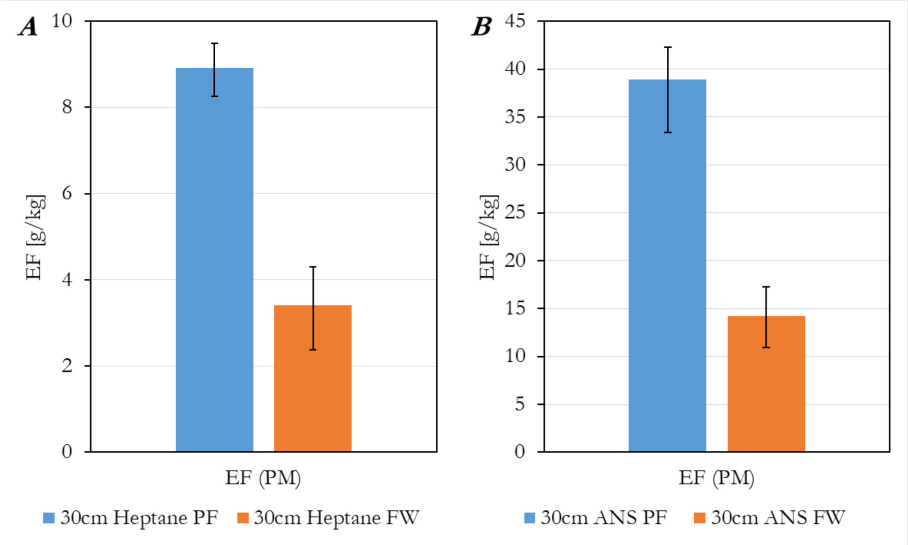

Figure 6.11. Comparison particulate matter EF for 30 cm heptane and ANS fires.

6.2.3. Gas Emissions

Gas emissions from medium-scale experiments were measured using a gas analyzer manufactured by Cal Instruments (ZPA ND-IR with O2 Analyzer) that measured CO, CO_2, and O_2. The details of the analyzer and calibration were presented in *Section 4* of this report. The results of O_2 measurements in terms of consumption factor for the tests with heptane and ANS crude oil in both flame regimes are presented in *Table 6.1*. Similar to the definition of an emission factor, a consumption factor is a normalized value obtained by dividing the total amount of consumed oxygen (kg) by the total mass of fuel that was burnt (kg). The general trend observed in the values are an increase in consumption factor when the flame regime is changed to a fire whirl. This increase occurs for both fuels and at both fuel pan diameters. The reason for this increased consumption is related to the unique flame geometry, providing a larger surface area for combustion to occur, and the dynamics of swirl that provide improved entrainment of air to the flame, leading to better mixing and combustion. The mixing and combustion efficiency are expected to continue to improve as turbulence increases with scale. This in turn reduces the production rate of CO and soot in the combustion process.

Table 6.1: Consumption factor of O_2 for medium-scale experiments in 20 and 30 cm. All reported numbers are in units of kg/kg-of fuel.

	Heptane		ANS crude oil	
Diameter	PF	FW	PF	FW
20 cm	8.21	13.2	12.4	12.5
30 cm	9.67	10.0	8.33	11.0

Figure 6.12 shows the CO_2 emission production rate (in units of g/s) of the experiments with heptane for both the 20 and 30 cm fuel pans. Data for a minimum of three tests are shown for both configurations. The fire whirl in a 20 cm fuel pool doubles its peak production rate (an increase from 1.5 g/s to about 3 g/s). The increase also occurs for the 30 cm pool, although the increase is less pronounced. In general, a higher instantaneous production rate of CO_2 is observed for fire whirls, which is mainly because of their higher mass-loss rate in the fire whirl configuration.

Figure 6.13 shows the CO_2 emission production rate of the experiments with ANS crude oil for both the 20 and 30 cm fuel pans. Data from a minimum of three tests, each without a boilover event, are shown for both configurations. ANS fire whirls show higher emissions of carbon dioxide, which is mainly due to their higher mass-loss rate. In particular, ANS fire whirls at the 20 cm pan diameter peaks at approximately 1.8 g/s while the peak for a similar size pool fire is near 1 g/s. Also, the burning duration is half that of the pool fire. Therefore, the total carbon dioxide produced (the area under the curves) should be close for the two burning regimes, with minor differences stemming from the different amounts of fuel consumed in each regime. On the other hand, the 30 cm ANS experiments show similar trends between the pool fire and fire whirl configuration.

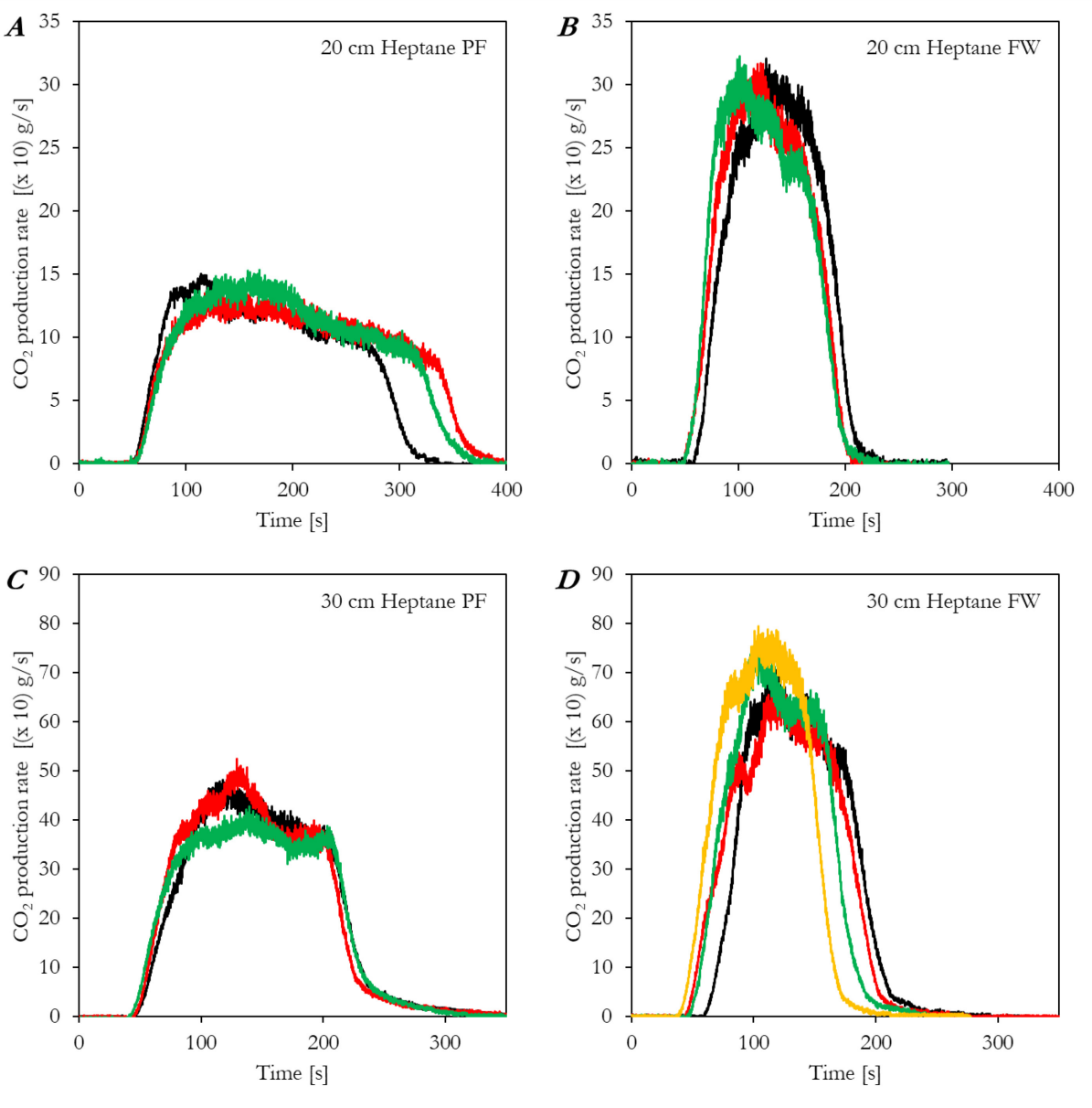

Figure 6.12: Comparison of CO_2 production rates from heptane fires, for 20 and 30 cm fuel pools.

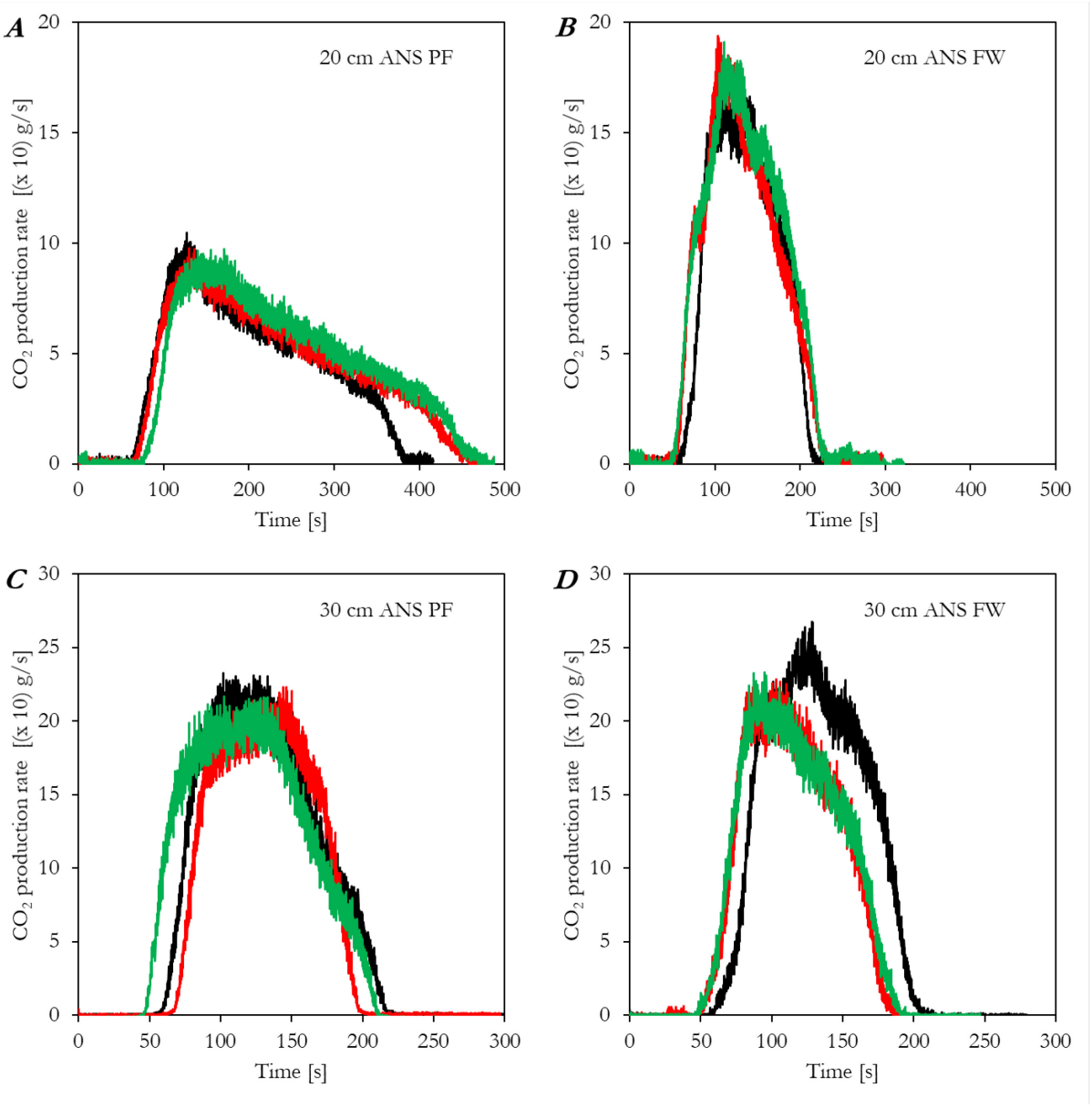

Figure 6.13: Comparison of CO_2 production rates from ANS fires, for 20 and 30 cm fuel pools.

The peak CO_2 concentration for fire whirls were higher than that of pool fires, which is a consequence of the higher burning rate. CO_2 concentrations therefore represented the burning rates and closely follow what was captured in the mass loss measurements. The CO_2 emission factors for fuel burning in the 20 cm pan are shown in *Figure 6.14* and a comparison is made between the

two burning configurations (pool fire vs. fire whirl). The CO_2 emission factors obtained from heptane and ANS crude oil in both flame regimes are quite similar.

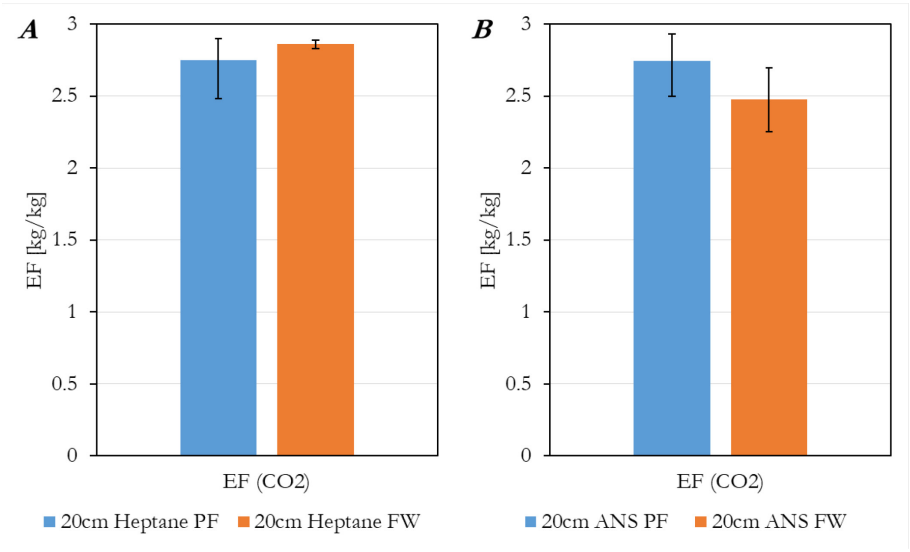

Figure 6.14: Comparison of CO_2 emission factors for Heptane (A) and ANS crude oil (B) burning in both pool fire and fire whirl configurations in the 20 cm pan.

The CO_2 emission factors for both fuels burning in the 30 cm pan are shown in *Figure 6.15* and a comparison is made between the two burning configurations (pool fire vs. fire whirl). CO_2 emission factors obtained for heptane and ANS crude oil in both flame regimes are relatively close and the differences observed are within the margin of the error of the calculations. At this scale, in the case of CO_2, while the instantaneous production rate of CO_2 is higher for fire whirls, the total amount of CO_2 formed cumulatively over the course of the experiment is similar for both flame regimes. The variability is minimal, as evident from the small spread of data in *Figure 6.13*.

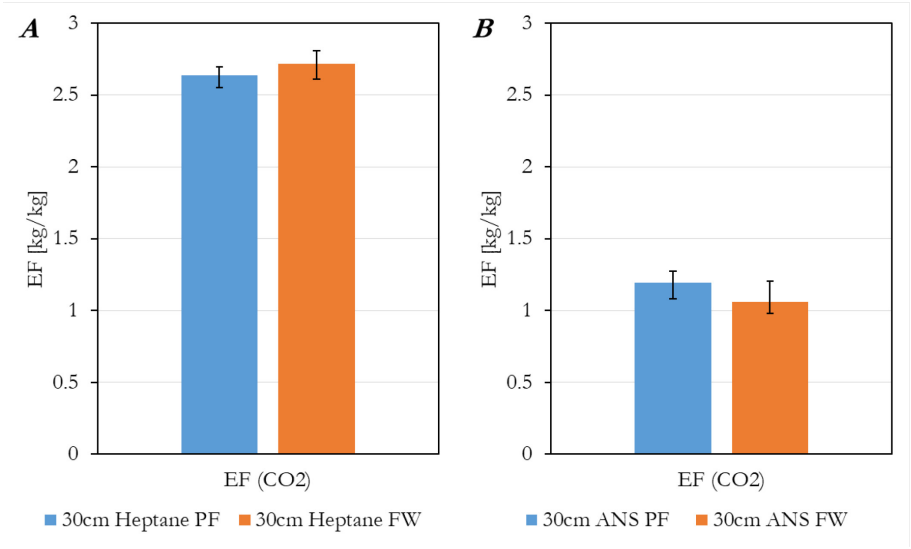

Figure 6.15: Comparison of CO_2 emission factors for Heptane (A) and ANS crude oil (B) burning in both pool fire and fire whirl configurations in the 30 cm pan.

Figure 6.16 shows the CO emission production rate (in units of g/s) of the experiments with heptane for both the 20 and 30 cm fuel pans. Data for a minimum of three tests are shown for both configurations. The CO production rate for heptane fires at the 20 and 30 cm scales are quite low, although a slightly higher CO production rate is seen at the 30 cm scale. There is a subtle increase in CO production rate of fire whirls compared to pool fire scenarios. This is due to higher burning rate of fire whirls, though since fire whirl burn in shorter span of time the fire whirl at both scale will have a smaller emission factor (as shown in *Figure 6.18*)

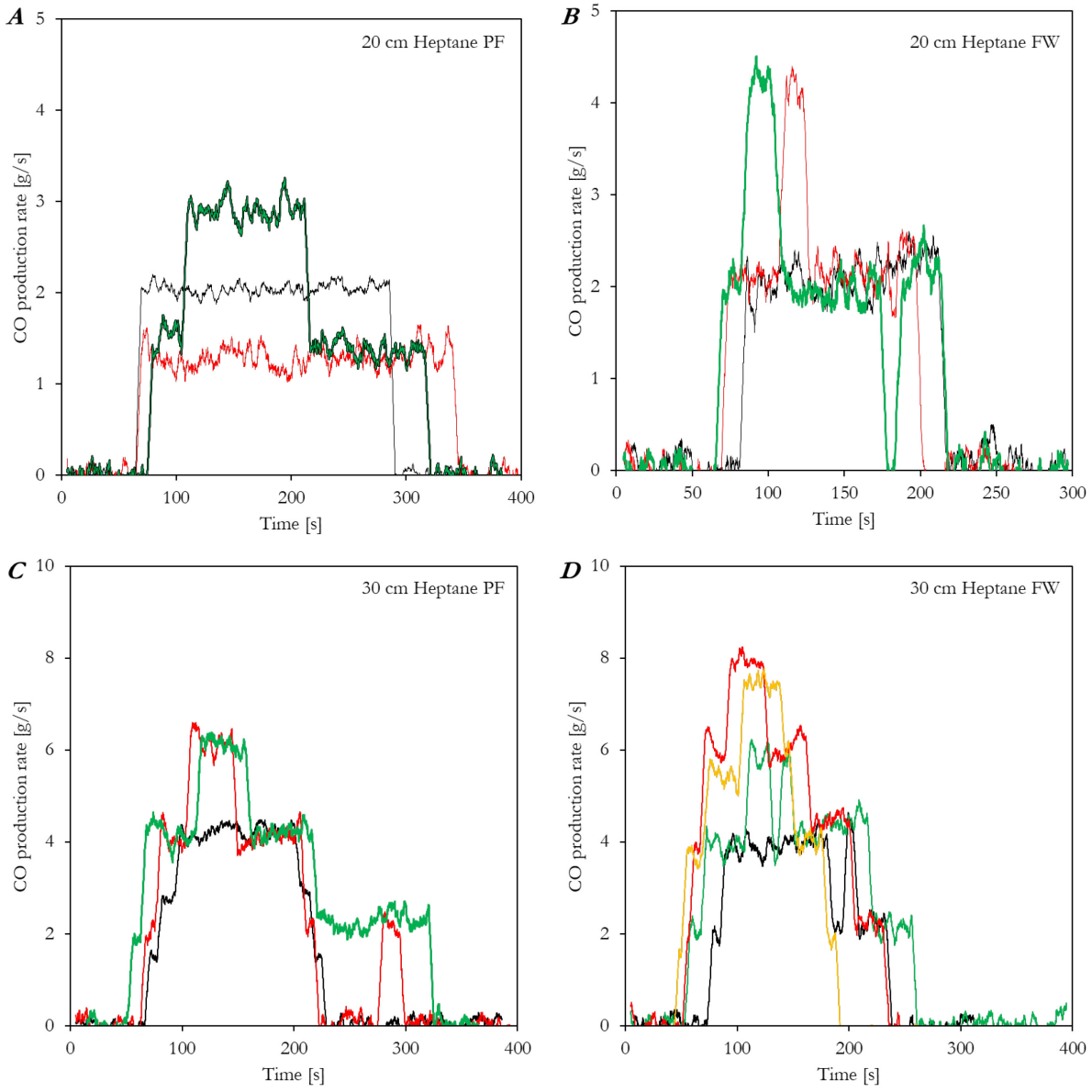

Figure 6.16: Comparison of CO production rates from heptane fires, for 20 and 30 cm fuel pools.

Figure 6.17 shows the CO production rate of the experiments with ANS crude oil for both the 20 and 30 cm fuel pans. Data from a minimum three repetitions are shown for both configurations. ANS fire whirls show higher emissions of carbon monoxide compared to heptane, which is expected due to the complex and heavy molecular components in crude oil. The CO production rate from the 20 cm ANS pool fire peaks around 10 g/s, and the fire burns for about 300 seconds. The production rate of the 20 cm fire whirl peaks at 30 g/s, though it has a much shorter burn

duration (140 s). The 30 cm ANS experiments show lower CO production rates in comparison to the 20 cm fires.

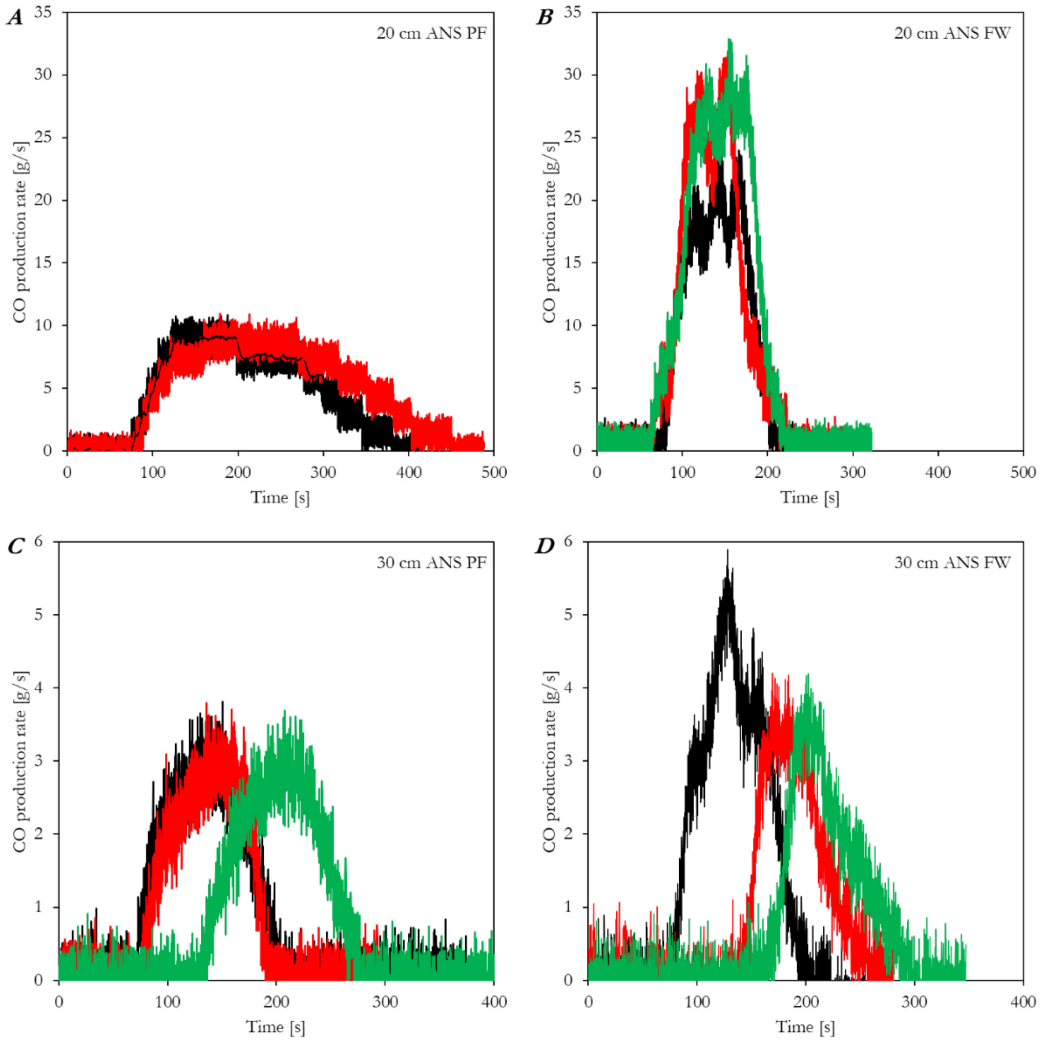

Figure 6.17: Comparison of CO production from ANS fires, for 20 and 30 cm fuel pools.

The CO emission factors for both 20 cm and the 30 cm pools are shown in *Figure 6.18 (A–D)*, and a comparison is made between the two burning regimes. The CO emission factors obtained from heptane and ANS crude oil in both flame regimes are relatively close and the differences observed are within the spread of experimental data. The 20 cm ANS emission factors, unfortunately, appear an order of magnitude higher than the other values shown in this figure. This

may be due to a sensor calibration issue or incorrect factor in the analysis, likely the latter because all other data gathered from 20 cm tests follow expected trends. These results will be presented as-is for the rest of the report; however, these off-trend values have to be re-analyzed in the future alongside repeated tests to ensure their accuracy.

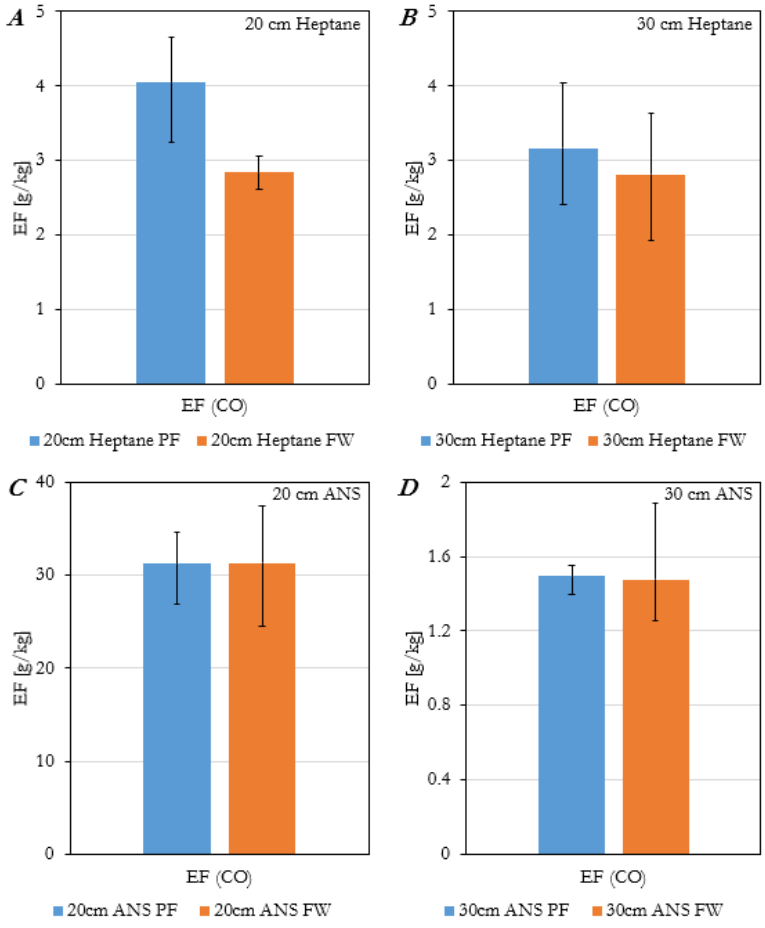

Figure 6.18: Comparison of CO emission factors for (A) 20 cm heptane, (B) 30 cm heptane, (C) 20 cm ANS, and (D) 30 cm ANS fires. Each panel shows data for both pool fire and fire whirl regimes.

6.2.4. Heat Feedback

Figure 6.19 shows the averaged heat feedback incident on the center of the fuel pan for both heptane (*A*) and ANS crude oil (*B*). The method used to determine the average heat flux feedback is similar to the case of the small-scale experiments. The initial and final temperature of the water

sublayer was used to determine the total energy transfer, which was then divided by the pool area and the burn duration. This results in a heat flux that is averaged temporally and spatially over the entire area of the fuel pool. The method does not provide an idea of the change in heat flux feedback values over the course of the experiment and thus peak values will be higher than the spatially and temporally averaged values calculated here. However, the average values present a good basis for comparing heating across scales and between the pool fire and fire whirl regimes. In the case of heptane fires, the average heat feedback is in the order of 12–18 kW/m^2, and the feedback from fire whirls is slightly higher. The trend is similar for both 20 and 30 cm diameter pans. For a given pool size, the ANS fires have a higher heat feedback compared to heptane fires, most likely due to a higher production of soot and therefore flame radiation. The average heat flux feedback values for ANS are in the range of 22–26 kW/m^2.

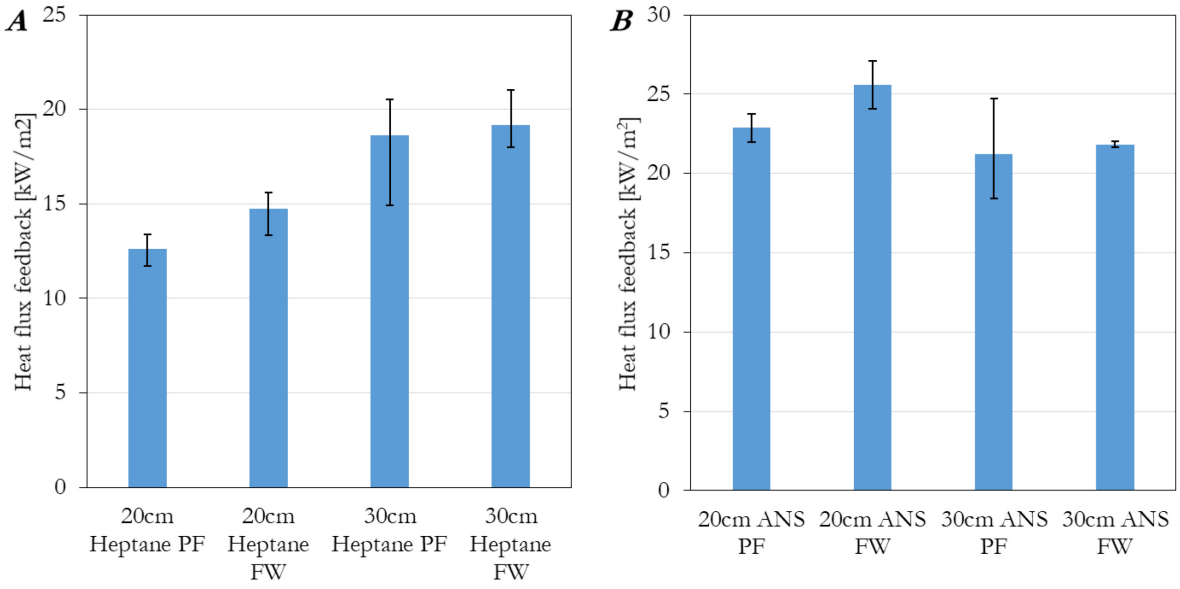

Figure 6.19: Averaged heat feedback from the flames to surface of (A) heptane and (B) ANS crude oil pools. Data is shown for both pool fire and fire whirl configurations.

Similar to flame temperature measurements of fires at the small scale, measurements of flame temperature at different heights above the fuel pool are shown in *Figure 6.20* and *Figure 6.21* for heptane and ANS fires respectively. In general, a significant reduction in temperature is observed with height for pool fires in all cases. In contrast, the vertical stratification in flame temperature

does not exist in the case of fire whirls. This rises the overall average temperature of fire whirls, which can result in enhanced convective and radiative heat flux feedback. An interesting aspect is that in case of the 30 cm ANS PF (*Figure 6.21–C*), even when boilover occurs towards the end of the burn duration (see the sharp spike in *Figure 6.21–C* at around 200 s), the stratification in the vertical temperature is retained.

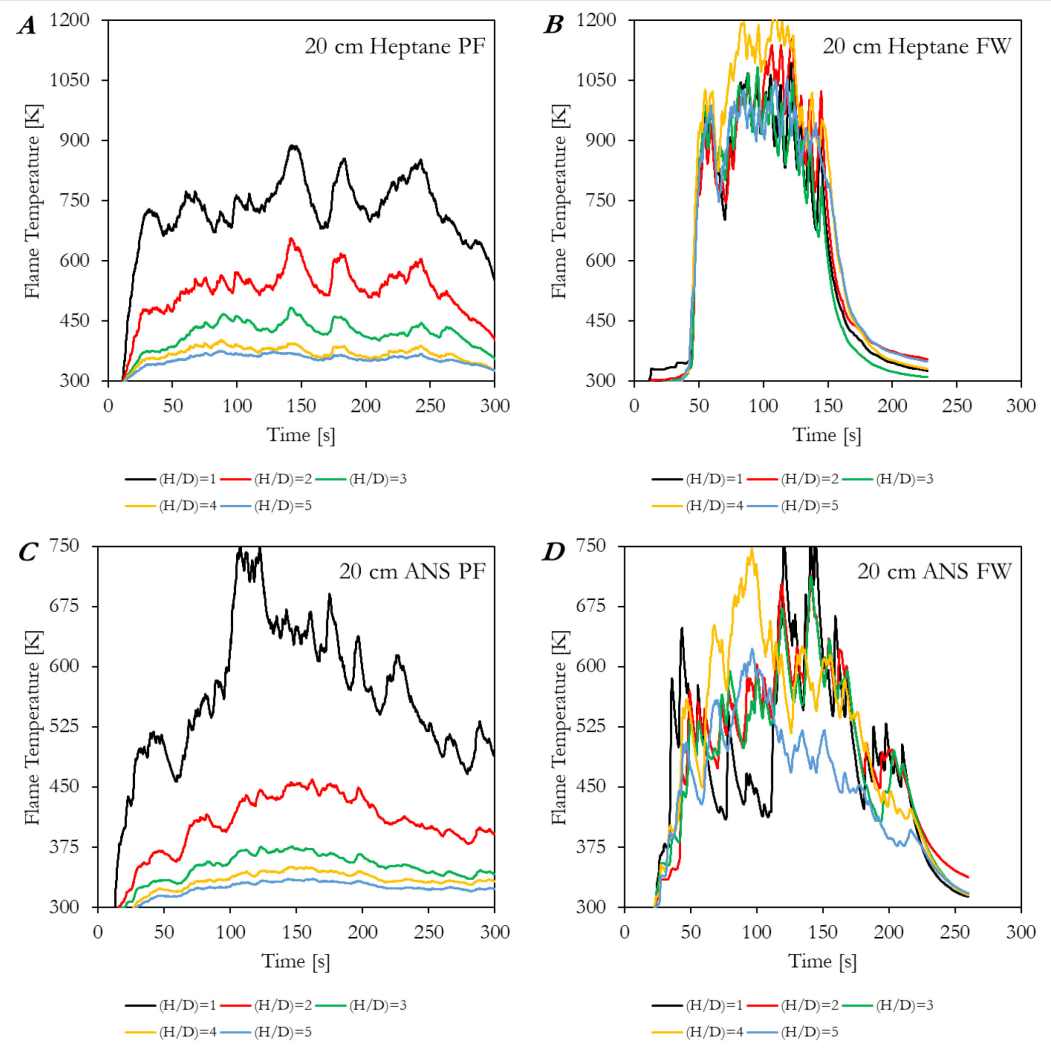

Figure 6.20: Flame temperatures at different heights (H) above the fuel layer, obtained for pool fires and fire whirls formed using heptane and ANS crude oil at the medium scale (D = 20 cm). Here, data from a single experiment is shown so that the data is not smeared by averaging. However, trends were very similar in other repetitions of the experiment.

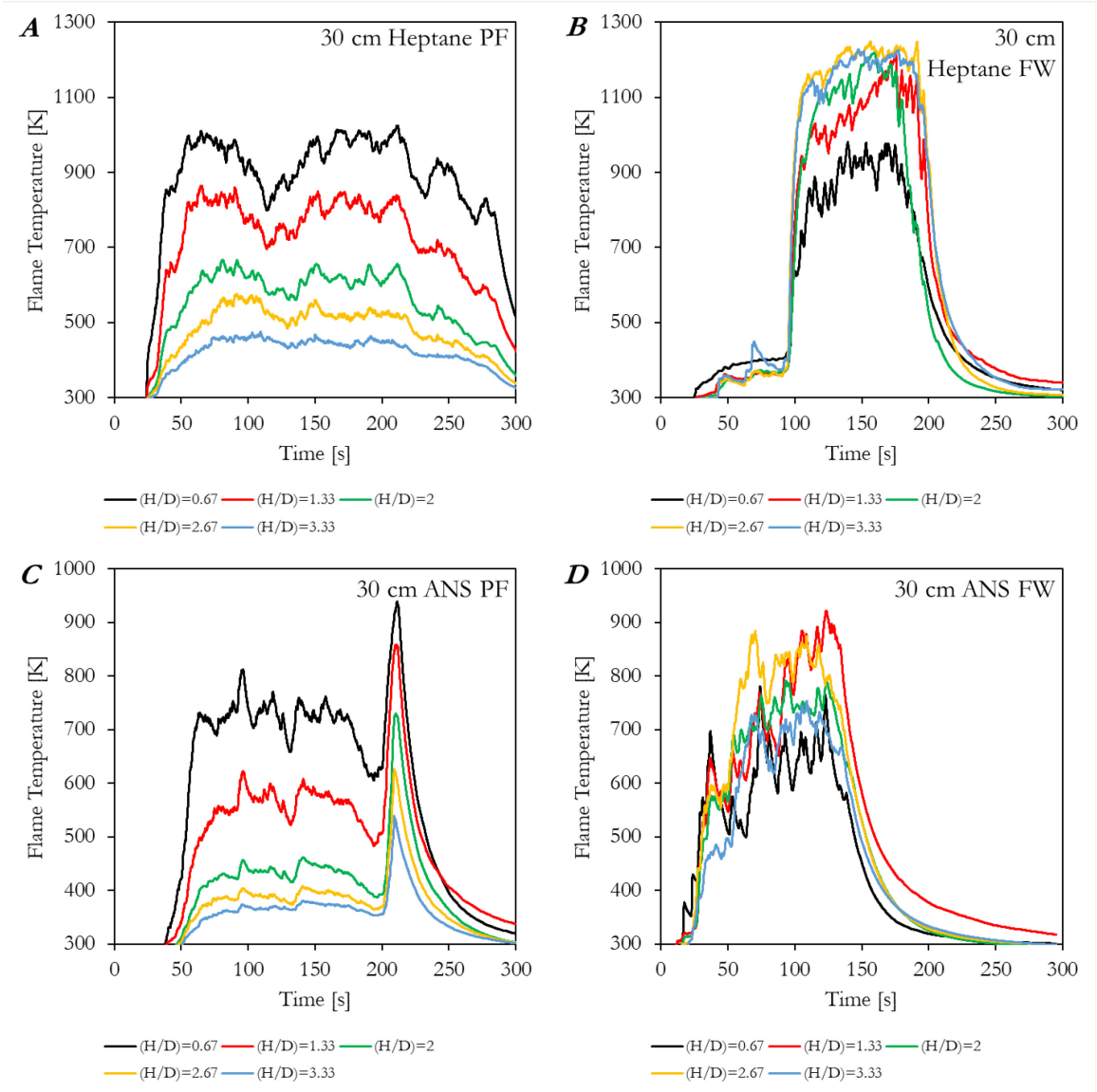

Figure 6.21: Flame temperatures at different heights (H) above the fuel layer, obtained for pool fires and fire whirls formed using heptane and ANS crude oil at the medium scale (D = 30 cm). Here, data from a single experiment is shown so that the data is not smeared by averaging. However, trends were very similar in other repetitions of the experiment.

6.2.5. Inlet Velocity

The inlet velocity and the calculated velocity for medium-scale fires are shown below in *Figure 6.22*. These values will be used in future sections to characterize the fire whirls formed in each of the cases to put them in the context of previous work, and potentially to help identify scaling trends. The results below were obtained with the Testo 405*i* vane anemometer.

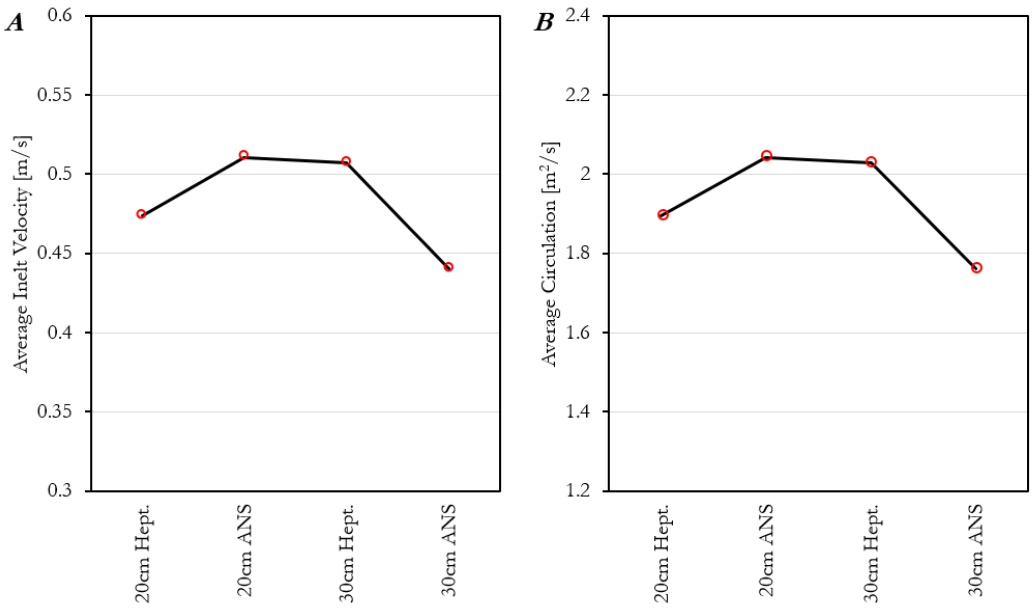

Figure 6.22: (A) Variation of average inlet velocity for medium-scale fires. (B) Average circulation calculated for each case using the enclosure side as the length scale, and the corresponding average inlet velocity.

6.3. Discussion of Medium-Scale Results

Our laboratory tests have consistently shown improved burning efficiencies of liquid hydrocarbon fires from fire whirls as compared to pool fires. This is particularly clear for mass-loss rate measurements, where fire whirls show significantly higher mass-loss rates, reducing the duration of burning when compared to corresponding pool fires. For crude oil (ANS), time dependent variations in the instantaneous mass-loss rate, although minimal, are attributable to the change in slick thickness over time and the evaporation order of different constituents of the fuel.

The amount of total fuel burned (removed) during ANS crude oil burns with a fire whirl also increased compared to that of a pool fire, indicating more efficacy in the combustion process. While the improvements were modest at the small scale, they increase at the medium scale, and the trend is expected to continue to the large-scale. The difference between pool fires and fire whirls is expected to continue to widen with the increased heat fluxes expected with fires at larger scales.

In terms of the total particulate matter released, *Figures 6.10* and *6.11* show that pool fires produce more PM per unit mass of fuel burned, and the trend is similar for both heptane and ANS crude. The stirrer used in the experiments at the small and medium scale have been shown to consistently prevent boilover for at least a majority of configurations tested. Measurements of temperatures in the fuel dish show that these effects are negligible during most experiments. The processes leading to boil over appear to occur very close to the interface between the fuel and water layer, which may provide an interesting topic for future study.

The CO_2 and CO emissions factors were presented in *Figures 6.16* and *6.18* and were crucial in understanding the emission behavior of fire whirls. In addition to these results, future measurement of unburned hydrocarbons will provide a more complete quantification of the differences between pool fires and fire whirls. As discussed in previous reports, the difference between combustion efficiency of pool fires and fire whirls becomes more apparent with increasing fuel-pool diameter. Consistent with this, the TPM emission factors for fire whirls showed a significant reduction from the corresponding values of pool fires, a trend that was visible with both heptane and ANS crude oil.

7. Large-Scale Experiments (Phase III)

Phase III was conducted at the Performance Fire Laboratory of the Worcester Polytechnic Institute between months 15 and 18 of the project. A fire whirl apparatus was constructed under the Large Oxygen Depletion System (LODS) of WPI. Experiments were conducted by burning ANS crude oil and heptane in both pool fire and fire whirl regimes. Results of the experiments at the large-scale are reported in this section.

7.1. Large-Scale Experimental Setup

The experimental configuration for the large-scale experiments is shown in *Figure 7.1*. The enclosure size was increased, along with the fuel pool diameter. The inlet gap width to enclosure length ratio (G/W) was again ¼ at this scale. The suction hood of LODS at WPI is 8 by 8 m at its outer skirt and is 6 m above the floor. Curtains with a height of 2 m were draped around the entire hood to ensure all effluents were collected. The large-scale setup consisted of three parts: walls, base floor, and the fuel/water container. The walls and base floor were constructed under the suction hood with 2 by 4 inch lumber (approximately 5 by 10 cm) frames and sheetrock boards forming the interior of the walls. The fuel/water container was made of stainless steel and had inlet/outlet ports for water circulation.

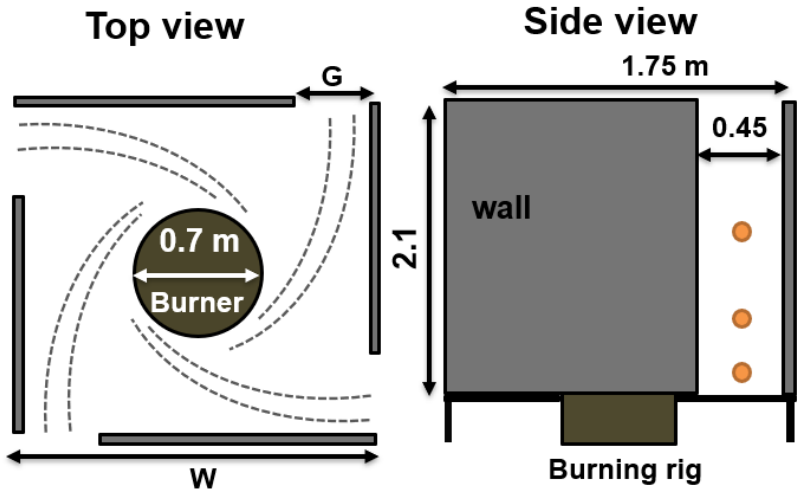

Figure 7.1: Experimental configuration for experiments at the large scale.

The four walls came together in the above formation to create a fire whirl enclosure floor area (1.75 m x 1.75 m) with each of the inlet gaps 0.45 m in width. The fuel/water container with a diameter of 0.7 m and depth of 0.35 m was placed in the center of the enclosure. This pan was filled with water for each experiment and the fuel layer was added prior to ignition. The four walls (3 m high, 2.4 m long) were constructed with coasters to allow flexibility in access to the fuel/water container at the center of the enclosure. A pump was used to circulate the water inside the pan through the inlet/outlet ports of the container. An additional inlet pipe (scape pipe) was also attached to the container to provide a port for passage of wires and tubes that were used within the container for instrumentation. The bottom surface of the enclosure consisted of a frame (built using lumber) above which a sheetrock board assembly was positioned such that a central opening 0.7 m in diameter enclosed the fuel/water container. The base floor surface was mounted flush with the pan, such that no lips was formed in the enclosure. *Figure 7.2* shows a photograph of the fuel/water container within the fire whirl enclosure. A section of the sheetrock base floor is removed to show the relative positioning.

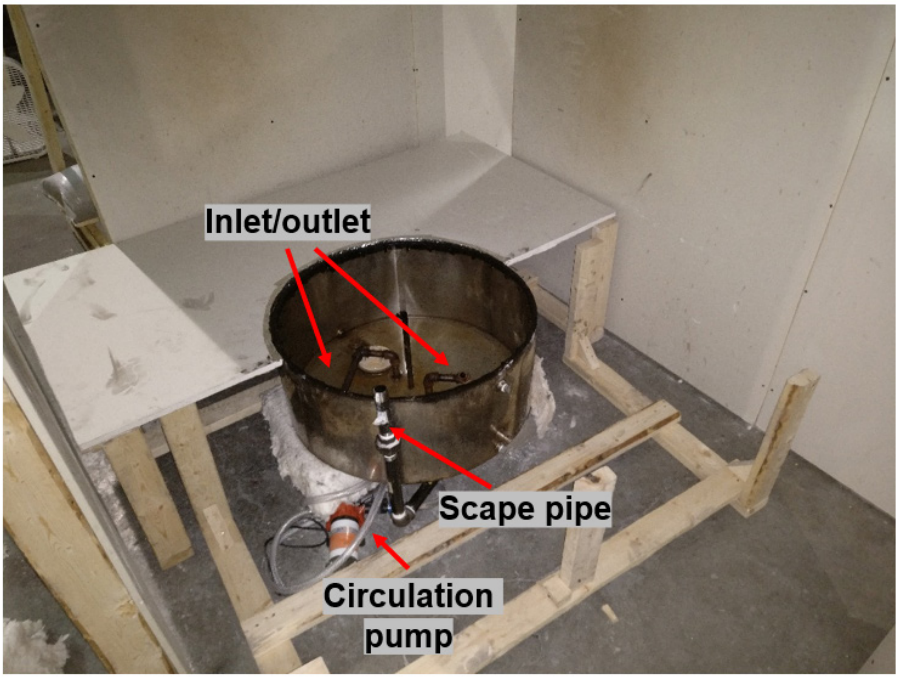

Figure 7.2: Fire whirl enclosure with the base floor partially removed. A circulation pump and other parts of the burning rig are labeled.

Preliminary experiments were performed to adjust the gap size for optimum fire whirl generation. A gap size of 0.45 m was found to consistently form fire whirls that were sustained for the burning duration. The walls were wheeled away for pool fire tests. *Figure 7.3* shows burning of ANS crude oil in the pool fire and fire whirl regimes.

Figure 7.3: Images of ANS crude oil pool fire (left) and fire whirl (right). The image of the pool fire was obtained with a roughly horizontal view, while the image of the fire whirl was obtained looking down from the top of the walls due to the limited visual access around the walls.

As mentioned earlier, curtains were hung around the hood to ensure all effluents were collected. The hood was connected to a long exhaust duct where effluents were sampled by a ring-shaped sampling tube, to sample from a circular region in the exhaust duct. The collected gases were pumped to the gas sensors and the DustTrak separately. The exhaust duct was also equipped with thermocouples and bidirectional pressure transducers to provide the flow rate of the gases through the duct. Concentrations of O_2, CO and CO_2 in the sampled effluents were measured with the gas analyzer. Details of the gas analyzer are provided in *Section 4* of this report. Particulate emissions were measured by the DustTrak DRX, and the average duct flow was used to convert the measured

concentration into a mass-emission rate of particulate matter from each fire. *Figure 7.4* shows the details of the instrumentation used at the large-scale phase.

The fire whirl enclosure and the burning rig were also instrumented with different sensors. Hot-wire and vane anemometers were used in the middle of the inlet gaps and at different height to measure the flow of the entrained air. The location of the anemometers is depicted in *Figure 7.4* with orange circles. A total of 32 thermocouples (type K, 24 gauge) were also placed in the centerline of the fire at different intervals. Thermocouples shown in *Figure 7.4*, labeled T1 through T32, were positioned up to a height of 120 cm above the fuel surface, and also in the liquid phase, down to 6 cm below the surface. The spacing between the thermocouples in the gas phase was 6 cm, in the liquid fuel 0.5 cm, and in the water 1 cm. Two water-cooled heat-flux gauges to measure total heat flux were also positioned in the enclosure. The first heat flux gauge with an operating range from 0 - 150 kW/m^2 was placed in two positions, at the center of the fuel pan (R0), and at a half radius of the pan (R1) to capture the heat feedback from the flame. This heat flux gauge was partially submerged in the liquid-phase, but its top surface was exposed to the gas-phase. The second heat flux gauge (0 - 20 kW/m^2 range) was intended to measure the external incident radiation of the fire whirl to an exterior wall, evaluating appropriate materials and separation distances for personnel. The second heat flux gauge was positioned at two elevations (S0 and S1) 50 cm away from the side of the pan.

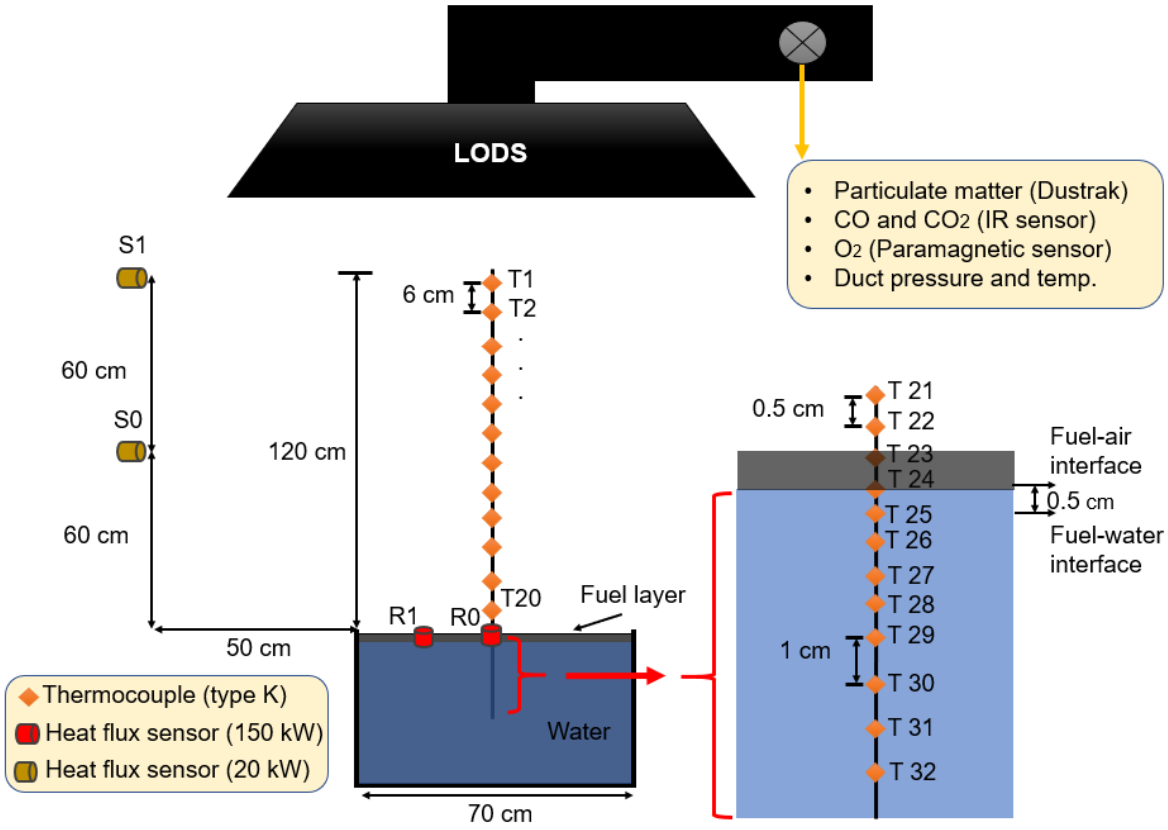

Figure 7.4: Instrumentation used for temperature and heat flux measurement in large-scale experiments.

Figure 7.5 shows the thermocouple tree installed in the center line of the pool, and the heat flux gauges in a submerged position within the container. In addition to the above sensors, cameras were placed at various locations to record the overall flame. Heptane and ANS crude oil were used, similar to the previous stages of the project. An initial fuel layer thickness of about 5 mm was used in all the tests with Heptane and ANS crude oil. Later on, ANS crude oil experiments were repeated with a thickness of ~7.5 mm to delay boilover, such that a longer duration prior to boilover was available for adequate gas and PM measurements.

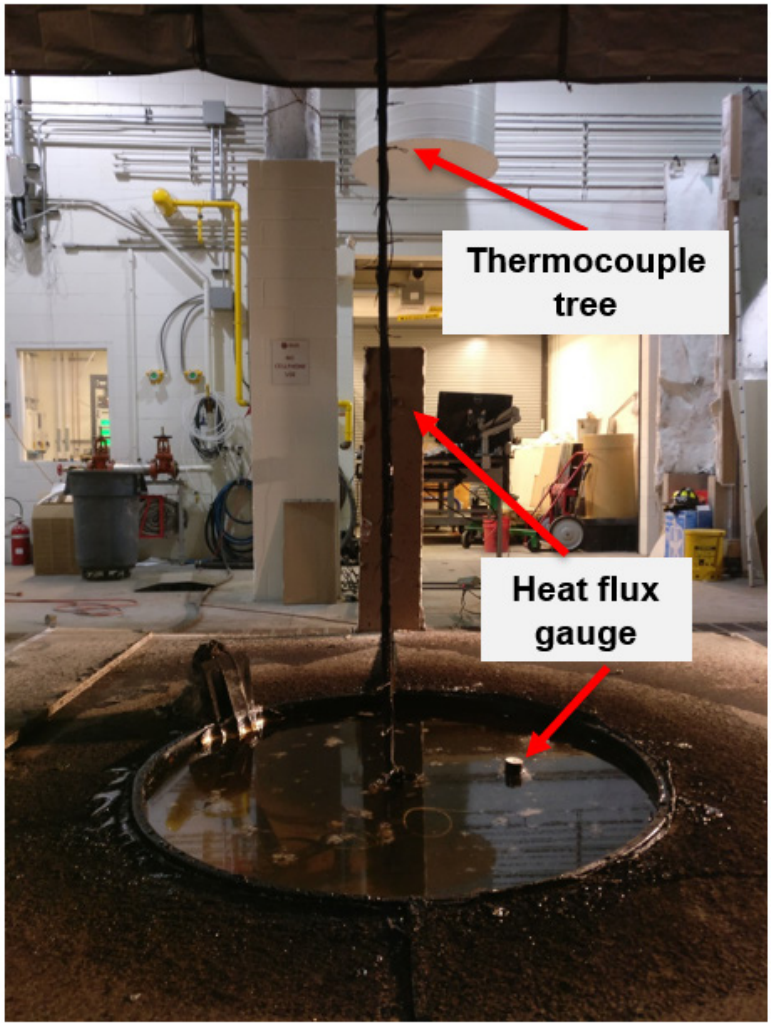

Figure 7.5: A photograph of the fuel pan showing the heat flux gauge and thermocouple tree.

7.2. Results and Discussion of Large-Scale Experiments

7.2.1. Mass Loss and Heat Release Rate

Heptane and ANS crude oil were used in the large-scale experiments similar to the previous stage of the project (with a 5 mm initial thickness). ANS crude oil tests were repeated with a 7 mm thickness to delay boilover as much as possible. In the large-scale tests, the residual ANS crude oil post-extinction was collected with absorbent pads (3M™ Petroleum Sorbent Static Resistant Pad HP-556). The weight of the pads used to collect the residue was measured before and after collection of the residue. *Table 7.1* shows the initial mass, residual weight, average burning rate, and consumption efficacy of the tests with ANS crude oil. Similar to previous experiments, Heptane was completely consumed with no residue. The ANS experiments underwent boilover at the end of burning, and thereby a minor portion of the fuel was splashed without burning. Nevertheless, the consumption efficacies of all the ANS tests were around 82-84%. The average burning rates reported in the below table involve the boilover phase, too.

Table 7.1: Consumption efficacy and average mass loss rate of the large-scale experiments.

	Initial mass [g] (Volume, [L])	**Residue [g]**	**Avg. mass loss rate [g/s]**	**Consumption efficacy [%]**
Heptane-5mm-PF	1250 (2 L)	-	8.3	~100
Heptane-5mm-FW	1250 (2 L)	-	10	~100
ANS-5mm-PF	1710 (2 L)	301	9.4	82
ANS-5mm-FW	1710 (2 L)	290	10.6	83
ANS-7mm-PF	2450 (3 L)	382	10.1	84
ANS-7mm-FW	2400 (3 L)	382	13.1	84

The excessive weight of the fuel/water pan in the experimental setup prevented the use of a load cell to measure the instantaneous mass loss of the fuel. However, it is possible to calculate the total

heat release rate (HRR) of the experiments using oxygen consumption calorimetry. This was done by multiplying the oxygen concentrations by a constant value of 13,100 MJ/kg-of-O_2, which is the constant amount of heat that is released per unit mass of oxygen consumed (assuming complete combustion). A reduction in the oxygen percentage was measured using a paramagnetic sensor, which was then converted to HRR. The HRR behavior of the large-scale experiments for both fuels and both flame regimes is shown in *Figure 7.6*. The peak HRR of all fire whirl cases are higher (around 0.6–0.8 MW) compared to pool fires (0.2–0.4 MW). There is also a significant jump in the HRR at the onset of boilover begins, which is roughly at the midpoint of the burn duration of ANS fires.

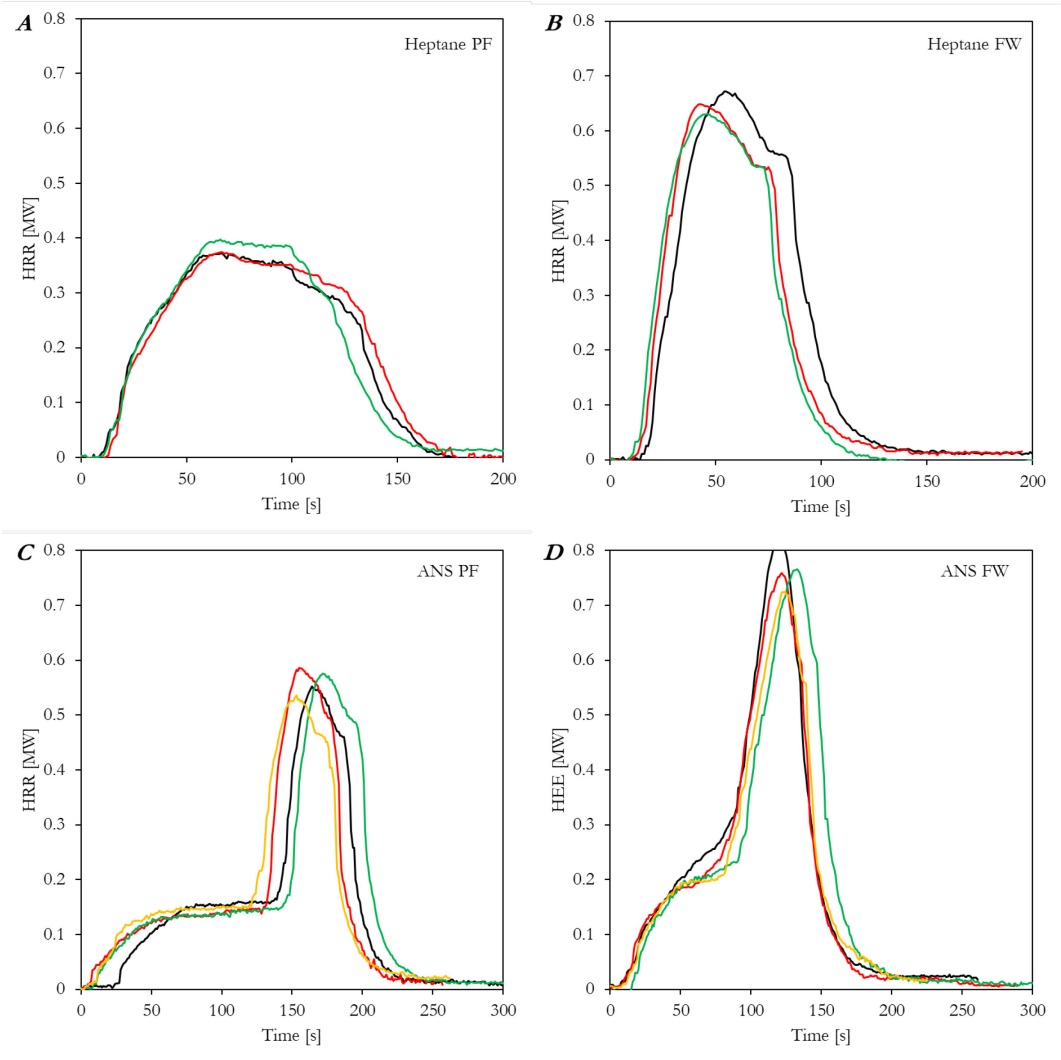

Figure 7.6: Heat-release rate behavior with time, calculated by oxygen consumption calorimetry for each case. The curves show data from individual experiments for each case.

7.2.2. Particulate Emissions

Particulate matter emission rates over time were captured for the large-scale fire whirls and pool fires formed using both heptane and ANS crude oil. The results for heptane fires are presented in *Figure 7.7* and show a comparison between the pool fire (A) and fire whirl (B). Three tests are reported for each burning regime with an initial volume of ~2 L corresponding to a 5 mm slick of fuel, the results of which shows good repeatability. Heptane fires consumed all the initial fuel, and showed a peak TPM emission rate of about 150-250 mg/s. The pool fire test lasted for a longer time from ignition to extinction (about 140 s) compared to the fire whirl tests. This means the burning rate of the pool fire tests was lower than that of the fire whirls. Meanwhile, the average and peak TPM rate of the pool fire tests show higher emission. The higher emission of TPM from pool fires is magnified when the results are normalized (as an emission factor) with the mass loss of the fuel.

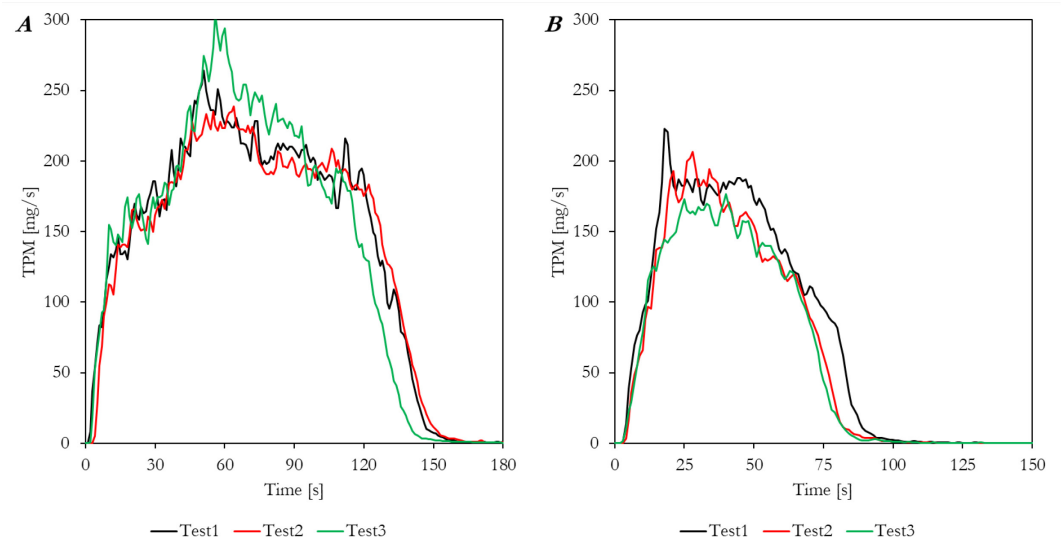

Figure 7.7: TPM emission rates – (A) Heptane pool fire, (B) Heptane fire whirl.

The results for ANS crude oil are presented in *Figure 7.8* and shows a comparison between a pool fire (A) and a fire whirl (B). The tests initially had ~3 L of ANS crude oil to delay the occurrence of boilover. Data from four individual experiments are reported for each burning regime, which show very good repeatability. The TPM emission rate increases sharply after some

time as lighter components of the oil are consumed, and particularly with the onset of boilover, when peak emission rates jump by nearly four times. ANS tests consumed about 80% of the initial oil, as explained previously. The burning of the ANS resulted in a peak particle emission rate of about 500-700 mg/s for normal burning, which increased to ~3000 mg/s during the boilover period. The pool fire tests lasted for a longer time from ignition to extinction (about 200 s) compared to the fire whirl tests (about 150 s).

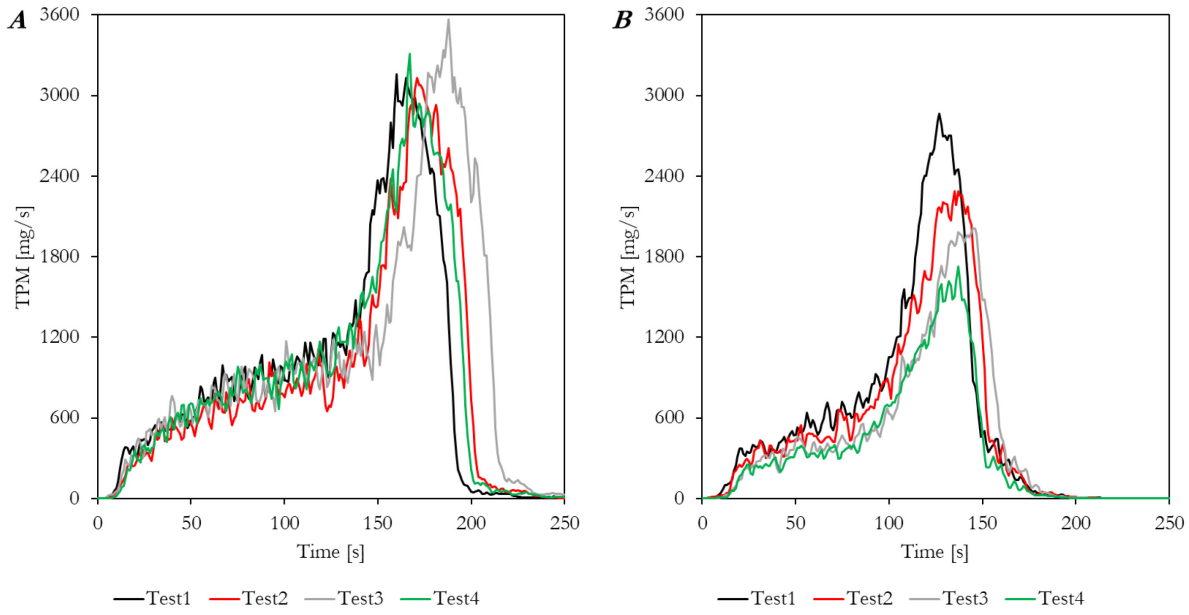

Figure 7.8: TPM emission rates – (A) ANS pool fire, (B) ANS fire whirl.

To compare the emissions from the large-scale experiments, TPM emission factors are shown in *Figure 7.9*. Emission factors represent the mass of particles produced per the mass of fuel consumed. *Figure 7.9–A* shows the results for heptane fires, indicating that the TPM emission factor for the heptane pool fire is about 18 g/kg-of-fuel, which is more than double of the heptane fire whirl (about 8 kg/kg-of-fuel). *Figure 7.9–B* shows the TPM emission factors from ANS fires, and the trends are similar to that of the heptane fires. The TPM emission factor from ANS pool fire is roughly double the fire whirl emission (60 g/kg-of-fuel). The emission factors presented for experiments at the large scale include emissions in the boilover period of burning. Further analyses

may benefit from separating and comparing emissions factors with and without boilover, perhaps alongside boilover data from the medium scale.

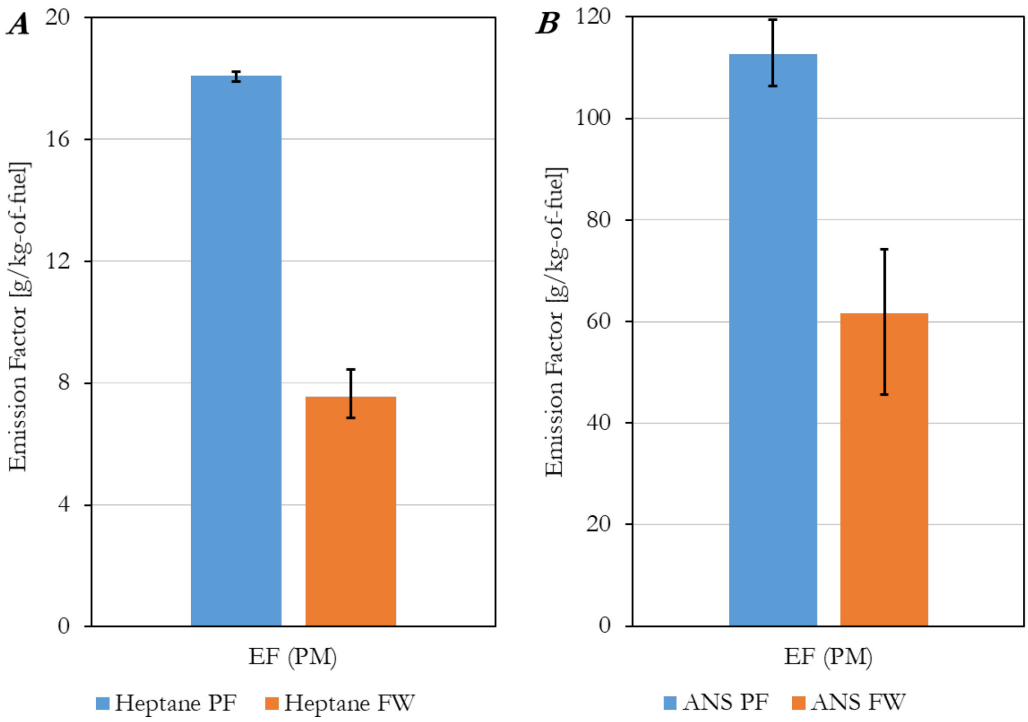

Figure 7.9: Comparison of PM emission factors for (A) heptane and (B) ANS fires.

7.2.3. Gas Emissions

The results of O_2 measurements for the heptane and ANS fires for both flame regimes are presented in *Figure 7.10* in terms of O_2 consumption rate. Heptane fires had an initial fuel slick of 5 mm, while ANS fires had an initial slick thickness of around 7 mm. The HRR data in *Figure 7.6* was derived from the data in *Figure 7.10*. Therefore, *Figure 7.10* can also be used to understand the mass loss rate behavior of the fire. For the fire whirl, the oxygen consumption rate peaks at a higher value compared to the pool fire due to higher burning rates. On the other hand, pool fires burn for a longer duration, and this is visible in O_2 consumption as well.

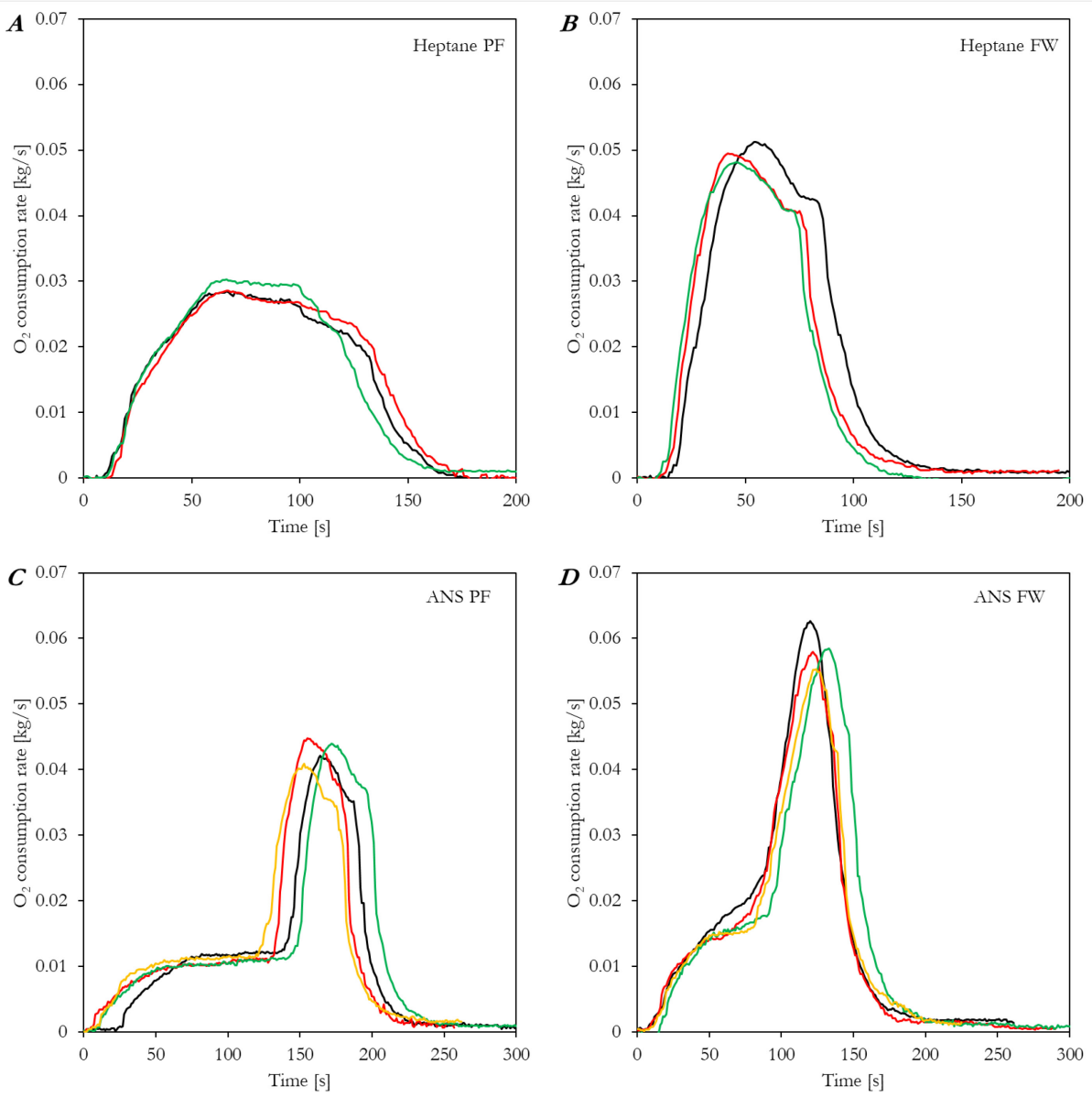

Figure 7.10: Oxygen consumption rate of the Heptane and ANS crude oil tests in both pool fire and fire whirl regime.

To normalize the oxygen consumption for every case, the total mass of O_2 consumed by the fire was calculated by calculating the area under each of the curves. Then, the total mass of consumed oxygen was divided by the amount of liquid fuel that was removed to obtain the consumption factor (CF) of oxygen. The O_2 consumption factors for the different fires are presented in *Figure*

7.11. Oxygen consumption in heptane fires was similar for both flame regimes, amounting to about 2.2 g/kg-of-fuel. However, the oxygen consumption factor of ANS fire whirls is about 25% greater that of the pool fire. This means that more oxygen is used for the same amount of fuel, partially explaining the resulting lower emissions of CO and PM.

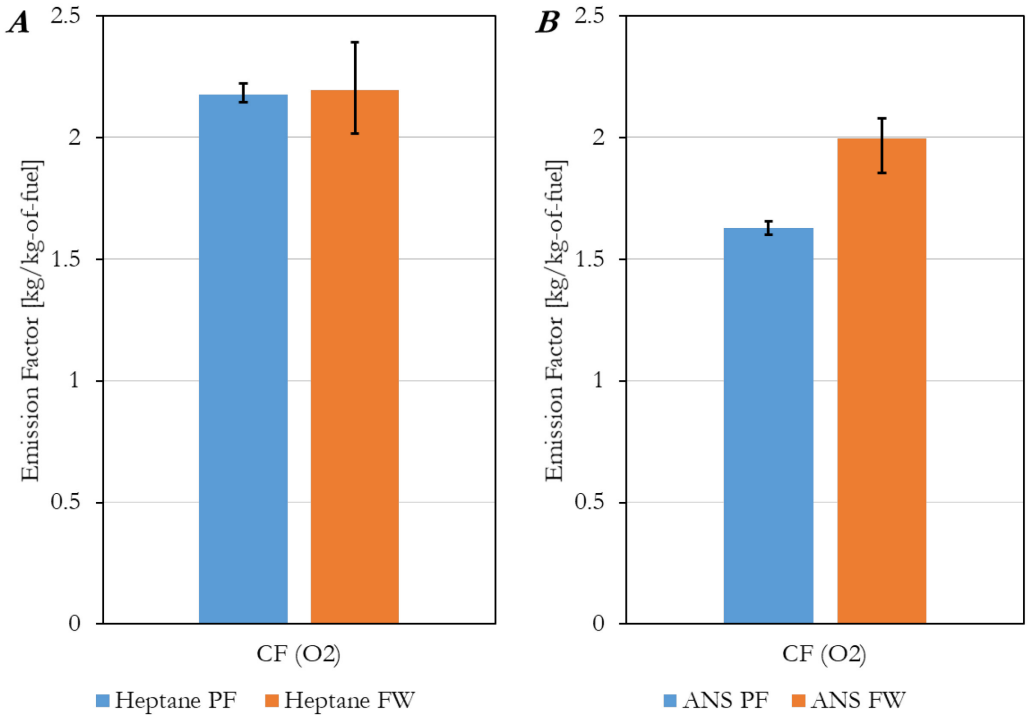

Figure 7.11: Comparison of O_2 consumption factor (CF) for (A) heptane and (B) ANS fires.

Figure 7.12 shows the CO_2 emission rates for the different fires at the large scale. Data for individual experiments show good repeatability. Similar to the oxygen consumption rate, the fire whirls show higher CO_2 emission rates, which can be attributed to the higher mass loss rate. *Figure 7.13* represents the different regimes and conditions, with averaged data for each condition, such that the emissions may be compared in a single figure.

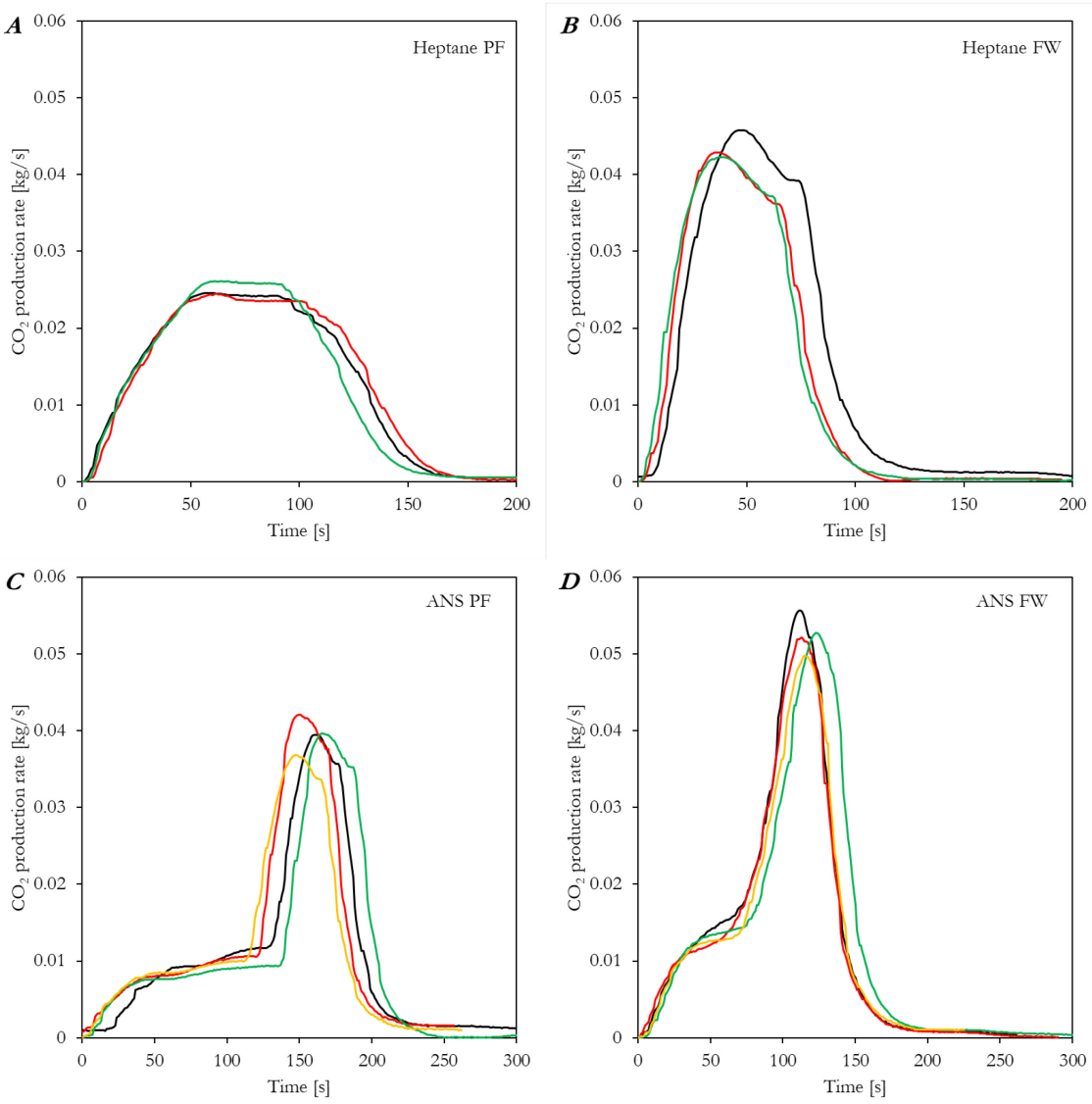

Figure 7.12: Comparison of CO_2 production rate from heptane and ANS fires.

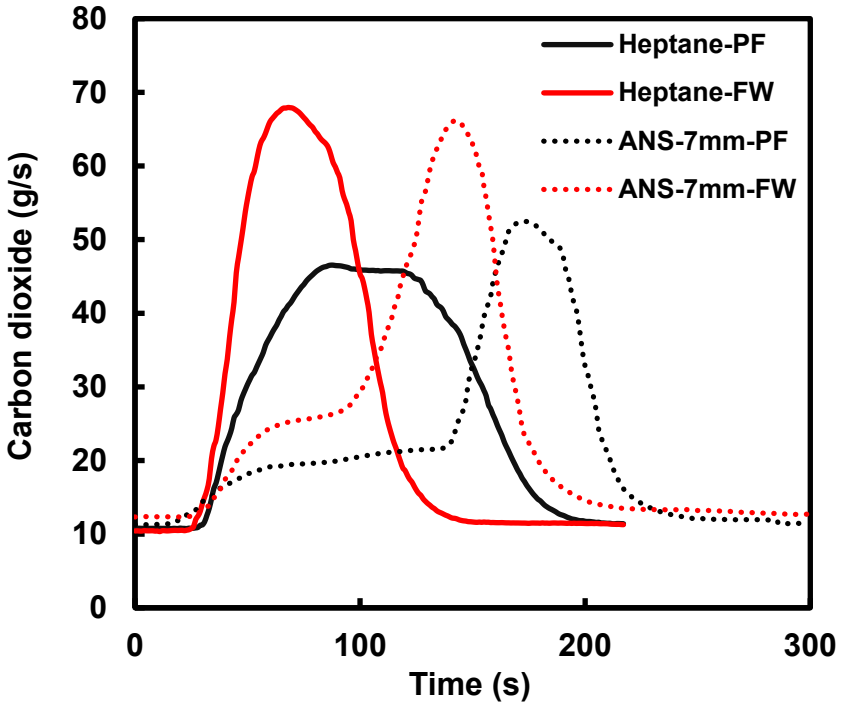

Figure 7.13: Comparison of CO_2 production rate for heptane and ANS fires, for both pool fire and fire whirl regimes.

The CO_2 emission factor for every case is reported in *Figure 7.14*. The total mass of CO_2 was divided by the amount of liquid fuel that was consumed in the fire to obtain the EF of CO_2. CO_2 emission factors for heptane fires was similar for both flame regimes, around 2 kg/kg-of-fuel. However, the CO_2 emission factor from ANS fire whirls was greater than that from ANS pool fires. This may be attributed to better air entrainment in the fire whirl regime that permitted enhanced combustion of the fuel. Therefore, more carbon dioxide was produced by the same amount of fuel.

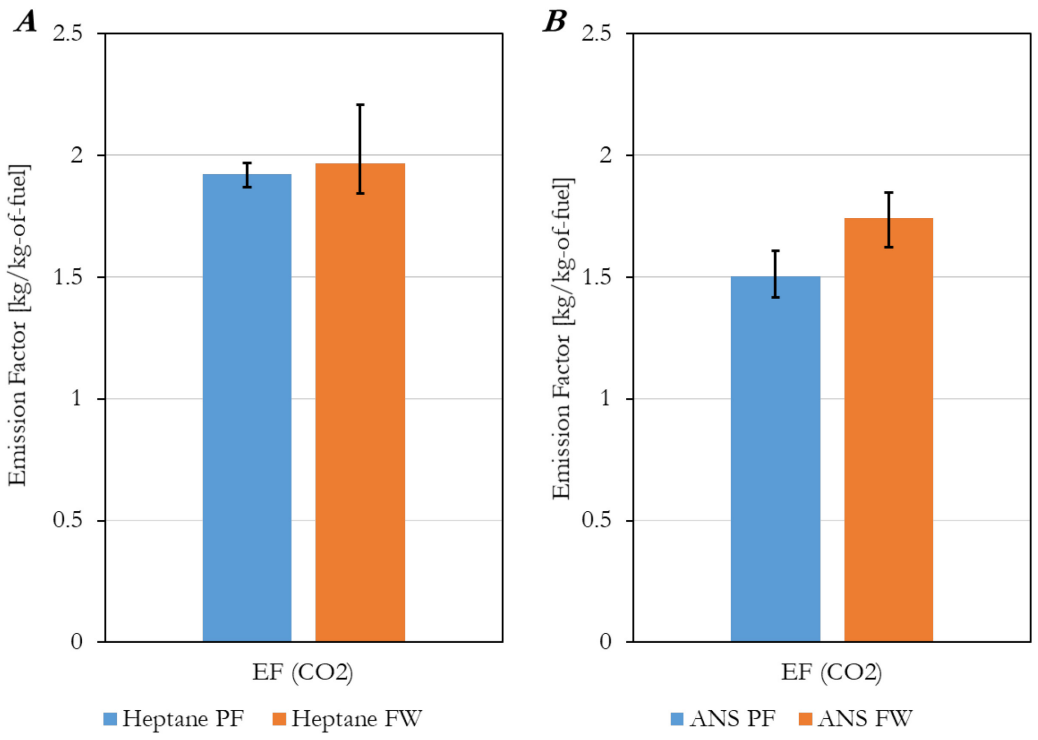

Figure 7.14: Comparison of CO_2 emission factors for (A) heptane and (B) ANS crude oil fires, for both pool fire and fire whirl regimes.

Figure 7.15 shows the CO emission rates for the different heptane and ANS fires. Data from individual experiments have minimal spread, and thus have high repeatability. Averaged trends for the different fires are combined in *Figure 7.16*. The production rates of CO from ANS fires were significantly higher than those from heptane fires.

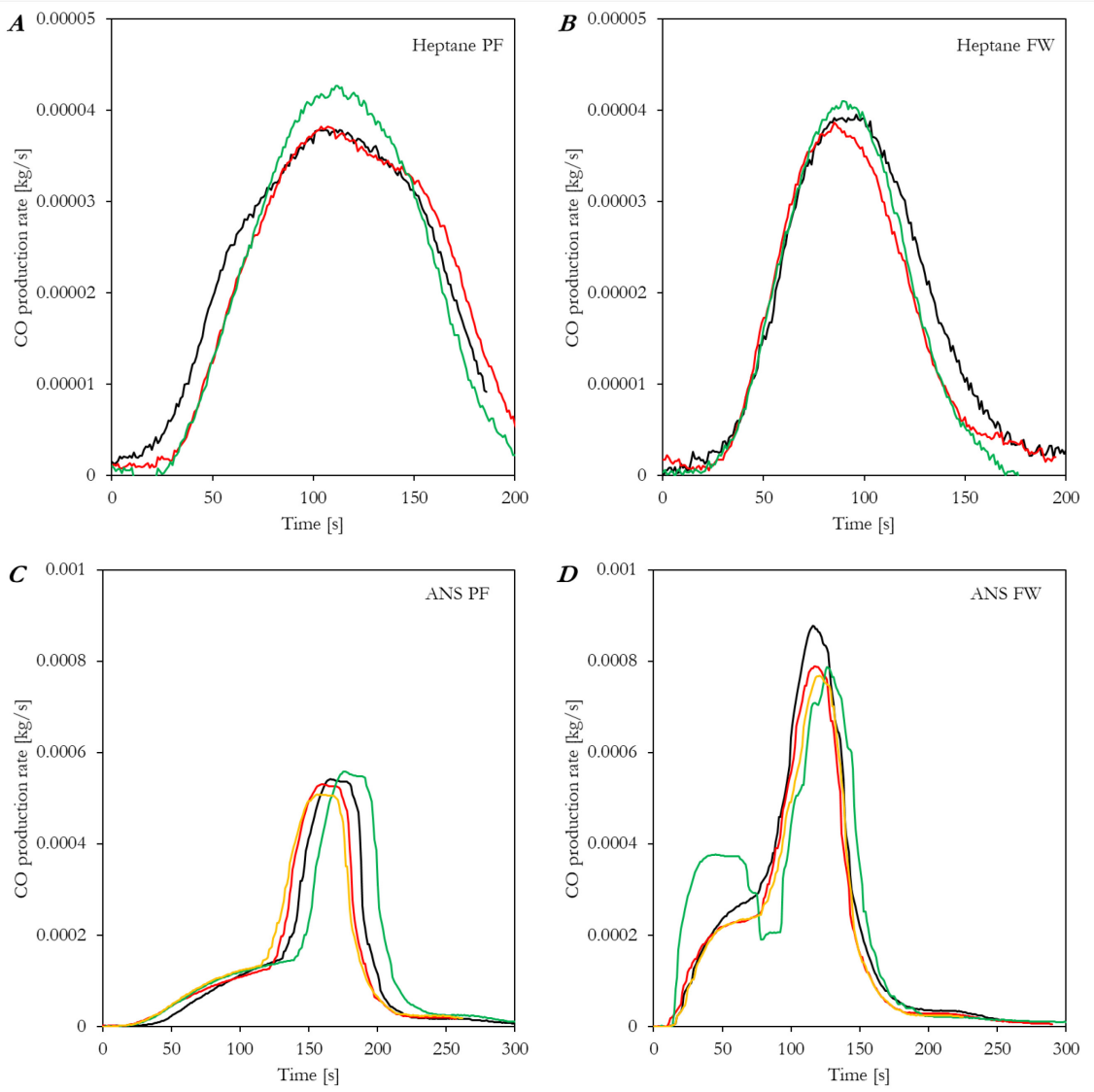

Figure 7.15: Comparison of CO production rates for heptane and ANS fires, for both pool fire and fire whirl regimes.

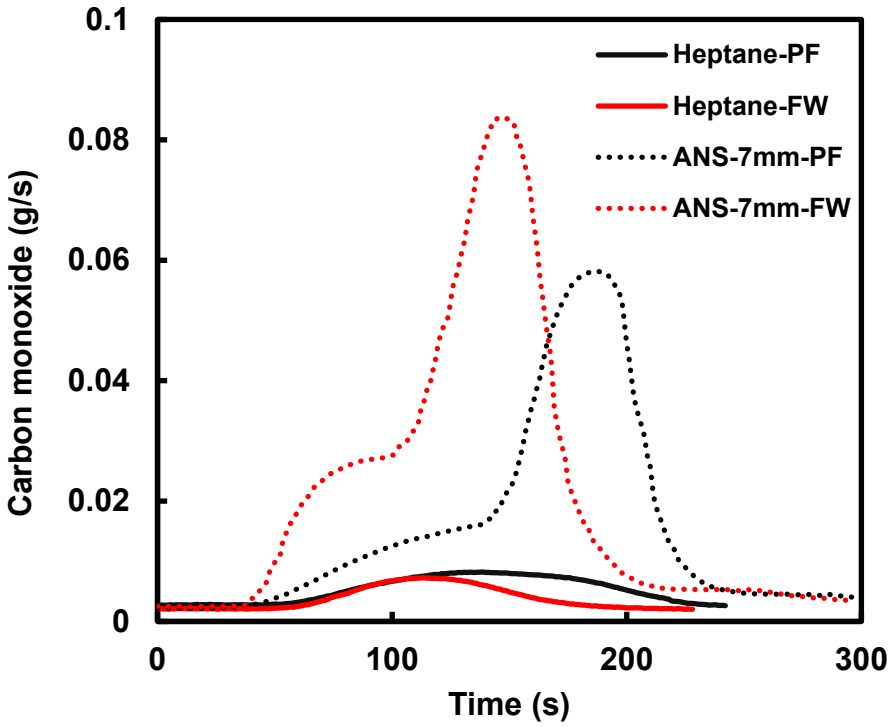

Figure 7.16: Comparison of CO production rates for heptane and ANS fires, for both pool fire and fire whirl regimes.

In addition, the CO emission factor for the different fires are reported in *Figure 7.17*. The total mass value of CO emitted was divided by the amount of the liquid fuel that was consumed in the fire to obtain the EF of CO. CO emission factors from heptane fires were much smaller than those from ANS fires. The ANS fire whirl had a greater CO emission factor compared to an ANS pool fire. One potential explanation for this is that the better mixing in the large-scale fire whirl, and the boilover condition permitted higher temperatures that allowed soot to oxidize partially to CO.

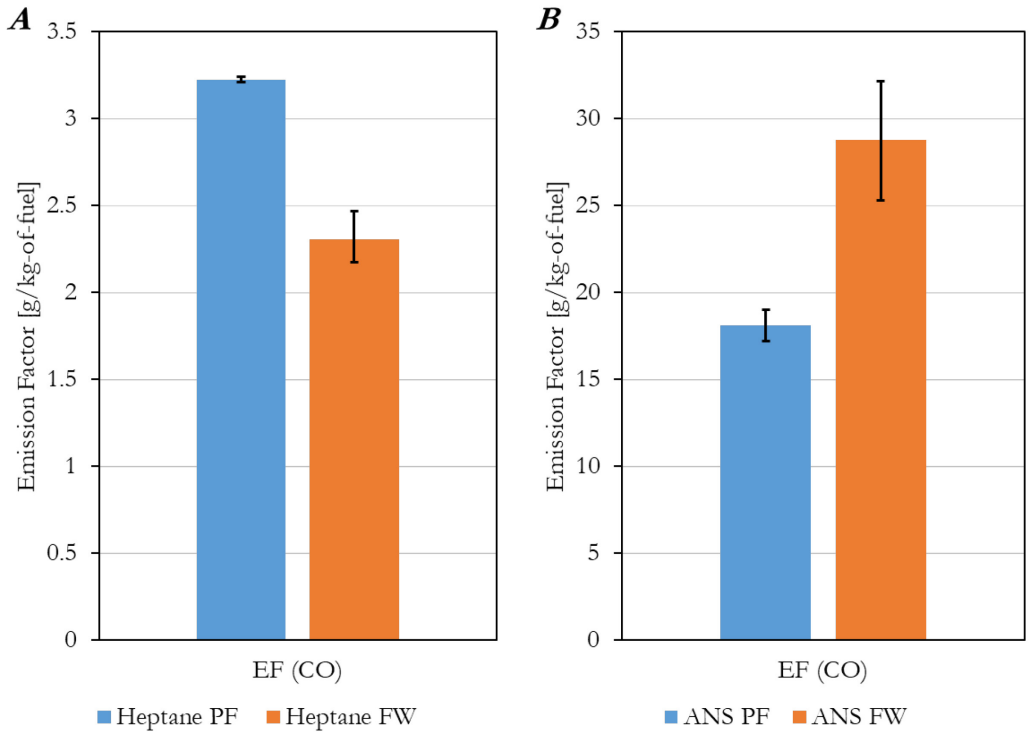

Figure 7.17: Comparison of CO emission factors for (A) heptane and (B) ANS fires, for both pool fire and fire whirl regimes.

Overall, there are two major trends that are observed in the gaseous emissions of the large-scale experiments. First, the emissions are generally lower for heptane fires, which is due to the nature of the fuel (pure, low boiling point, simple molecular structure), and the absence of the boilover. Use of the fire whirl regime to burn heptane resulted in lower emissions of soot and carbon monoxide compared to burning in the pool fire regime. Second, for a multi-component fuel with a complicated molecular structure, the use of the fire whirl reduces the emission of soot, and it is supposed that some of the lower particulate emissions may result in slight increase in CO emissions.

7.2.4. Temperature and Heat Flux Measurements

The temperature of both gas and liquid phase at the center line of the pool was recorded using the thermocouple tree shown in the experimental setup section. *Figure 7.18* shows the temperature

measurements of a few select thermocouples over the duration of the experiment with heptane in both pool fire and fire whirl regimes. The temperature measurements show similar trends in repeated experiments except for persistent fluctuations for every test. The results presented herein are representing one test for each case and are not averaged to avoid smearing the data.

In the liquid-phase temperatures, T23 was the submerged thermocouple closest to liquid surface and shows a gradual increase from the initial temperature of heptane (18 ºC) to values near its boiling temperature (95 ºC) for fire whirl cases. The temperature increase in pool fire case was relatively slower. The next thermocouple, T24, was closest to the fuel-water interface and followed T23 readings closely. Note the low values recorded by T25 in both flame regimes, which indicated minimal effect from both fires. In the gas phase, three locations (top, middle, and bottom) on the thermocouples three were selected to present here, T1, T11, T22, with a distance of ~60 cm between them. Temperatures in the gas-phase peak around (950 ºC), but because of the movement of the flame, specifically flame wander in the fire whirl regime, the temperature fluctuations had a rough cyclic nature. It is important to note these measurements are *not* corrected for radiation losses and, due to their slow response with a large bead size, necessary to avoid damage during testing, provide an estimated temperature in the flame zone.

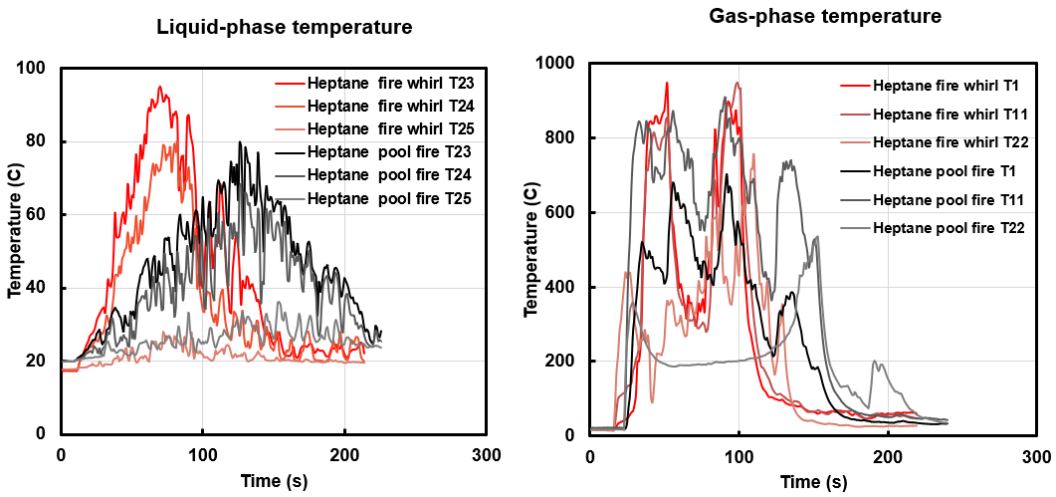

Figure 7.18: Liquid and gas phase temperature for heptane fires in both pool fire and fire whirl regimes.

Figure 7.19 shows temperature readings from select thermocouples over the duration of the experiment with ANS crude oil in both pool fire and fire whirl regimes. In the liquid-phase, T23 showed a gradual increase from the initial temperature of ANS (18 ºC) to values near its boiling temperature (250 ºC). The next thermocouple, T24, was closest to the fuel-water interface and increased to values near the boiling point of water in the moments that boilover occurred. Note the low values recorded by T25 in both flame regimes, which indicated minimal thermal penetration from both fires. In the gas phase, three locations (top, middle, and bottom) were selected to present here, T1, T11, T22, with a distance of about 60 cm between them. Again, temperatures in the gas-phase peak around (950 ºC).

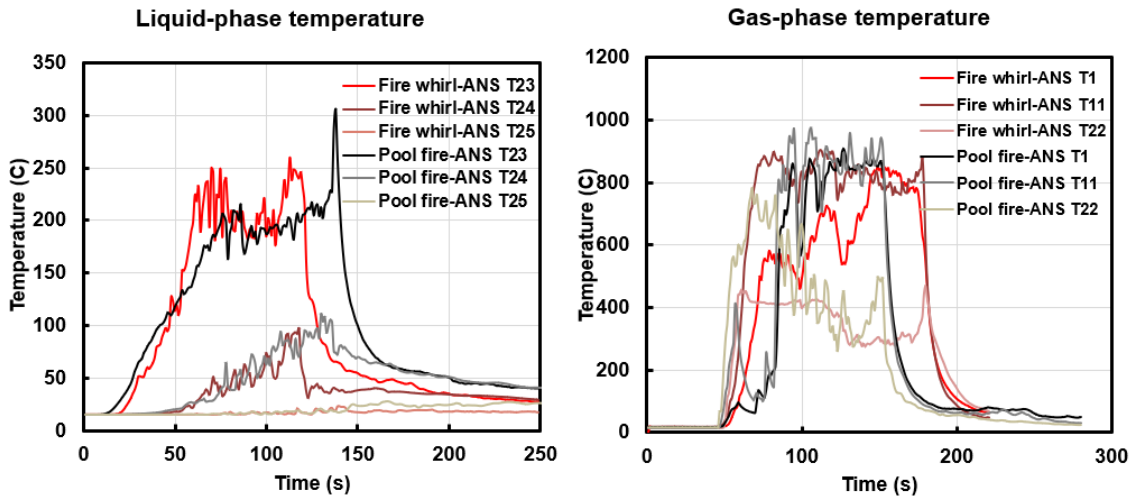

Figure 7.19: Liquid- and gas-phase temperature for ANS fires in both pool fire and fire whirl regimes.

The heat feedback to the pool of liquid at both flame regimes were measured with a heat flux gauge (radiation + convection) that was partially submerged within the liquid fuel. The heat flux gauge was placed facing up in the center of the pool (R0) and also at half-radius distance from center (R1). *Figures 7.20* and *7.21* show the heat feedback for ANS and heptane fires at the center and half-radius distance from the center of pool, respectively. The heat flux measurements show similar trends in repetitions of experiments, except for persistent fluctuations for every test. The results presented are from one experiment for each case and are not averaged to prevent temporally smearing the data. As shown in *Figure 7.20*, the heat flux measurements for heptane fires show

different trends between pool fire and fire whirl regimes. The heat feedback of heptane pool fire increased to 40 kW/m^2 after ignition, and then declined to a steady 20 kW/m^2, before rising again prior to extinction. The fire whirl scenario however showed a different behavior and increased to a relatively steady value of about 70 kW/m^2 before decreasing continuously until extinction. The difference could potentially be explained using the flame geometry. For the heptane pool fire, the flame evolved to a semi-conical shape as it began steady burning, which moved the reacting gases (flame sheet) away from the center. Inside of the flame sheet, high concentrations of heptane vapor existed, with excess air outside of the flame sheet. Therefore, the convection portion of the heat feedback was reduced, thereby reducing measurements at the heat flux gauge. For burning of heptane in fire whirl regime, the geometry was completely transformed to a narrow cylindrical shape with flames inclined toward the fuel surface at the bottom.

The ANS experiments show similar trends in both flame regimes, although fire whirls show slightly higher heat feedback (peak at ~60 kW/m^2) compared to pool fires (peak at ~50 kW/m^2). This could explain the higher burning rate for ANS fire whirl scenarios.

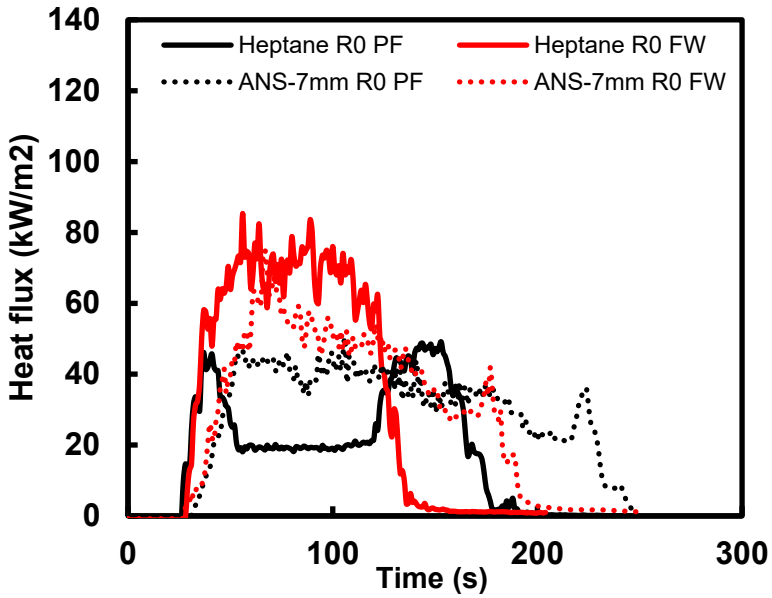

Figure 7.20: Heat feedback from the flames to the fuel layer at the center in both pool fire and fire whirl regimes.

The heat feedback received at a half-radius from the center also shows a similar trend for heptane fires. The only difference is that the amount of heat feedback to the half-radius location is slightly higher compared to the center location for the fire whirl. This could explain the higher burning rate for the fire whirl scenarios compared to the pool fire cases. The heat feedback from ANS fires at the half-radius location shows higher feedback for the fire whirl compared to pool fire tests. Overall, the relation between the flame geometry and heat feedback to the burning rate and emissions are crucial to understanding the fire whirl phenomenon.

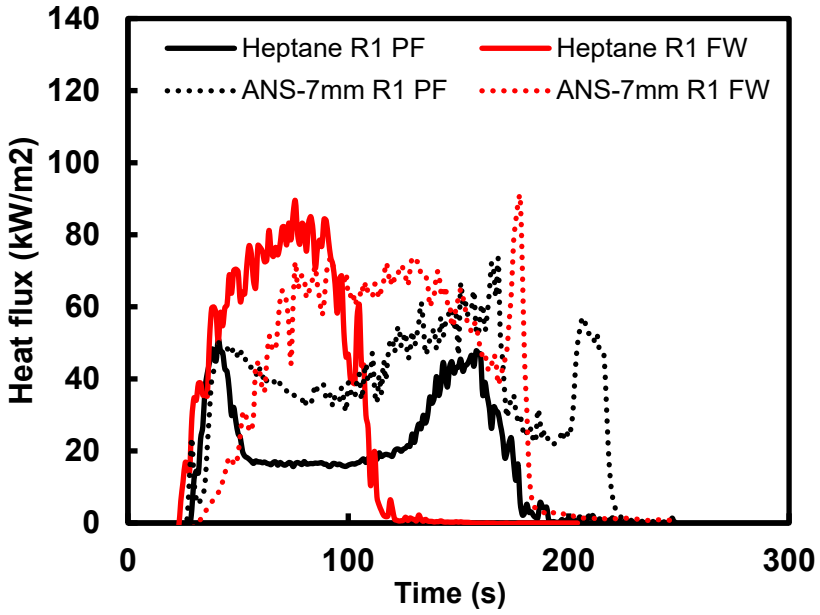

Figure 7.21: Heat feedback from the flames to the fuel layer at half radius in both pool fire and fire whirl regimes.

In addition to the heat flux measurement for heat feedback analysis, a heat flux gauge was embedded in the fire whirl enclosure wall to capture the incident heat flux impinged on external walls. As shown in the experimental setup the heat flux gauge was placed 0.5 m away from the fuel/water container, at a 0.6 m height from the floor. These measurements are required for both safety and design purposes. As seen in *Figure 7.22*, the incident heat to the wall is lower than the heat feedback to the fuel surface but it is still significant. Fire whirls were observed to remain well-controlled within the test enclosure during experiments, however it is essential that any practical

applications be constructed out of materials that will withstand sustained heat fluxes up to the levels observed in tests. For heptane fires in both regimes, the obtained heat flux values are similar and on order of 20 kW/m^2. Because fire whirls exhibit some flame "wandering" around the enclosure apparatus, i.e. the sweeping motion at the beginning of the experiment before becoming stationary, momentary higher heat fluxes should also be designed for to exterior walls. Results for ANS fires showed lower incident heat compared to heptane fires during the steady burning period. However, after the onset of boilover, the amount of incident heat is doubled due to a dramatic increase in the width of the flame.

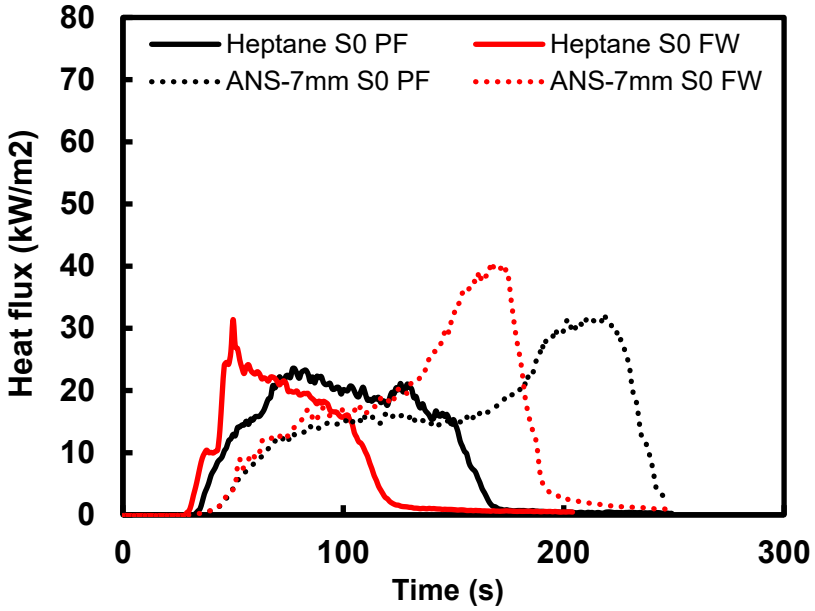

Figure 7.22: Incident heat flux on the walls, in both pool fire and fire whirl regimes.

7.2.5. Inlet Velocity

For the fire whirl experiments in the large-scale stage of the project, a constant gap size of 45 cm was used, and inlet velocity measurements were conducted using a combination of hot-wire anemometers and vane flow meters. The entrained air velocity and their variation with height are shown in *Figure 7.23–A and B)*. Also, circulation of air in the fire whirl enclosure calculated with the enclosure side length as the length scale, and shown in *Figure 7.23–C and D*. The average inlet velocity for heptane fire whirls was between 0.7–0.8 m/s, and showed minimal decrease with

height, up to 1 m above the lower surface, which was the upper limit for experiments at this scale. However, ANS crude tests showed a considerable decline in the average inlet velocity with height. Nevertheless, this data is useful in estimation of the air entering the enclosure and scaling the behavior of the fire whirl. This will be especially useful for comparison between different scales and will allow for an estimate of larger configurations that may also form reliable fire whirls.

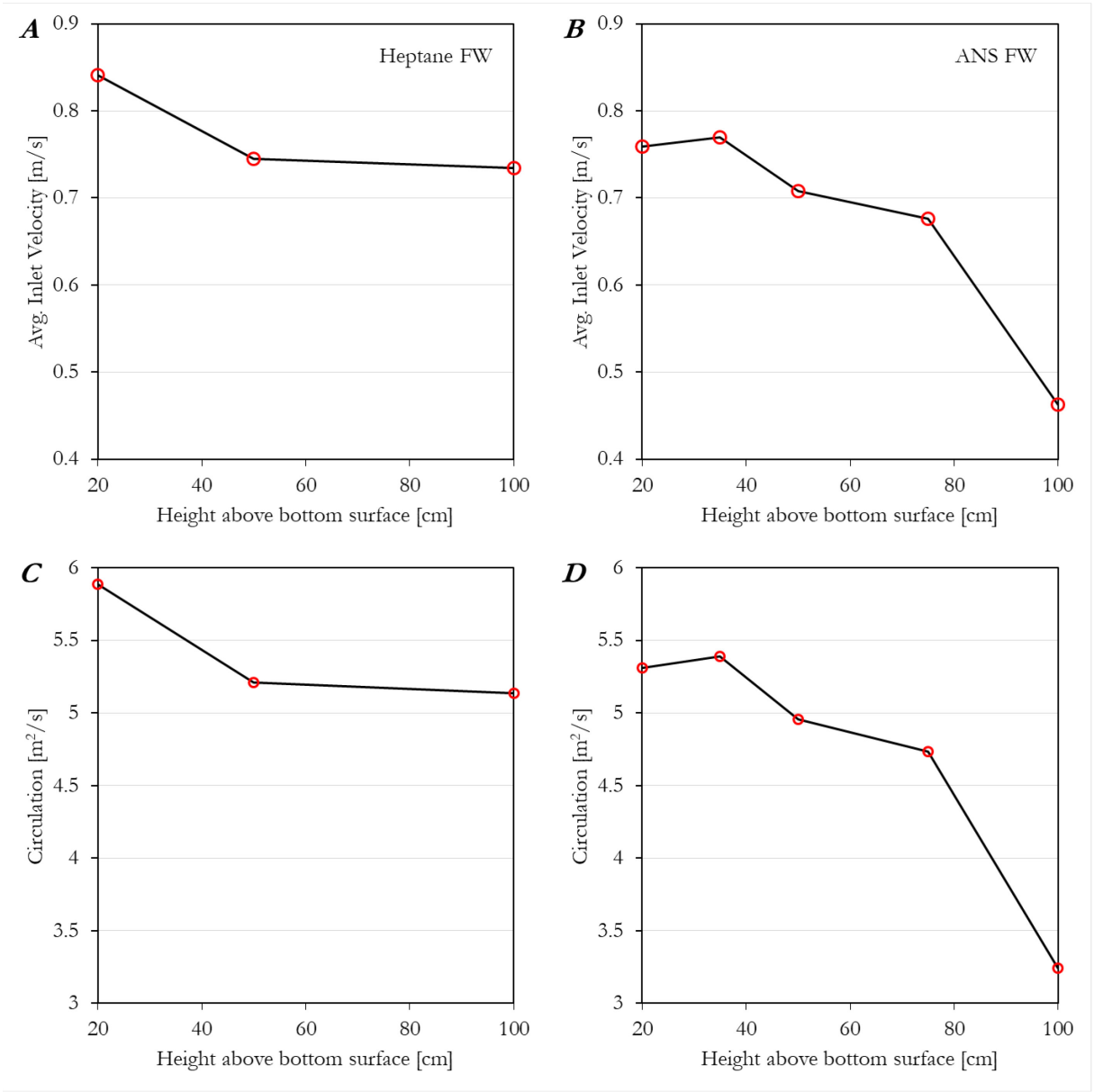

Figure 7.23: Average inlet velocity at various heights above the bottom surface for (A) heptane fire whirls, and (B) ANS fire whirls. Circulation calculated from the avg. inlet velocity at each different height for (C) heptane fire whirls, and (D) ANS fire whirls.

7.3. Discussion of the Large-Scale Results

The large-scale experiments showed an overall improved condition for burning in the fire whirl regime similar to results from smaller scales during this project. The fire whirl regime showed higher burning rates. In experiments with crude oil, the consumption efficacies of fire whirls were marginally higher than pool fires. This could be because of improved heat feedback, fuel layer thickness and the fuel properties. Most importantly this improvement is now observed from bench-scale experiments up to practical scales, i.e. 70 cm diameter fuel pools.

Consistent with results at smaller scales discussed in earlier sections, emissions were improved by implementing the fire whirl regime. This is true for both fuels tested, with major differences observed especially in the form of lower particulate matter emissions. The fire whirl regime shows significantly lower particulate matter produced when compared to corresponding pool fires. PM emission factors obtained from crude oil experiments show around a 50% reduction going from the pool fire to fire whirl regime.

Heat feedback can influence the energy balance of a burning liquid fuel and subsequently alter its burning rate. Heat feedback measured by partially submerged heat flux gauges showed different amounts of heat flux transferred to the fuel layer for the pool fire and fire whirl regimes. *Figure 7.24* shows a conceptual drawing delineating the different heat feedback between the two flame regimes. The swirling motion of the entrained air induces an Ekman boundary layer that pushes the flame down near the fuel surface. The concave flame shape at the base of fire whirl potentially increases the heat flux feedback to fuel surface, thus increasing the burning rate when compared to a pool fire.

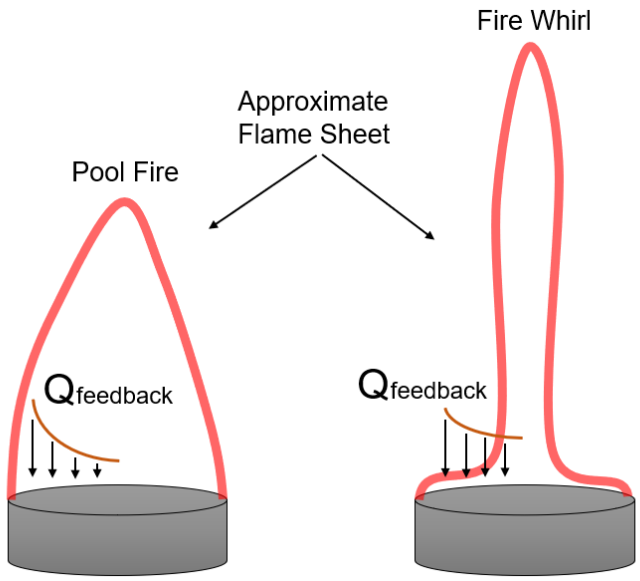

Figure 7.24: Heat feedback scenarios for pool fire and fire whirl based on the flame geometries governed by the air entrainment [26].

8. Scaling Behavior

The results of the analysis have produced data which may, in the future, assist in developing scale models of fire whirl behavior that could be used to design configurations for practical use, and also to predict their emissions and fuel consumption behavior. Various data related to the burning rate or heat-release rate of the fire, as well as the inlet flow velocity for fire whirls have been collected and analyzed in this work. *Figure 8.1* shows a comparison of the measured circulation vs. the measured heat-release rate from fire whirls and pool fires using ANS and heptane at all scales. A relatively linear trend is observed between these quantities, indicating the existence of a simple relationship to relate the governing quantities for fire whirls from bench to field scale. These could be useful in the future to decide on an appropriate fire size for ISBs, and also to design the dimensions of the required enclosure or swirl generation device to form controlled fire whirls. This also presents a basis for relating the data from this work to earlier work on fire whirls formed in other configurations.

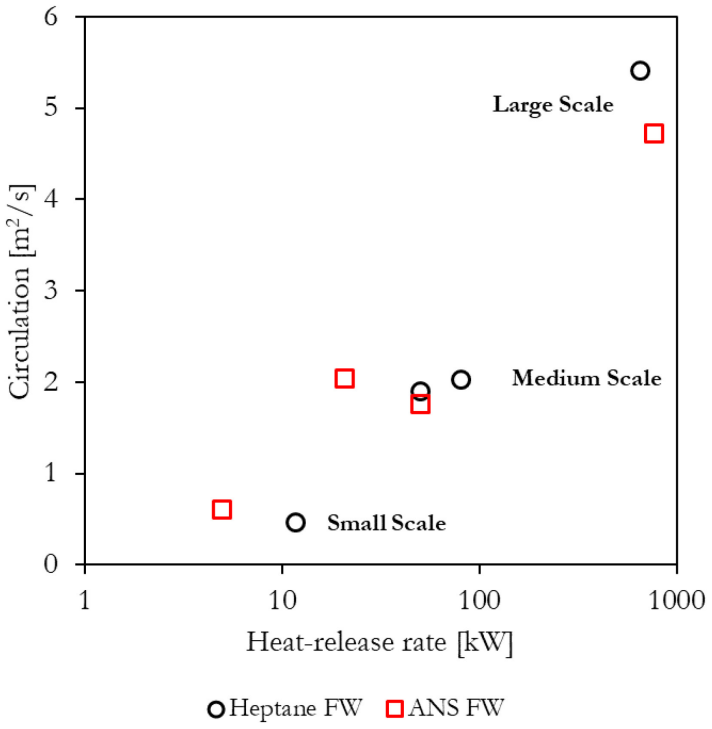

Figure 8.1: The scaling conditions for the different fire whirls investigated in this work.

8.1. Scaling of Consumption Efficacy of Fire Whirls

One of the practical aspects of the current project that was addressed was the consumption efficacy of the fire whirl. Comparisons of the ratio of the mass of fuel burned to the initial mass of fuel (consumption efficacy) were made at different scales. And the results were compared for pool fire and fire whirl regimes. This quantity is relevant only to fires burning ANS crude oil. Generally, experiments were conducted with a fuel slick thickness of 5 mm thickness of ANS crude oil. Some experiments were conducted with a 7 mm slick at the large scale, although the results were very similar.

The consumption efficacy for pool fires and fire whirls was expected to converge with increasing scale and reach an asymptote. As the pan size increased to 70 cm, efficacies of about 80–90% were seen for both pool fires and fire whirls. A removal efficiency of around 90% is normally observed in large scale field tests. As shown in *Figure 8.2*, when compared to pool fires, the fire whirl regime yields higher consumption efficacies when the pool size is smaller, and the efficacy is roughly the same at the 70 cm scale. The increase in consumption efficacy with scale shows a non-linear increase for the fire whirl regime. With scale, the trend is more linear for pool fires.

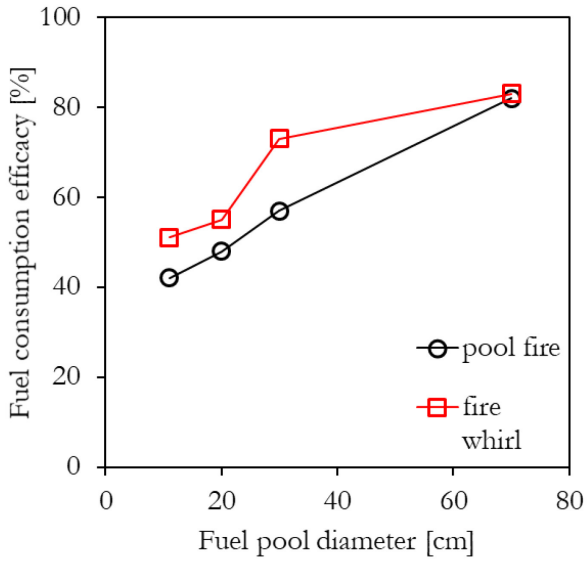

Figure 8.2: Scaling of consumption efficacy of pool fire and fire whirl regimes. All experimental conditions shown here used an initial fuel slick thickness of 5 mm.

8.2. Scaling of Emission from Fire Whirls

In general, emissions from pool fires and fire whirls formed using liquid fuels show reduced emissions in the fire whirl regime. *Figure 8.3 (A–H)* shows the scaling of the various emission factors for the pool fire and fire whirl regimes. Panels *(A–D*) show results for heptane fires, and panels (*E–H*) show the corresponding results for ANS fires. Emission factors of soot (PM) for both fuels consistently decrease with increasing scale when the fire whirl regime is used. This is a promising outcome as particulate matter from combustion has been identified to be very dangerous for human health. Fire whirls in general showed higher burning rates compared to pool fire regime. Because of this, the rate of carbon dioxide production was found to be higher as the two parameters correlate closely. However, the emission factor of CO_2 for heptane fire whirl experiments only showed slightly higher values across all scales when compared to heptane pool fires, though little increase would really be expected as CO_2 is generally closely related to the heat-release rate of the fuel.

Results for 20 cm diameter tests, unfortunately, do not conform to the overall trends observed in *Figure 8.3*. As reported earlier, emissions values for these 20 cm tests are sometimes double what would be expected and may be due to a calibration or analysis error. The source of this error was not discovered before the preparation of this report and, unfortunately, additional ANS crude required to re-perform the necessary experiments was not available in time to include in this report. These will be conducted in the future and updated before final submission of manuscripts to journals.

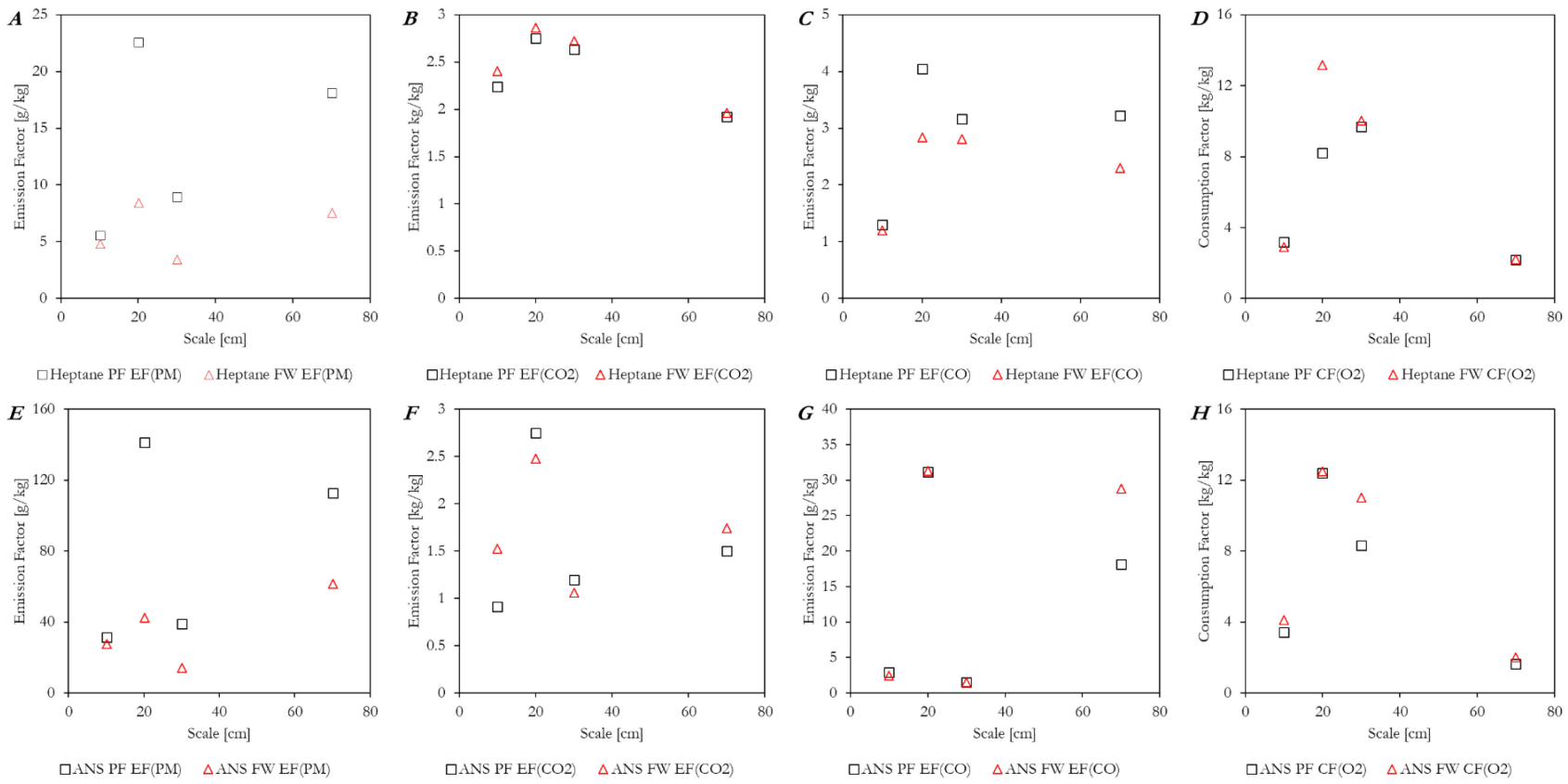

Figure 8.3: Emission factors from heptane and ANS crude oil fires at different scales. Top row shows emission factors from heptane fires, for (A) PM, (B) CO_2, (C) CO, and consumption factor of (D) O_2. Bottom row shows emission factors from ANS crude oil fires, for (E) PM, (F) CO_2, (G) CO, and consumption factor of (H) O_2.

9. Conclusions

The primary objectives of this work were to (1) Describe and characterize the structure and behavior of fire whirls over open water; (2) understand the effects and advantages of fire whirls on ISB; and to understand and quantify emissions from ISBs with and without fire whirls in scenarios ranging from (3) small to (4) large scale test burns. At the conclusion of this work we have adequately addressed all four objectives, demonstrating the effectiveness of fire whirls to reduce emissions and improve burning rates when burning both heptane and crude oil.

Throughout this work we have further understood the structure and behavior of fire whirls over open water, addressing objective 1. In particular, a relationship between ambient circulation and the heat-release rate of the fire was shown to be linearly correlated from small (11 cm diameter) to large (70 cm diameter) scale. This is an impressive range and represents a means to design fire whirls at larger scales, as desired. Collection of heat fluxes and flame temperatures has also helped to demonstrate the mechanisms by which improved burning efficiency is achieved, namely higher heat fluxes to the fuel surface and higher flame temperatures, both augmented by the fluid dynamic structure of the fire whirl and radiation within the swirling fire plume.

Emissions measurements have directly led to quantification of the advantages of fire whirls on ISB, addressing objective 2. In particular, particulate emissions are significantly reduced when burning crude oil in a fire whirl configuration vs. a traditional pool fire configuration, typically by at least half. The rate of burning is also dramatically increased, which would result in reduced operational burning times in the field. These results are shown using fuel pool diameters of 10, 20, 30, and 70 cm, demonstrating the ability for improvement to be achieved from small (objective 3) to large (objective 4) scale. By coupling detailed measurements at the small scale with larger-scale results, a comprehensive data set is now available to extract both the mechanisms responsible for improvement in combustion efficiency with fire whirls and a proof-of-concept established which shows this technique could be applied at practical scales.

10. Proposed Future Work

As of March 2019, all the tasks related to Phase I, II, and III of the projects are complete. While these objectives have been completed, work will still continue on this project. Additional manuscript preparation for submission to multiple journals will continue as more analysis is being conducted on the results obtained. Further analysis of issues related to the 20 cm pan diameter emissions will take place as well as separating boilover and non-boilover conditions for an assessment of their separate impact on emissions factors at various scales. Still, there is additional work which is now possible as a result of this first project. These potential future steps are proposed below.

The first is optimization of the fire whirl configuration; essentially manipulation of the burning rate and circulation, to establish an entrainment condition that leads to reduced emissions. At direction of BSEE initial tests focused on emissions only for the most ideal configurations, however finding a means to predict this ideal condition and assessing the effects of conditions on potential emissions would be practically and scientifically important. For this, the change in dimensions of the fire whirl configurations (enclosure area, opening area, wall height) will be studied at the small-scale to assess the effect on fire whirl formation and shape properties, and also circulation and burning rate. This knowledge is important for implementing the fire whirl in ISB applications, in particular how far the wall height can be reduced to still achieve ideal emissions conditions. Their effect on emissions will aid in identifying the right entrainment conditions – naturally or forced – for *in-situ* implementation.

Another aspect of this work is to investigate the effect of fuel layer thickness on emissions. Boil over was observed at some point at all scales, however it is not observed in field conditions. By varying the fuel layer thickness a longer burning period and combustion of a broader range of hydrocarbons present in crude oil will be achieved. Boil over will also be avoided for a longer period of time, thereby the analysis of emission will be less dependent on tests conditions, e.g. pool diameter. This is a practical step toward use of fire whirl for ISB. Eventually further tests on different fuels at various stages of weathering will also aid in assessing how effective this technique can be in practical application.

References

[1] G.M. Solomon, S. Janssen, Health effects of the gulf oil spill, Disaster Med. Public Health Prep. 4 (2010) 273–276. doi:10.1001/dmp.2010.45.

[2] S.R. Pezeshki, M.W. Hester, Q. Lin, J.A. Nyman, The effects of oil spill and clean-up on dominant US Gulf coast marsh macrophytes: A review, Environ. Pollut. 108 (2000) 129–139. doi:10.1016/S0269-7491(99)00244-4.

[3] J.P. Zock, G. Rodríguez-Trigo, F. Pozo-Rodríguez, J.A. Barberà, L. Bouso, Y. Torralba, J.M. Antó, F.P. Gómez, C. Fuster, H. Verea, Prolonged respiratory symptoms in clean-up workers of the Prestige oil spill, Am. J. Respir. Crit. Care Med. 176 (2007) 610–616. doi:10.1164/rccm.200701-016OC.

[4] R.J. Law, J. Hellou, Contamination of fish and shellfish following oil spill incidents, Environ. Geosci. 6 (1999) 90–98.

[5] C.H. Peterson, S.D. Rice, J.W. Short, D. Esler, J.L. Bodkin, B.E. Ballachey, D.B. Irons, Long-Term Ecosystem Response to the Exxon Valdez Oil Spill, Science (80-.). 302 (2003) 2082–2086. doi:10.1126/science.1084282.

[6] J.M. Teal, R.W. Howarth, Oil spill studies: A review of ecological effects, Environ. Manage. 8 (1984) 27–43. doi:10.1007/BF01867871.

[7] NOAA, Oil and Chemical Spills, Off. Response Restor. (2017).

[8] M.A. Peters, Oil geopolitics and eco-nightmares, Educ. Philos. Theory. 49 (2017) 435–438. doi:10.1080/00131857.2017.1286135.

[9] M.F. Fingas, G. Halley, F. Ackerman, R. Nelson, M. Bissonnette, N. Laroche, Z. Wang, P. Lambert, K. Li, P. Jokuty, G. Sergy, E.J. Tennyson, J. Mullin, L. Hannon, W. Halley, J. Latour, R. Galarneau, B. Ryan, R. Turpin, P. Campagna, D. V Aurand, R.R. Hiltabrand, THE NEWFOUNDLAND OFFSHORE BURN EXPERIMENT—NOBE, Int. Oil Spill Conf. Proc. 1995 (1995) 123–132. doi:10.7901/2169-3358-1995-1-123.

[10] J.L. Ross, R.J. Ferek, P. V Hobbs, Particle and Gas Emissions from an In Situ Burn of Crude Oil on the Ocean Particle and Gas Emissions from an In Situ Burn of Crude Oil on the Ocean, J. Air Waste Manag. Assoc. Air Waste Manag. Assoc. 463 (1996) 251–259. doi:10.1080/10473289.1996.10467459.

[11] I. Buist, Window-of-Opportunity for In Situ Burning, Spill Sci. Technol. Bull. 8 (2003) 341–346. doi:10.1016/S1353-2561(03)00050-1.

[12] A.A. Allen, R.J. Ferek, ADVANTAGES AND DISADVANTAGES OF BURNING SPILLED OIL, Int. Oil Spill Conf. Proc. 1993 (1993) 765–772. doi:10.7901/2169-3358-1993-1-765.

[13] I. Buist, K. Trudel, J. Morrison, D. Aurand, LABORATORY STUDIES OF THE PROPERTIES OF IN-SITU BURN RESIDUES, Int. Oil Spill Conf. Proc. 1997 (1997) 149–156. doi:10.7901/2169-3358-1997-1-149.

[14] I. Buist, S. Potter, T. Nedwed, J. Mullin, Herding surfactants to contract and thicken oil spills in pack ice for in situ burning, Cold Reg. Sci. Technol. 67 (2011) 3–23. doi:10.1016/j.coldregions.2011.02.004.

[15] Q. Lin, I.A. Mendelssohn, K. Carney, S.M. Miles, N.P. Bryner, W.D. Walton, In-situ burning of oil in coastal marshes. 2. Oil spill cleanup efficiency as a function of oil type, marsh type, and water depth, Environ. Sci. Technol. 39 (2005) 1855–1860. doi:10.1021/es0490626.

[16] C. Bech, I. Buist, S.L. Ross, IN-SITU BURNING OF EMULSIONS: THE EFFECTS OF VARYING WATER CONTENT AND DEGREE OF EVAPORATION, (n.d.).

[17] S.& T.C. NATIONAL RESPONSE TEAM, GUIDANCE ON BURNING SPILLED OIL IN SITU, Office of Response and Restoration, 1995.

[18] IPIECA, IOGP, In-Situ Burning of Spilled Oil - Good practice guidelines for incident management and emergency response personnel, London, UK, 2016.

[19] A. Tohidi, M.J. Gollner, H. Xiao, Fire Whirls, Annu. Rev. Fluid Mech. 50 (2018) annurev-

fluid-122316-045209. doi:10.1146/annurev-fluid-122316-045209.

[20] O. US EPA, Particulate Matter (PM) Basics, (n.d.).

[21] T. Incorporated, Theory of Operation - DustTrak DRX Aerosol Monitor, 2012.

[22] T. Incorporated, DustTrak DRX Aerosol Monitor Model 8534 Operation and Service Manual, 2017.

[23] L. van Gelderen, L.M.V. Malmquist, G. Jomaas, Vaporization order and burning efficiency of crude oils during in-situ burning on water, Fuel. 191 (2017) 528–537. doi:10.1016/j.fuel.2016.11.109.

[24] N.A. May, Moisture Content Effects on Energy and Emissions Released During Combustion of Pyrophytic Vegetation, University of Maryland, College Park, 2017.

[25] P. Wang, N. Liu, K. Hartl, A. Smits, Measurement of the Flow Field of Fire Whirl, Fire Technol. 52 (2016) 263–272. doi:10.1007/s10694-015-0511-0.

[26] R. Dobashi, T. Okura, R. Nagaoka, Y. Hayashi, T. Mogi, Experimental Study on Flame Height and Radiant Heat of Fire Whirls, Fire Technol. (2015). doi:10.1007/s10694-015-0549-z.

[27] Yu, Dehai, and Peng Zhang. "Circulation-controlled fire whirls with differential diffusion." Combustion and Flame 189 (2018): 288-299.

[28] Jomaas, G. "Experimental Procedure for Laboratory Studies of In Situ Burning: Flammability and Burning Efficiency of Crude Oil." Journal of visualized experiments: JoVE 135 (2018).

[29] Alva, U. Rojas, Bjørn Skjønning Andersen, and Grunde Jomaas. "Pumice stones as potential in-situ burning enhancer." Cold Regions Science and Technology 146 (2018): 167-174.

[30] Zhao, J., Huang, H., Jomaas, G., Zhong, M., & Yang, R. (2018). Experimental study of the burning behaviors of thin-layer pool fires. Combustion and Flame, 193, 327-334.

11. Appendix

11.1. Construction of fire whirl apparatus for large-scale experiments

Figure A1. Lumber frame for holding sheetrock boards. Lumber cross-section were (2” x 4”).

Figure A2. Sheetrock installed on the lumber frame. The side visible was on the outside of the fire whirl enclosure.

Figure A3. Fuel/water container being tested for leaks. Also visible are the inlet/outlet ports for water recirculation, and the scape pipe for running instrumentation wires.

Figure A4. Fuel/water container shown here positioned in the center of the enclosure. The enclosure base was partially removed to show the support frame.

Figure A5. Fuel/water container shown with the full enclosure base in position.

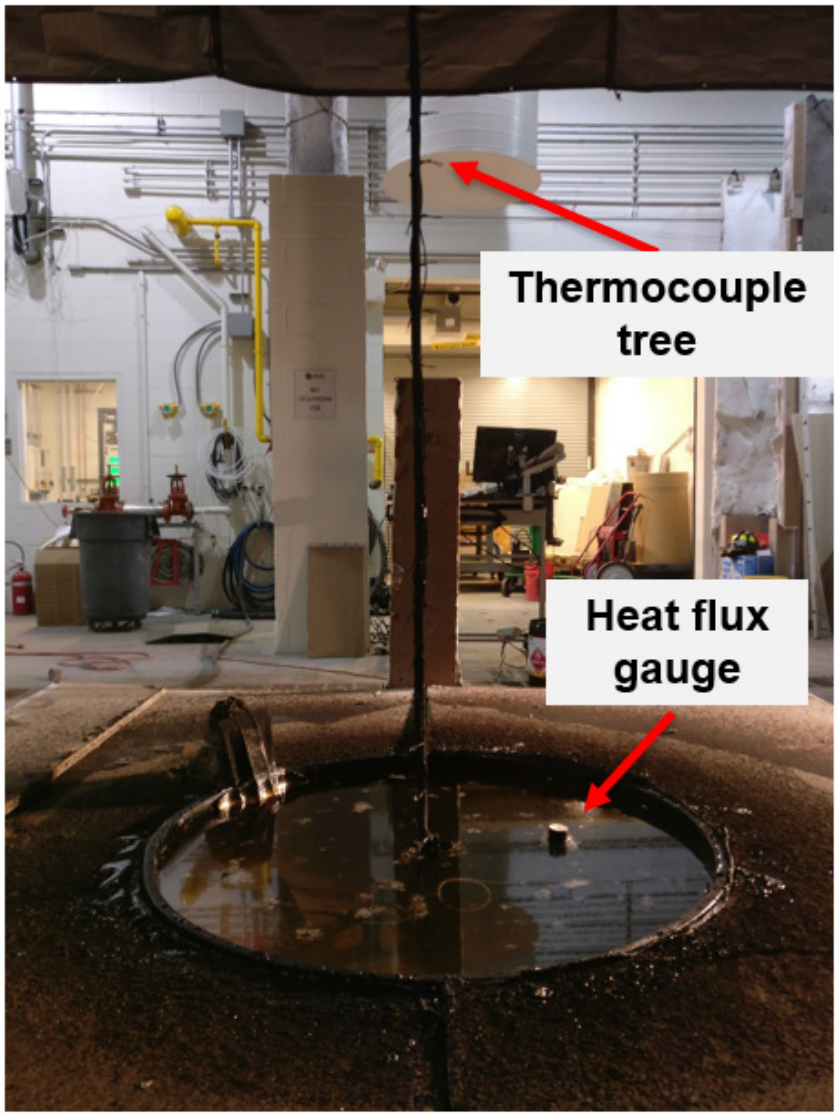

Figure A6. Image showing the fuel/water container filled with water. Also labelled are the submerged heat flux gauge and thermocouple tree installed in the center of the container.

Additional images

Figure A7. An image showing boilover during an experiment at the small scale. This image was submitted to the 2019 Combustion Art Competition, to be held at the 11th US National Combustion Meeting.